The Dissertation Committee for Chia-Yin Wei Certifies that this is the approved version of the following dissertation:

Ensemble and Single-Molecule Studies of Polymer Dynamics Near the Glass Transition

Committee:

David A. Vanden Bout, Supervisor

Paul F. Barbara

Peter J. Rossky

Jason B. Shear

Charles B. Mullins

Ensemble and Single-Molecule Studies of Polymer Dynamics Near the Glass Transition

by

Chia-Yin Wei, B.S.

Dissertation

Presented to the Faculty of the Graduate School of

The University of Texas at Austin

in Partial Fulfillment

of the Requirements

for the Degree of

Doctor of Philosophy

The University of Texas at Austin

May 2007

Dedication

To my family

Acknowledgements

This dissertation would not have been possible without the mentorship of my supervisor, Dr. Vanden Bout, who has inspired and motivated me throughout these years in graduate school. He has shown great passion for his work and genuine kindness to those around him, which I admire and look up to. I want to thank my parents, who have provided me with all possible resources so that I had the chance to become who I am today. I hope I can live up to them someday. My brothers, David and Jim, have also been a source of inspiration even though I don't see them much. I would like to acknowledge all the members of the Vanden Bout group for their friendship and support. I wish to thank Yeon Ho in particular, who has not only been my project partner but also my hero, helping me tremendously with the experiments and every other problem that I encountered. I also want to acknowledge all the administration and technical staff in the Department of Chemistry for their assistance. I want to express my appreciation to Chia-Jung and Ying-Cheng for hosting me when I first came to the U.S.; and I would like to thank Wei-Shun for his guidance in academia and life. I've had great fortune to make a lot of friends here in Austin and I deeply cherish their wonderful friendships. Thanks to all those who have supported me along the way.

Ensemble and Single-Molecule Studies of Polymer Dynamics Near the Glass Transition

Publication No._____

Chia-Yin Wei, Ph.D.

The University of Texas at Austin, 2007

Supervisor: David A. Vanden Bout

Rotational dynamics of polymers are studied by both ensemble and single-molecule spectroscopy. Polarized fluorescence recovery after photobleaching (FRAP) is used to measure bulk rotational diffusion of probe molecules in poly(cyclohexyl acrylate) matrix at various temperatures above the glass transition temperature of the polymer. The anisotropy decay is fit by a stretched exponential function: $f(t) = \exp[-(t/\tau)^{\beta}]$, and is a nonexponential decay with small β values ~ 0.6. The dependence of rotational time on temperature follows the well-established Williams-Landel-Ferry equation, which describes the primary relaxation of polymers, and therefore demonstrates that the rotational times of probes are indeed reflective of their host material. The same polymer is also investigated by single-molecule fluorescence spectroscopy. The rotational motion of the probe molecule can be elucidated by the auto-correlation function of the reduced linear dichroism signals. Each auto-correlation function is fit to the stretched exponential function, and the results from all single molecules show wide distributions of correlation times and β. The average rotational

time from the single-molecule experiment agrees with that measured by the ensemble technique, and the sum of all correlation functions forms a nonexponential decay that is almost identical to the bulk anisotropy decay. Both results suggest that the polymer system has inhomogeneous dynamics that are not pure diffusion.

Table of Contents

List of Tables

List of Figures

Chapter 1: Introduction and Dissertation Overview

DYNAMICS IN GLASS-FORMING MATERIALS

A liquid which can be rapidly cooled below its melting temperature without crystallizing is called a supercooled liquid. Molecular motions in supercooled liquids become extremely slow that at some point the entire material appears to be "frozen" on the timescale of experimental observation, and becomes glassy. This non-first order phase change is called the glass transition, and the slowing of the dynamics is not accompanied by a drastic structural change [Figure 1.1]. The glass transition temperature can be defined in many ways, such as the temperature at which a change occurs in the expansion coefficient, specific heat capacity, elastic modulus, or dielectric constant. Since the glass transition is a gradual transformation, measurement of T_g is very sensitive to parameters such as the heating and cooling rate. Thus T_g is not an exact value, and may be different depending on how it is defined. T_g is one of many important characteristics for determining properties of glass-forming materials such as polymers, viscous liquids, amorphous metal alloys, and other disordered solids. For more extensive reviews refer to these references[1-6].

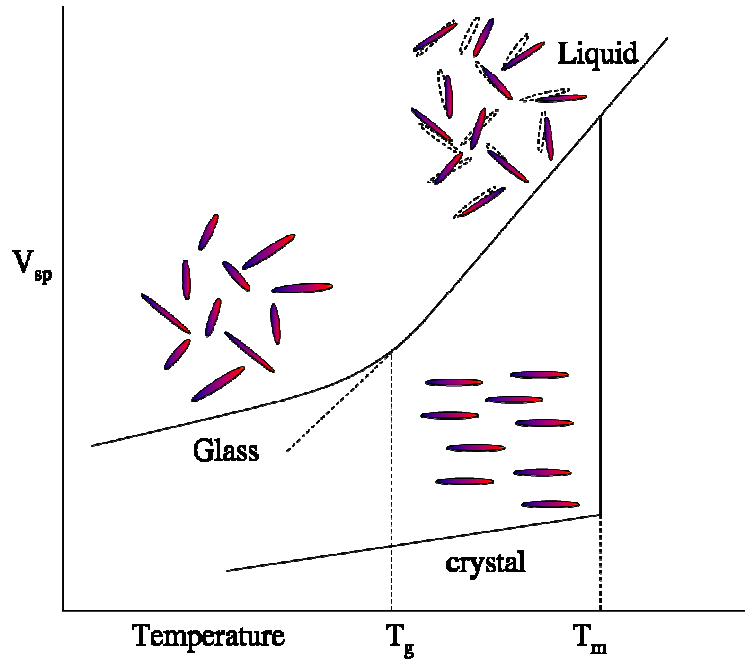

Figure 1.1: Phase diagram of a liquid shown as specific volume versus temperature. The liquid can crystallize at T_m, or continue to be cooled below the melting point without ordering. Dynamics slow down dramatically until at T_g, where molecular motions stop and the disordered structure is retained in the glassy state.

One of the most noticeable and intriguing features of supercooled liquids is the nonexponential relaxation as response to various perturbations. In a normal liquid, relaxation is a single exponential decay, as would be expected from Brownian motions. In supercooled liquids, not only does the relaxation take very long time, its nonexponential nature is often regarded as indicative of heterogeneity. It has long been debated which underlying scheme can describe such non-diffusive behaviors: (1) heterogeneous scenario, where different sub-environments exist throughout the system, and that each molecule relaxes exponentially in its local environment, but timescales vary substantially among the sub-environments, thus resulting in an overall

nonexponential manner; or (2) homogeneous scenario, in which each molecule relaxes identically on the same timescale, but in an intrinsically nonexponential fashion. See Figure 1.2 for a schematic illustration of both cases.

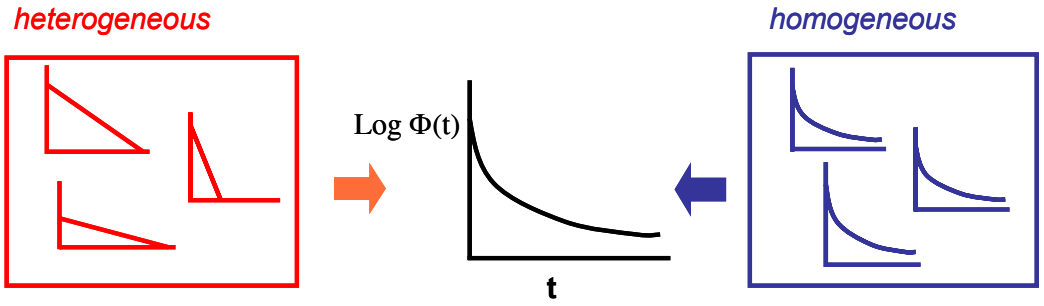

Figure 1.2: Illustration of nonexponential decay described by the heterogeneous or homogeneous scenario. The heterogeneous scheme consists of single exponential decays of different times, whereas the homogeneous scheme consists of identical nonexponential decays.

The heterogeneous idea has been addressed in early glass transition theories[7-13], and many experiments have made strong arguments for spatially heterogeneous dynamics[14-22]. Despite the general conception that dynamics are *heterogeneous*, the debates continue: what exactly does the experiment measure? How do results compare from one technique to another? How does the experimental time frame compare to the molecular dynamics? How large are the spatial domains? How does the molecule switch from one diffusion time to another? etc. The challenge in establishing an all-encompassing model to successfully explain the entire phenomenology of the glass transition dynamics lies in the complexity of the problem itself, and it remains an active area of scientific research for experimental and theoretical scientists across disciplines.

What we hope to investigate within the scope of our research is the rotational dynamics in a glass-former on a single-molecule level in order to differentiate the scenarios for nonexponential relaxations. Most experiments measure a bulk property that is averaged over an ensemble of molecules. Although enhanced signals provide more accurate information, such results do not reveal the behaviors of individual components which may be very different from one another. From Figure 1.2, we can see clearly that in order to make an unambiguous distinction between homogeneous and heterogeneous, one should probe directly individual molecular dynamics.

SINGLE-MOLECULE SPECTROSCOPY

Single-molecule spectroscopy offers ultimate sensitivity in the detection of only one molecule upon radiation. This provides a powerful means to study individual behaviors of molecules in a complex environment directly and obtain a distribution rather than only the average. By removing ensemble averaging, hidden details of molecular dynamics can be probed, from which new physical effects may be observed, and microscopic theories on spatial or temporal inhomogeneity can be investigated. The most practical method to detect signals from single molecules by optical means is laser-induced fluorescence. Even though the first optical single-molecule detection was done using phase-modulated absorption method[23], it was soon identified that fluorescence methods showed much higher sensitivity, in which a small red-shifted emission can be detected above almost zero background through effective filtering. Early experiments were carried out at low temperatures, and the first room-temperature single-molecule imaging was done by near-field scanning optical microscopy[24-26]. As the technique developed over the years, room-temperature, far-field confocal microscopy, along with

other methods, have been widely adopted in many fields for single-molecule studies[21,27-34].

The main requirements for carrying out a single-molecule experiment include exciting only one molecule at the focal volume, and providing a good signal-to-noise ratio for detection. To guarantee that only one molecule is at resonance with the excitation beam, it is often accomplished by focusing the laser beam to a very small spot. In addition, very low concentrations of probe molecules are dispersed into the host matrix, normally in the nM range for a probed volume of 10 μm^3. The other very important issue for a single-molecule experiment is to optimize the signal-to-noise ratio. This is achieved by maximizing the signal while minimizing the backgrounds. To achieve a large signal, one needs to choose a good fluorophore with a high fluorescence quantum yield, short excited state lifetime, and low intersystem-crossing rate. In other words, a good fluorophore can be excited repeatedly, and emits a photon upon every cycle back to the ground state. It should only rarely intersystem-cross to the triplet state which has a longer lifetime, because when it does so, $S_1 - S_0$ cycles will cease until it returns to the singlet ground state. Thus fluorescence emission rate can be maximized by using high photon flux and large absorption cross section.

There are a number of limitations for fluorescence measurements as well. Among these limitations is optical saturation, which happens when the laser intensity is increased, but the relaxation from the excited state to the ground state is not fast enough for the molecule to reabsorb photons. Therefore, when the pumping laser has reached the saturation intensity, the fluorescence signal no longer increases anymore, yet the background signals will grow. In addition, triplet bottleneck occurs when the molecule occasionally undergoes intersystem-crossing to the triplet state, thus both absorption and emission cease for a triplet lifetime. Photobleaching is another event that limits

fluorescence signal intensities and the observation time. There are several mechanisms through which photobleaching takes place, and the molecule is transformed to another species which does not absorb or emit photons, upon which fluorescence detection is over. Eliminating atmospheric oxygen and adding triplet quenchers will reduce the rate of photobleaching[35,36]. Overall, there is a tradeoff between excitation power, signal, and observation time. Higher pumping power boosts the emission rate and thus the signal, but also leads to faster photobleaching rate and shorter survival time of the molecule. Therefore, for imaging purposes, higher laser power can give better resolution, but lower power is desired for acquiring long transient data. Moreover, while not ensemble-averaged, the single-molecule measurement is inherently time-averaged as the data for a single molecule are collected over a period of repeated excitation. Thus it is very crucial that we know which properties are really being measured, and how the experimental time resolution compares to the molecular dynamics. Due to photobleaching, a fluorophore cannot be observed for an infinite long period of time and statistical errors grow as the transient length shortens[37-39]. This leads to an inherent bias with single-molecule measurements, in such that it is possible to make very short observations of a system where all the molecules are in fact identical, and yet obtain distinct properties for each of the molecules as a result of the large uncertainties associated with the short measurement time. Ideally, aside from measuring a distribution of properties, one would also like to examine how this distribution changes with time. Therefore, it is very important to understand how observation time in single-molecule experiments affects the inherent distribution of properties measured. Two important comparisons should be made when characterizing a distribution measured from single molecules. First, the ensemble of single molecules measured individually should yield the bulk average result. This requires a clear understanding of how to directly

compare the single-molecule and ensemble measurements. Second, the distribution should be compared to the distribution expected to arise merely as a result of the statistics associated with the measurement.

DISSERTATION OVERVIEW

Chapter 1

The goal of this chapter is to familiarize readers with sufficient background information on a few key notes of our studies. A general introduction on the dynamics of glass-forming materials is presented, with the emphasis on the nonexponential relaxations near the glass transition temperature that are signature of their dynamical properties. The possible scenarios of homogeneous and heterogeneous schemes that may lead to such nonexponentiality are discussed, followed by a short overview of single-molecule spectroscopy, along with discussions on some technical aspects of the experiment.

Chapter 2

The ensemble anisotropic relaxations of probe molecules in poly(cyclohexyl acrylate) are investigated by polarized fluorescence recovery after photobleaching (FRAP) technique at various temperatures above the polymer T_g. The anisotropy decay is fit by a stretched exponential function : $f(t) = \exp[- (t / \tau)^{\beta}]$, and is a nonexponential decay with small β values of 0.5 to 0.6, which suggests that the measured rotational dynamics are heterogeneous. The dependence of relaxation time on temperature follows the empirical Williams-Landel-Ferry equation, demonstrating that the primary relaxation

of the polymer is measured, and that probe dynamics are in fact heavily dependent on its local environment.

Chapter 3

A report by Hinze *et al.*[40] demonstrated that the correlation function of the fluorescence dichroism signal, measured as a probe of single molecule rotational dynamics, should not manifest a single exponential decay even for isotropic diffusion. This has called into question the attribution of nonexponential behaviors in supercooled fluids and polymer systems to dynamical heterogeneity. In this chapter, it is shown that for the case of a high-numerical aperture objective, the dichroism decay becomes indistinguishable from a single exponential. As a consequence, observed nonexponential decays can be associated with complex rotational dynamics. These effects are illustrated via simulated rotational trajectories for isotropic diffusion of a dipole[41].

Chapter 4

In this chapter, single-molecule spectroscopy is exploited to study rotational motions of single Rhodamine 6G probe molecules in poly(cyclohexyl arylate) in order to investigate any heterogeneity in the amorphous polymer system. The rotational dynamics of the probe molecule is measured by the auto-correlation function of the linear dichroism signals. Each correlation function is fit to the stretched exponential function, and the results from all single molecules show wide distributions of correlation times τ and β. Statistical errors arising from finite-sampling effects are also taken into consideration to properly interpret the experimental distributions.

Chapter 5

This is the overview of the entire dissertation. Comparisons of ensemble anisotropy decay and single molecule rotational correlation functions are made quantitatively to explore the dynamics of PCA. A demonstration of how to relate the properties measured in both experiments is first presented theoretically, and later validated by experimental results. The ensemble results yield nonexponential decays which suggest that dynamics are not pure diffusion; while single-molecule results of the same system reveal broad distributions of rotational correlation functions that are not identical, and yet the average of all rotational constants agrees with the ensemble decay time. An intermediate scenario is proposed to attribute the nonexponential relaxation dynamics to heterogeneous, non-pure diffusions, instead of the two extreme cases of homogenous or heterogeneous.

REFERENCES

(1) Ediger, M. D.; Angell, C. A.; Nagel, S. R. *J. Phys. Chem.* **1996**, *100*, 13200.

(2) Phillips, J. C. *Rep. Prog. Phys.* **1996**, *59*, 1133.

(3) Sillescu, H. *J. Non-Crys. Solids* **1999**, *243*, 81.

(4) Angell, C.A.; Ngai, K. L.; McKenna, G. B.; McMillan, P. F.; Martin, S.W. *J. Appl. Phys.* **2000**, *88*, 3113.

(5) Ediger, M. D. *Ann. Rev. Phys. Chem.* **2000**, *51*, 99.

(6) Lubchenko, V.; Wolynes, P. G. *Annu. Rev. Phys. Chem* **2007**, *58*, 235.

(7) Adams, G.; Gibbs, J. H. *J. Chem. Phys.* **1965**, *43*, 139.

(8) Pomeau, Y.; Resibois, P. *Physics Reports* **1974**, *19*, 65.

(9) Cohen, M. H.; Grest, G. S. *Phys. Rev. B* **1981**, *24*, 4091.

(10) Bengtzelius, U.; Goetze, W.; Sjolander, A. *J. Phys. C* **1984**, *17*, 5915.

(11) Leutheusser, E. *Phys. Rev. A* **1984**, *29*, 2765.

(12) Kirkpatrick, T. R.; Thirumalai, D.; Wolynes, P. G. *Phys. Rev. A* **1989**, *A40*, 1045.

(13) Mazenko, G. F.; Yeo, J. *Transp. Theory Stat. Phys.* **1995**, *24*, 927.

(14) Schmidt-Rohr, K.; Spiess, H. W. *Phys. Rev. Lett.* **1991**, *66*, 3020.

(15) Cicerone, M. T.; Blackburn, F. R.; Ediger, M. D. *Macromolecules* **1995**, *28*, 8224.

(16) Cicerone, M. T.; Ediger, M. D. *J. Chem. Phys.* **1995**, *103*, 5684.

(17) Böhmer, R.; Chamberlin, R. V.; Diezemann, G.; Geil, B.; Heuer, A.; Hinze, G.; Kuebler, S. C.; Richert, R.; Schiener, B.; Sillescu, H.; Spiess, H. W.; Tracht, U.; Wilhelm, M. *J. Non-Crys. Solids* **1998**, *235-237*, 1.

(18) Bartko, A. P.; Dickson, R. M. *J. Phys. Chem. B* **1999**, *103*, 11237.

(19) Ha, T.; Laurence, T. A.; Chemla, D. S.; Weiss, S. *J. Phys. Chem. B* **1999**, *103*, 6839.

(20) Lunkenheimer, P.; Schneider, U.; Brand, R.; Loidl, A. *Contemp. Phys.* **2000**, *41*, 15.

(21) Deschenes, L. A.; Vanden Bout, D. A. *J. Phys. Chem. B* **2002**, *106*, 11438.

(22) Richert, R. *J. Phys.: Condens. Matter* **2002**, *14*, R703.

(23) Moerner, W. E.; Kador, L. *Phys. Rev. Lett.* **1989**, *52*, 2535.

(24) Betzig, E.; Chichester, R. J. *Science* **1993**, *262*, 1422.

(25) Trautman, J. K.; Macklin, J. J.; Brus, L. E.; Betzig, E. *Nature* **1994**, *369*, 40.

(26) Ambrose, W. P.; Goodwin, P. M.; Martin, J. C.; Keller, R. A. *Science* **1994**, *265*, 364.

(27) Basché, T.; Moerner, W. E.; Orrit, M.; Wild, U. P. *Single-molecule optical detection, imaging and spectroscopy*; VCH: Cambridge, 1997.

(28) Nie, S.; Zare, R. N. *Annu. Rev. Biophys. Biomol. Struct.* **1997**, *26*, 567.

(29) Xie, X. S.; Trautman, J. K. *Annu. Rev. Phys. Chem* **1998**, *49*, 411.

(30) Tamarat, P.; Maali, A.; Lounis, B.; Orrit, M. *J. Phys. Chem. A* **2000**, *104*, 1.

(31) Moerner, W. E.; Fromm, D. P. *Rev. Sci. Instrum.* **2003**, *74*, 3597.

(32) Kulzer, F.; Orrit, M. *Ann. Rev. Phys. Chem.* **2004**, *55*, 585.

(33) Barbara, P. F. *Acc. Chem. Res.* **2005**, *38*, 503.

(34) Michalet, X.; Weiss, S.; Jäger, M. *Chem. Rev.* **2006**, *106*, 1785.

(35) Deschenes, L. A.; Vanden Bout, D. A. *Chem. Phys. Lett.* **2002**, *365*, 387.

(36) Lakowicz, J. R. *Principles of Fluorescence Spectroscopy*, 2nd ed.; Kluwer Academic/Plenum Publishers: New York, NY, 1999.

(37) Zwanzig, R.; Ailawadi, K. *Phy. Rev.* **1969**, *182*, 280.

(38) Box, G. E. P.; Jenkins, G. M. *Time Series Analysis Forecasting and Control*; Holden-Day: San Francisco, 1970.

(39) Lu, C.-Y.; Vanden Bout, D. A. *J. Chem. Phys.* **2006**, *125*, 124701.

(40) Hinze, G.; Diezemann, G.; Basché, T. *Phys. Rev. Lett.* **2005**, *93*, 203001.

(41) Wei, C.-Y. J.; Kim, Y. H.; Darst, R. K.; Rossky, P. J.; Vanden Bout, D. A. *Phys. Rev. Lett.* **2005**, *95*, 173001.

Chapter 2: Ensemble Fluorescence Recovery After Photobleaching

INTRODUCTION

Disordered systems, such as viscous liquids, polymers, and glassy solids, have versatile material properties that can be used in a wide range of applications. When cooled, instead of forming an ordered crystal, these materials can be cooled below the melting temperature to become a supercooled liquid. Molecular dynamics in supercooled liquids slow down several orders of magnitude as the temperature is lowered, and eventually they no longer have enough energy to rearrange and are thus frozen in the glassy state[1-3]. Many polymers do not ever crystallize and only exist as rubbers or glasses. This transformation is called the glass transition and the glass transition temperature (T_g) can be measured in different ways, such as the temperature at which the thermal expansion coefficient changes. These glass-forming materials can be used either below or above their glass transition temperatures to provide different mechanical and transport properties, and thus a fundamental understanding of the glass-transition phenomenology is of great interest and importance to physical scientists and engineers.

The dynamics of supercooled liquids and polymers can be probed by introducing a perturbation, and subsequently monitoring the response time for the system to return to its original state[4-8]. The result is a universally observed nonexponential relaxation at temperatures near and above T_g. A homogeneous system in which the dynamical motions are governed by a single timescale should yield a single exponential decay, and

therefore the nonexponential relaxations are often interpreted as existence of heterogeneities[9-15].

In this work, we designed an experiment to study the rotational dynamics of poly(cyclohexyl acrylate) by means of fluorescence recovery after photobleaching (FRAP), also known as dynamic hole-burning[5,16,17]. This is done by selectively photobleaching fluorescent probe molecules with a linearly-polarized high-intensity bleaching beam, thus creating an initial anisotropy for the system. The remaining unbleached molecules can then be probed by a weaker-intensity reading beam, whose polarization is parallel or perpendicular to the bleaching polarization. By monitoring the rotational motions of the remaining molecules, the dynamics of the system can be elucidated. As the molecules reorient back to a random distribution, the system anisotropy decays to zero. The anisotropy decay measures the C_2 rotational correlation function that is expressed as $e^{-(6Dt)}$, where D is the rotational diffusion constant. The decays can be fit with the Kohlrausch-Williams-Watts (KWW) stretched exponential function: $f(t) = \exp[-(t/\tau)^{\beta}]$. $\beta = 1$ would indicate dynamics are simply Brownian motion; $\beta < 1$ would suggest complex or heterogeneous dynamics. The polymer system was studied at various temperatures above T_g, and the dependence of anisotropy decay times on temperatures follows the well established, semi-empirical Williams-Landel-Ferry (WLF) equation, which is often used to describe viscosity or relaxations in polymers[18,19].

EXPERIMENTAL SECTION

Samples

For the ensemble experiment, a bulk sample containing concentrated probe molecules was needed. Poly(cyclohexyl acrylate) was purchased from Scientific Polymers as a solution in toluene, and the approximate MW is 150,000. Rhodamine 6G dyes (Spectra-Physics) were used as fluorescent probes. See Figure 2.1 for chemical structures.

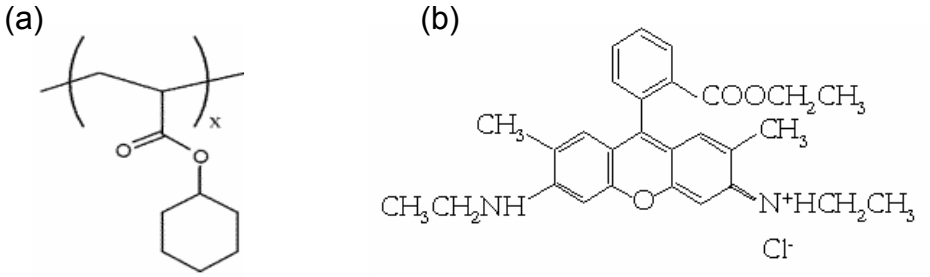

Figure 2.1: Chemical structures of (a) poly(cyclohexyl acrylate); (b) Rhodamine 6G.

The initial experimental design was to prepare thick polymer films with concentrated Rhodamine 6G dyes and collect fluorescence signals at 45˚ relative to the excitation. It was later discovered, however, that there are several difficulties with this setup (which will be discussed later). Therefore, the apparatus was redesigned to employ 90˚ detection geometry, and thus a polymer melt has to be made inside a cuvette, instead of a film on a glass cover slip.

To prepare the polymer melt, PCA was first precipitated by adding cold methanol to the toluene solution, and then filtered. Rhodamine 6G were dissolved in dichloromethane or THF/methanol, and then added into the polymer. The concentration of R6G in the polymer was in the range between 10 to 100 ppm by weight. The mixture was sonicated for several hours in warm water to fully mix the dyes with the polymer. The sample was then dried in the hood under flowing air overnight, and then placed under vacuum to remove any residual solvent. The dried sample was scraped off and transferred to a 4 mm-diameter cuvette, and heated to about 90 ˚C in the oven for 2 to 3 days to form a melt. To remove gas bubbles that were trapped inside the melt, the sample was then put under vacuum, heated to 110 ˚C for several days until it formed a homogeneous melt inside the cuvette.

Three different PCA/R6G samples were made at different times, each with different concentrations of R6G dyes. The reported literature value of T_g for PCA is about 19 ˚C, therefore substantial cooling was not required. Temperature was controlled by either a water chiller manufactured by PolyScience or a Janice ST-100 cryostat with a LakeShore temperature controller.

Photobleaching and probing

The basic principle of polarized fluorescence recovery after photobleaching (FRAP) is use high-intensity bleaching beam to purposely photobleach probe molecules that have absorption dipoles oriented along the excitation polarization, thus creating an initial anisotropy. A weaker reading beam either parallel or perpendicular to the bleaching beam is then followed to probe the orientation of the remaining molecules. As the molecules rotate, the system anisotropy decays towards zero as the ensemble becomes isotropic again[5,16,17] .

Figure 2.2 is an illustration of the setup. The excitation source is a continuous-wave 532-nm diode laser made by Power Technology. An electro-optic modulator (EOM) (commonly know as Pockels cells) manufactured by FastPulse Technology is used to modulate the beam polarization between 90˚ and 0˚ at 10 Hz frequency. The modulation frequency is controlled by a function generator (Stanford Research Systems), which outputs a square wave to a Trek voltage amplifier, and then the modulated high-voltage between 0 and 430 V is applied on the EOM. The index of refraction of the crystal inside the EOM will change when an electric field is applied, producing a phase retardation that is directly proportional to the electric field[20]. Depending on the wavelength, an appropriate voltage can be applied to achieve half-wave retardation, thus rotating the polarization of the incoming light by 90˚. A ½-wave plate is placed after the EOM to rotate the exiting beam polarization by 45˚ to produce a probing beam that is switching between ± 45˚ from vertical. Fluorescence is detected at 90˚ through a polarizer at the "magic angle" of 35.3˚ from vertical. This detection configuration allows the observation of absorption intensities proportional to the probing beam polarization[17].

Photobleaching is done by sending synchronized digital signals to pull the solenoid holding the neutral density filter (to remove the filter out of the beam path), and disable the voltage amplifier output to the EOM (to pause polarization modulation), therefore producing a high-intensity bleaching beam linearly polarized at 45˚. After a few seconds of photobleaching, another set of digital signals are sent to the solenoid to return the neutral density filter to its original location to attenuate the laser intensity, and at the same time polarization modulation starts again. By varying bleaching power and duration, different bleach depths can be achieved. Typical bleaching power ranges from 0.5 to 3.5 mW, and reading power ranges from 0.5 to 3.5 μW. Bleaching duration is

between 1 sec to 6 sec. Bleach depth is between 10% to about 40%. All fluorescence signals are collected by a single Hamamatsu photomultiplier tube (PMT), and the raw data are later sorted to separate fluorescence signals parallel ($I_{//}$) and perpendicular ($I_{\perp}$) to the bleaching polarization.

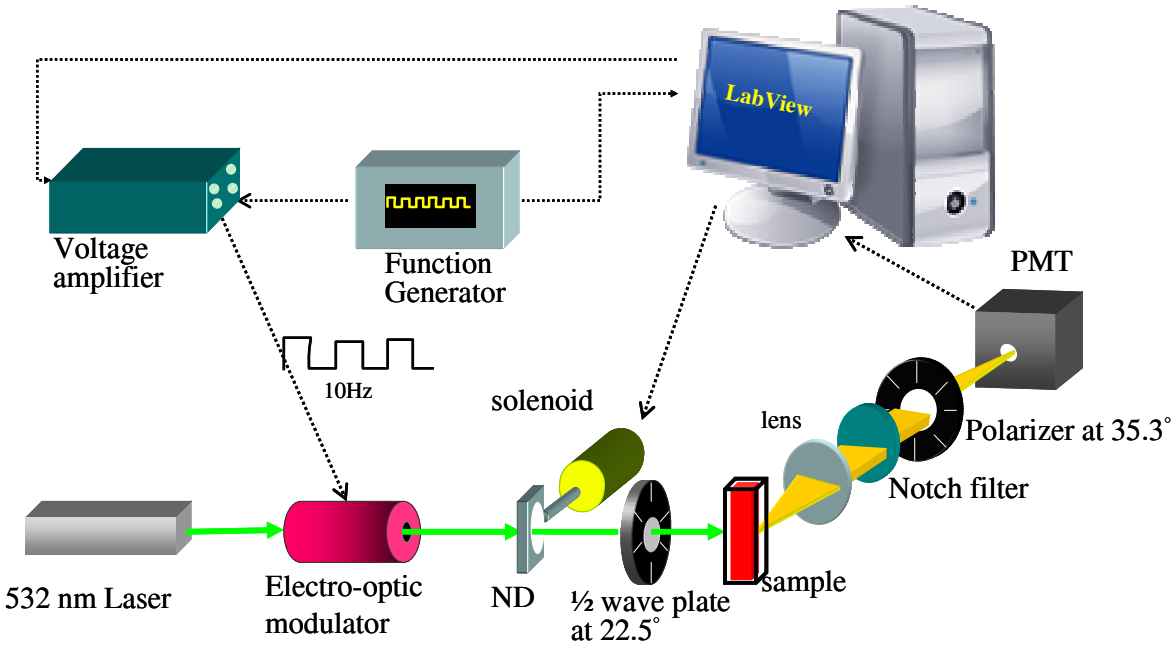

Figure 2.2: Schematic representation of ensemble FRAP setup. Laser polarization is modulated by the electro-optic modulator, whose frequency is controlled by the function generator. The solenoid holding and the neutral density filter (ND) are used to switch between high-intensity bleaching beam and low-intensity reading beam. The configuration of the ½-wave plate at 22.5˚ and detection at 90˚ angle with a polarizer at 35.3˚ allows for probing intensities of the absorption dipoles moments. Data collection and integration of all the devices are controlled by the LabVIEW program on a computer.

Instrument control

Data collection and communication between individual pieces of equipment are accomplished via a National Instruments LabVIEW Data Acquisition Card (DAQ), which is equipped with 64 channels for Digital Input/Output, Analog I/O, Counting, etc., and integrated by a LabVIEW program with a *Virtual Instrument* (VI) written specifically for the experiment. The experiment timing, such as photon-counting period, voltage monitoring, and the start/finish of photobleaching action, is controlled by the LabVIEW vi, which uses the hardware clock on the DAQ as the master timebase. Polarization modulation frequency is controlled by the function generator, and is not directly controlled by the LabVIEW VI. Since the function generator is not equipped with an input port for receiving a start trigger from LabVIEW DAQ, it is used instead to trigger the master timing of LabVIEW, and therefore polarization modulation can be synchronized with the rest of the instrument.

See Appendix A for the LabVIEW FRAP.vi.

Data Analysis Procedure

All fluorescence photons are collected by the same photomultiplier tube as a single wave of data points. In order to separate the signals that have polarizations parallel ($I_{//}$) and perpendicular ($I_{\perp}$) to the bleaching polarization, the exact switching time of the EOM must be known. There is a monitor channel on the voltage amplifier which generates a monitor voltage that is 1/200 the amplified voltage output. Therefore this monitor voltage is recorded simultaneously with the photon counts from the PMT. In other words, when the voltage is high, EOM is on, and the beam is +45˚ polarized; when the voltage is nil, EOM is off, and the beam is −45˚ polarized. As mentioned in the

experimental section, during photobleaching, the voltage amplifier output is disabled, i.e. the EOM is off and thus the bleaching beam is -45° polarized. In such case, signals that are collected when the reading beam is -45° polarized are designated as $I_{//}$, and $+45^\circ$ as $I_\perp$.

The only data that are collected are photon counts and monitor voltage. Using the monitor voltage as the reference, the raw data for photon counts can be sorted into $I_{//}^{0}, I_{\perp}^{0}$ for initial signals *before* photobleaching and $I'_{//}, I'_{\perp}$ for signals *after* photobleaching. Therefore, anisotropy can be calculated as:

$$r(t) = \frac{(I'_{//} - I^0_{//}) - (I'_{\perp} - I^0_{\perp})}{(I'_{//} - I^0_{//}) + 2(I'_{\perp} - I^0_{\perp})} = \frac{\Delta I_{//} - \Delta I_{\perp}}{\Delta I_{//} + 2\Delta I_{\perp}} \tag{2.1}$$

Data analysis is carried out using IGOR software. See Appendix A for complete procedure codes.

RESULTS AND DISCUSSION

Analysis of anisotropy relaxation

Figure 2.3 to 2.6 are examples of the aforementioned data analysis results. Fig. 2.3 shows the initial fluorescence signals before photobleaching, $I^0_{//}$ and $I^0_{\perp}$. The system is originally isotropic, therefore both polarizations have the same intensities. Fig. 2.4 is the fluorescence signals after photobleaching, $I'_{//}$ and $I'_{\perp}$. Immediately after photobleaching, $I'_{//}$ is smaller than $I'_{\perp}$, because molecules oriented parallel to the bleaching polarization have been depleted most effectively. As the remaining molecules rotate, the system returns to an isotropic configuration, and the two signals have the same

intensity. Note there is residual photobleaching occurring even when the low-intensity reading beam is used. However, now bleaching takes place on both polarizations, thus both intensities decrease gradually at the same rate. To illustrate more clearly how fluorescence signals in either polarizations change as the molecules reorient, in Fig. 2.5 the signal differences between *before* and *after* photobleaching, $\Delta I_{//}$ and $\Delta I_{\perp}$ are normalized to the total intensity, $(\Delta I_{//} + 2\Delta I_{\perp})$. $\Delta I_{//}$ decreases while $\Delta I_{\perp}$ increases, and eventually they are equal when the system is randomly distributed again.

Anisotropy can now be calculated using Eq. 2.1, and the result is shown in Fig. 2.6, with the fit to the stretched exponential function:

$$r(t) = A \exp[\, -(t/\tau)^{\beta}\,] \tag{2.2}$$

where A is the amplitude of the decay, τ is the decay time, and β is the stretching exponent: $\beta = 1$ for a single exponential decay, $\beta \neq 1$ for a nonexponential decay.

For the data shown in Fig. 2.7, the fit yields $\beta = 0.58$, $\tau = 95.82$ sec. The anisotropy relaxations are nonexponential decays in all our measurements: β is about 0.5 to 0.6, and is never close to 1. Table 2.1 shows the fitting results of decay times as a function of temperature for PCA sample #1. Temperature was controlled by the water chiller. Rotational dynamics become slower as temperature is lowered, and this trend can be better seen as plotted in Figure 2.7.

Same experiments were carried out for PCA sample #2 and #3, using the cryostat for temperature control. The results for PCA sample #2 are tabulated in Table 2.2 and plotted in Fig. 2.8; the results for PCA sample #3 are tabulated in Table 2.3 and plotted in Fig. 2.9.

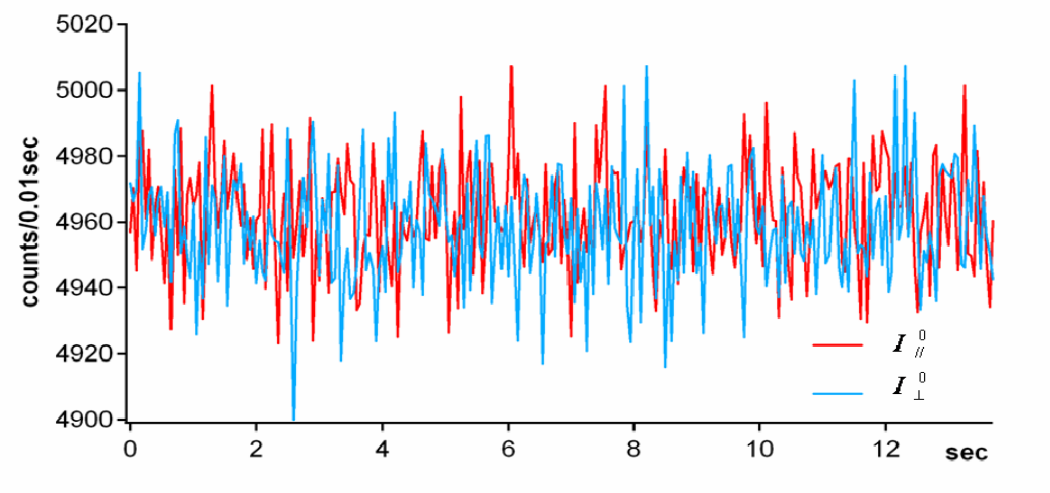

Figure 2.3: Fluorescence signals before photobleaching.

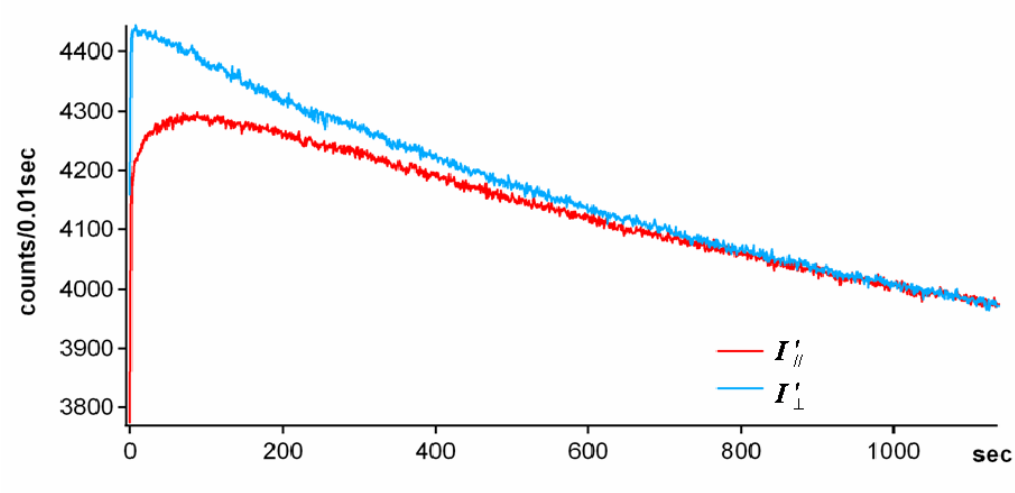

Figure 2.4: Fluorescence signals after photobleaching.

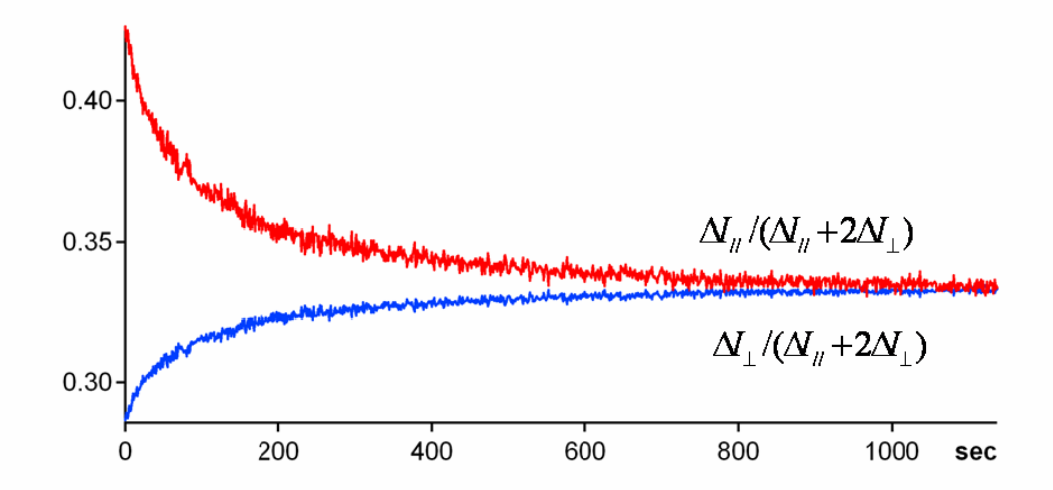

Figure 2.5: Normalized delta-signals after photobleaching.

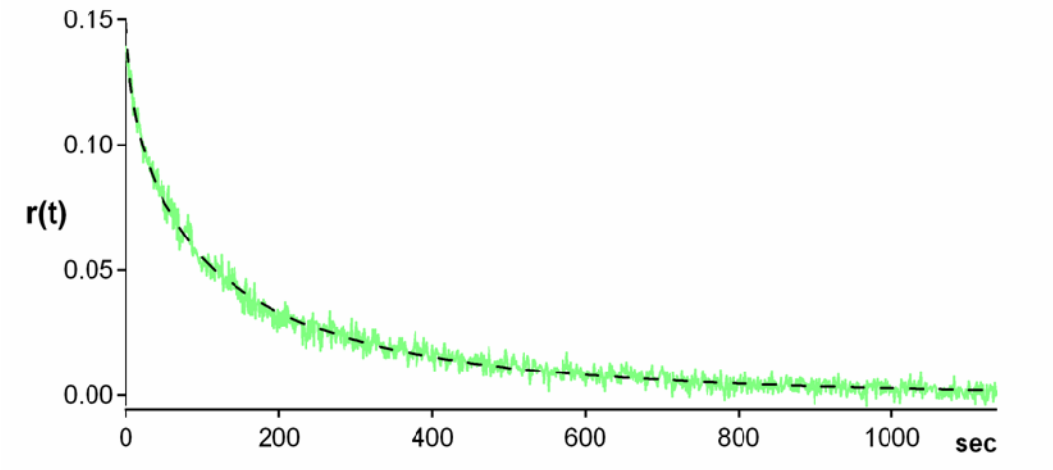

Figure 2.6: Anisotropy decay, $r(t)$, and the fit to the stretched exponential function (dashed line), giving: $\beta = 0.58$, $\tau = 95.82$ sec.

Temperature (˚C)	τ_{fit} (sec)	β_{fit}
20.0	212.121 ± 21.726	0.568 ± 0.033
21.3	124.005 ± 31.471	0.5223 ± 0.050
21.8	113.548 ± 24.470	0.571 ± 0.017
22.0	113.508 ± 10.579	0.522 ± 0.067
23.0	69.625 ± 3.840	0.551 ± 0.030
27.6	9.163 ± 3.082	0.462 ± 0.094
28.2	10.452 ± 1.051	0.545 ± 0.044
28.6	8.909 ± 1.589	0.522 ± 0.051
29.5	5.123 ± 0.963	0.511 ± 0.034
32.0	3.471 ± 0.727	0.533 ± 0.024

Table 2.1: Anisotropy decay measurements for PCA sample #1 at various temperatures.

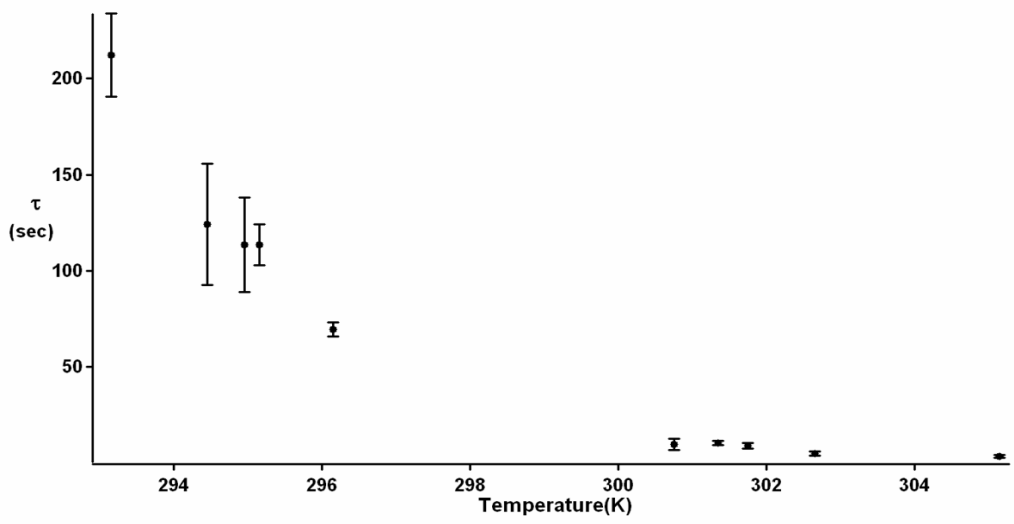

Figure 2.7: Relaxation time vs temperature for PCA sample #1.

Temperature (˚C)	τ_{fit} (sec)	β_{fit}
14.0	277.414 ± 27.470	0.689 ± 0.026
15.0	216.654 ± 32.870	0.640 ± 0.032
16.0	160.785 ± 12.809	0.612 ± 0.017
17.0	116.36 ± 18.646	0.616 ± 0.025
18.0	89.282 ± 7.012	0.615 ± 0.020
19.0	69.712 ± 7.125	0.663 ± 0.074
21.0	30.137 ± 2.903	0.628 ± 0.094
22.0	20.775 ± 1.325	0.623 ± 0.041
25.0	8.459 ± 1.270	0.628 ± 0.051
27.0	4.937 ± 1.611	0.633 ± 0.132

Table 2.2: Anisotropy decay measurements for PCA sample #2 at various temperatures.

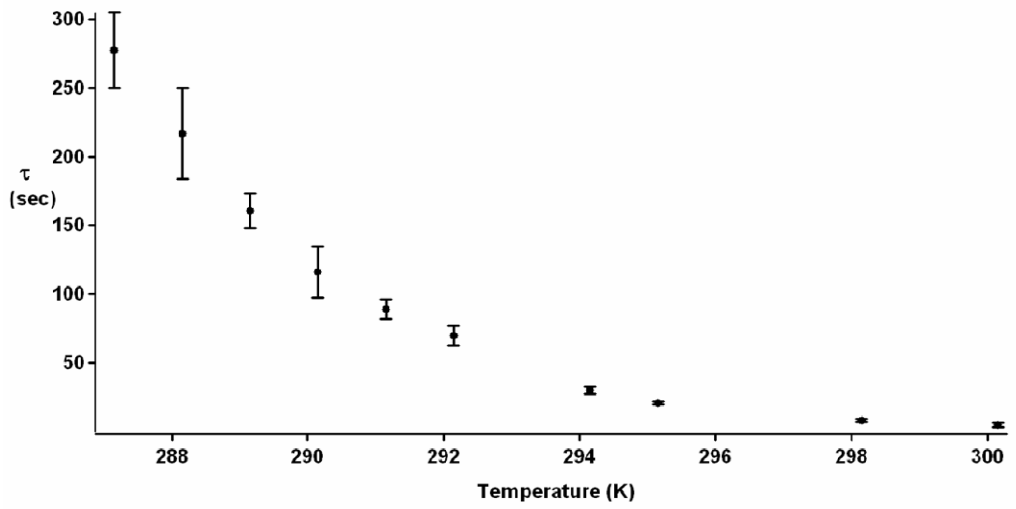

Figure 2.8: Relaxation time vs temperature for PCA sample #2.

Temperature (˚C)	τ_{fit} (sec)	β_{fit}
25.0	495.416 ± 81.922	0.679 ± 0.024
28.0	157.013 ± 11.443	0.546 ± 0.047
30.0	90.603 ± 4.057	0.587 ± 0.070
32.0	40.148 ± 4.589	0.595 ± 0.080
34.0	17.985 ± 1.421	0.461 ± 0.030
36.0	8.952 ± 0.686	0.417 ± 0.032
38.0	5.391 ± 1.876	0.417 ± 0.063

Table 2.3: Anisotropy decay measurements for PCA sample #3 at various temperatures.

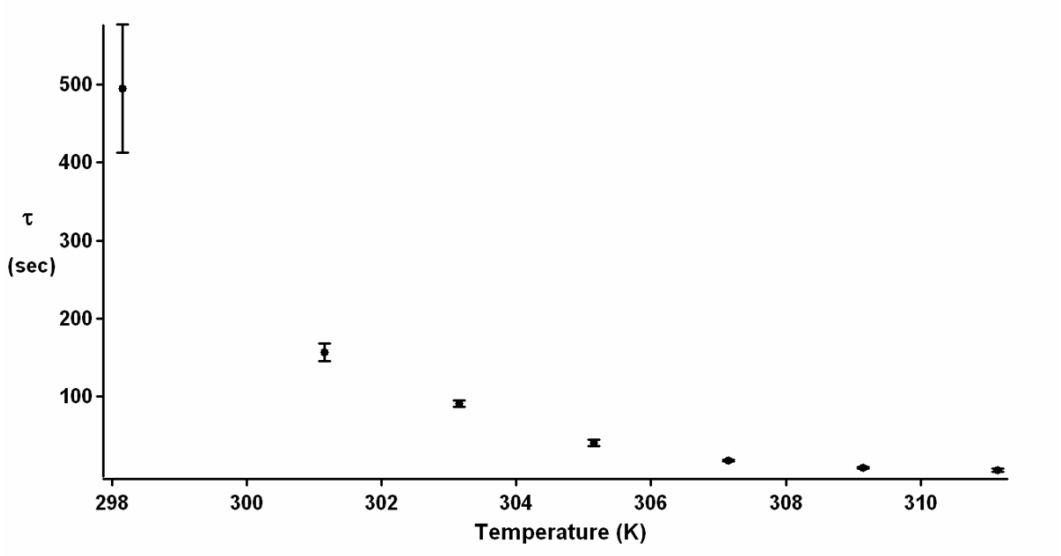

Figure 2.9: Relaxation time vs temperature for PCA sample #3.

From these results, it can be seen that the anisotropy decays for PCA are nonexponential with fitted values $\beta << 1$, and that the rotational timescale slows down dramatically near T_g. It is generally conceived that $\beta < 1$ suggests heterogeneous dynamics in the system. The magnitude of β is often used to describe the degree of heterogeneity: the smaller the β, the more heterogeneous the system. From this perspective, it should be expected that β would be small at low temperatures, and become closer to 1 at higher temperatures. This correlation between magnitude of β and temperature was not observed in our experiments, although the values of β are ~ 0.5 and 0.6.

In addition, past studies by Cicerone *et al.*[21] have shown a strong dependence of observed correlation time on the bleach depth in supercooled ortho-terphenyl (OTP). The relationship that τ increases greatly with bleach depth is contributed to faster molecules being bleached more easily, thus the interpretation is that this condition results in a wide distribution of relaxation times that is evidence for spatially heterogeneous dynamics in OTP. However, in our FRAP experiments, such a relationship between τ and bleach depth was not observed.

At higher temperatures when dynamics are faster, it becomes difficult to create deep anisotropy, i.e., the decay measured has a smaller initial anisotropy value. This is the result of molecules reorienting during bleaching period, and thus when the bleaching beam is switched to reading beam, anisotropy has already decayed. Due to the time resolution of experimental setup (polarization modulation at 10 Hz and data acquisition at 100 Hz), when relaxations are on the timescale of only a few seconds, signals become noisy and the small initial anisotropy amplitude makes it difficult to fit to the stretched exponential.

Temperature dependence of relaxation time

The measured parameter τ corresponds to the averaged rotation time for the unbleached R6G molecules in PCA. Probe dynamics are very sensitive to their local environments, therefore they serve as reporters of the surrounding polymer structure. To validate our data, we fit the results to the semi-empirical Williams-Landel-Ferry equation (WLF), where A, C_1 and C_2 are empirical coefficients:

$$\log(\tau) = A - \frac{C_1 \times (T - T_g)}{(C_2 + T - T_g)} \tag{2.3}$$

The WLF equation is mathematically equivalent to the frequently applied Vogel-Fulcher equation and many other empirical equations that are used to describe viscosities and relaxations in polymers. This equation implies that rotational dynamics become orders of magnitude slower as temperature approaches T_g, and there is a temperature C_2 at which the dynamics diverge[3]. The fact that our experiment results can be fit by the WLF equation confirms that polymer relaxations are indeed measured, and that rotation of probe molecules is dependent on the dynamics of the polymer.

The fitting to the WLF equation for three PCA/R6G samples are plotted together in Figure 2.10. There is a linear temperature shift among these three samples, and from fitting to the WLF equation, we obtained T_g = 19 ˚C for sample #1, T_g = 15 ˚C for sample #2, and T_g = 26 ˚C for sample #3. This difference may be due to the individual sample history as the result of preparation procedure and the time it has been exposed to the ambient environment. Alternatively, there may be impurities in the sample that have reacted with the polymer and altered its structure. Trace amount of solvent trapped inside the polymer melt may also result in faster dynamics.

Even though the same preparation procedure was followed, the conditions varied slightly. For example, one sample annealed in the cuvette under vacuum at 110 ˚C in just three days, but the others required more than one week. Mechanical stress created by the glass cuvette may also have affected the polymer structure. Nevertheless, the WLF trend can be used to compare rotational times at temperatures relative to each sample's T_g. For example, at T_g + 2 ˚C, the measured rotational time is 124.01 sec for PCA sample #1 (T_g = 19 ˚C), 116.36 sec for PCA sample #2 (T_g = 15 ˚C), and 157.01 sec for PCA sample #3 (T_g = 26 ˚C). It is evident that the rotational times measured have the same order of magnitude at T_g + 2 ˚C across different samples, and it also shows that polymer dynamic measurements are not affected by the concentration of the probes.

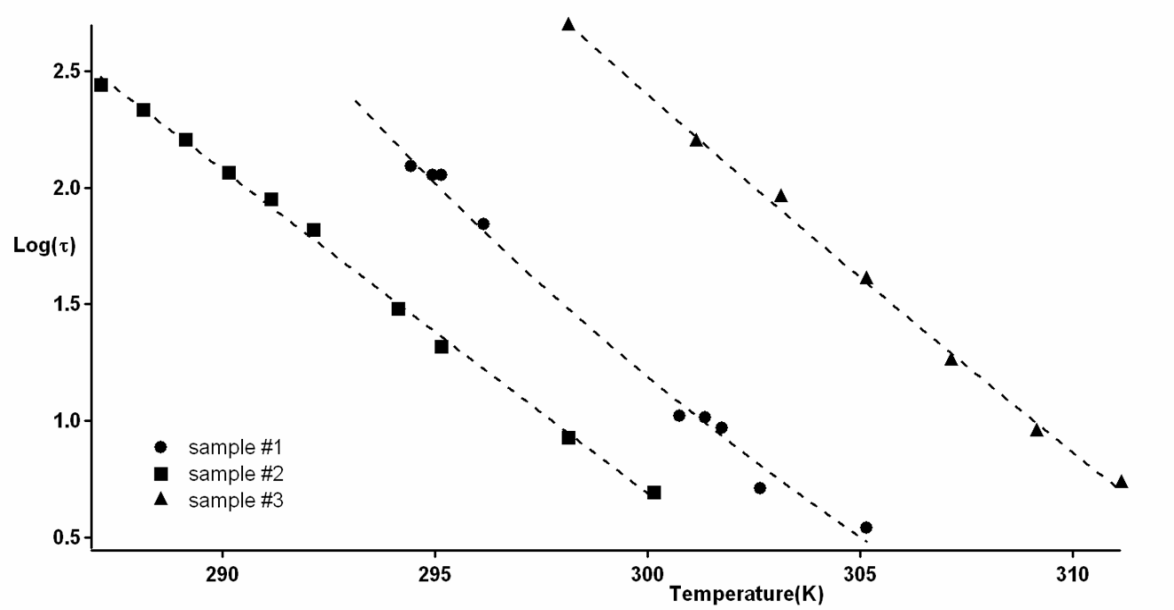

Figure 2.10: Temperature dependence of relaxation times for three PCA samples. The dashed line is the fit to the WLF equation. T_g values determined from fitting data to the WLF equation are: T_g = 19 ˚C for sample #1, 15 ˚C for sample #2, and 26 ˚C for sample #3. WLF equation is expressed as: $\log(\tau) = A - \frac{C_1 \times (T - T_g)}{(C_2 + T - T_g)}$.

Technical notes on the experimental setup

The first version of the experimental setup was to use film samples because it is a simpler way to prepare samples in terms of doping dyes into the polymer and removal of the solvent. In order to detect fluorescence signals from a film, 45˚ detection geometry was employed. A simple schematic representation of this setup is shown in Figure 2.11.

There were several problems encountered with this setup. First it was difficult to align the optics along the 45˚ collection beam path. According to Wegener[17], when the excitation polarization is vertically (or horizontally) polarized, detecting at 45˚ through a magic angle of 54.7˚ from vertical will result in observed fluorescence intensities that are proportional to the vertical (or horizontal) absorption dipole moments. In other words, when probing an isotropic system, the two orthogonal signals should be the same with this configuration. However, we were never able to obtain equal signals at this magic angle of 54.7˚ (or any other angle). The relative intensity of horizontal and vertical signals also varied with different polymer films, i.e. it was very sensitive to the morphology and thickness of the film. This made it even more difficult to reproduce the results. In addition, with such configuration, a cryostat cannot be used to control the temperature because the cryostat has a rectangular chamber with four glass windows on each side, which is not designed for 45˚ detection. When cooling the sample film in ambient atmosphere, there was substantial amount of water condensation on the cover slip, which might have affected the index of refraction of the sample and the polarization of detected fluoresce signals.

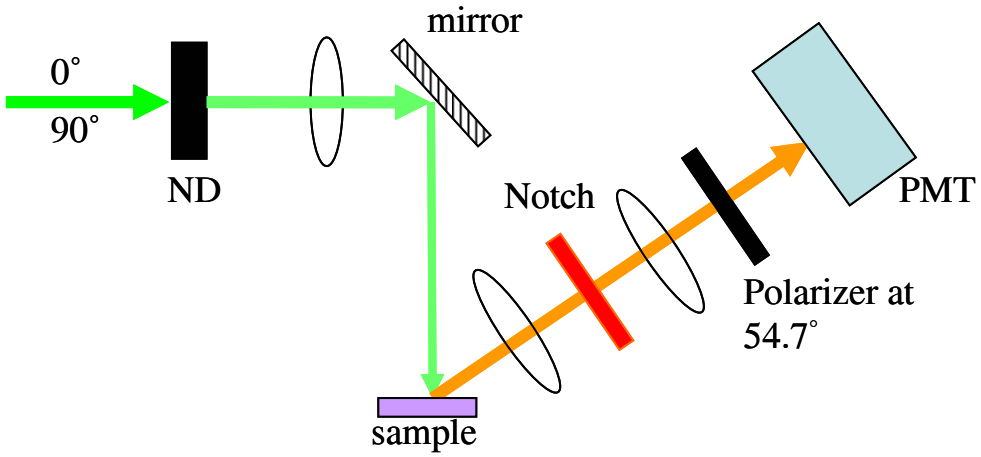

Figure 2.11: Illustration of the 45° detection configuration for a film sample. The probing beam polarization is modulated between 0° and 90°, and fluorescence signals are detected through a polarizer set at the magic angle of 54.7°.

The modified version of the experiment was to replace the film sample and employ a 90° detection scheme. It was very similar to Fig. 2.11, except that a cuvette was in place of the film and fluorescence signals were detected at 90° direction. For this geometry, the excitation light has to be ± 45° polarized and the detection magic angle is 35.3° from vertical. A ½-wave plate was placed after the EOM at 22.5° to rotate the beam by 45°. However, fluorescence signals from both probing polarizations were still not the same when the sample was isotropic. It was later discovered that the dielectric mirror, which was used to direct the beam onto the sample, actually changed the polarization of the excitation beam, which was no longer ± 45° after it was reflected off the dielectric mirror. Therefore the setup was rearranged again to remove unnecessary mirrors, and finally became what is shown in Figure 2.2. It should also be mentioned that the ½-wave plate has great impact on this experimental configuration, i.e., the ratio

of the observed orthogonal signals changes substantially when the ½-wave plate angle is slightly adjusted.

The limitation of this FRAP experiment is the time resolution, i.e. only slow dynamics can be probed due to polarization modulation frequency and data acquisition rate. The EOM seems to have a slow response time to the applied voltage and therefore with a modulation frequency faster than 10 Hz, the output beam is somewhere between the desired polarizations. The solenoid-ND filter mechanism is also a limitation factor. It takes roughly 0.2 sec to completely remove the filter out of the beam path or put it back, thus the first 0.2 sec of data right after photobleaching are omitted during data analysis. In general, rotational dynamics on the order of few seconds is the fastest timescale that this setup can measure.

CONCLUSIONS

Rotational dynamics of poly(cyclohexyl acrylate) were studied by probing the reorientation rate of the embedded fluorescent probe molecules. The results yield nonexponential decays for PCA anisotropy relaxations, with β values around 0.5 to 0.6 when fit to the stretched exponential function. This suggests that the dynamics are inhomogeneous. The observed PCA relaxation times follow the temperature-dependence described by the Williams-Landel-Ferry (WLF) equation, confirming that the primary relaxation dynamics of the polymer are indeed measured. The relaxation time at T_g + 2 $^{\circ}$C is on the order of 100 sec. In addition, our results also show that probe dynamics are in fact dependent on its surrounding polymer matrix, and therefore the use of fluorescent dyes as reporters of non-fluorescent systems is validated.

REFERENCES

(1) Ediger, M. D.; Angell, C. A.; Nagel, S. R. *J. Phys. Chem.* **1996**, *100*, 13200.

(2) Phillips, J. C. *Rep. Prog. Phys.* **1996**, *59*, 1133.

(3) Angell, C.A.; Ngai, K.L.; McKenna, G. B.; McMillan, P. F.; Martin, S. W. *J. Appl. Phys.* **2000**, *88*, 3113.

(4) Schmidt-Rohr, K.; Spiess, H. W. *Phys. Rev. Lett.* **1991**, *66*, 3020.

(5) Cicerone, M. T.; Ediger, M. D. *J. Phys. Chem.* **1993**, *97*, 10489.

(6) Stickel, F.; Fischer, E. W.; Richert, R. *J. Chem. Phys.* **1995**, *102*, 6251.

(7) Wang, C.-Y.; Ediger, M. D. *J. Phys. Chem. B* **1999**, *103*, 4177.

(8) Böhmer, R.; Diezemann, G.; Hinze, G.; Rössler, E. *Prog. Nucl. Magn. Reson. Spectrosc.* **2001**, *39*, 191.

(9) Cicerone, M. T.; Blackburn, F. R.; Ediger, M. D. *Macromolecules* **1995**, *28*, 8224.

(10) Böhmer, R.; Chamberlin, R. V.; Diezemann, G.; Geil, B.; Heuer, A.; Hinze, G.; Kuebler, S. C.; Richert, R.; Schiener, B.; Sillescu, H.; Spiess, H. W.; Tracht, U.; Wilhelm, M. *J. Non-Crys. Solids* **1998**, *235-237*, 1.

(11) Sillescu, H. *J. Non-Crys. Solids* **1999**, *243*, 81.

(12) Ediger, M. D. *Ann. Rev. Phys. Chem.* **2000**, *51*, 99.

(13) Deschenes, L. A. *Single-molecule studies of heterogeneous dynamics near the glass transition*, The University of Texas at Austin, 2002.

(14) Richert, R. *J. Phys.: Condens. Matter* **2002**, *14*, R703.

(15) Russell, E. V.; Israeloff, N. E. *Nature* **2000**, *408*, 695.

(16) Velez, M.; Axelrod, D. *Biophys. J.* **1988**, *53*, 575.

(17) Wegener, W. A. *Biophys. J.* **1984**, *46*, 795.

(18) Williams, M. L.; Landel, R. F.; Ferry, J. D. *J. Am. Chem. Soc.* **1955**, *77*, 3701.

(19) Matsuoka, S. *J. Rheology* **1986**, *30*, 869.

(20) Goldstein, R. *Lasers & Applications* **1986**, *Lasermetrics Technical Notes*

(21) Cicerone, M. T.; Ediger, M. D. *J. Chem. Phys.* **1995**, *103*, 5684.

Chapter 3: Origins of Nonexponential Decay in Single-Molecule Measurements of Rotational Dynamics

INTRODUCTION

Single-molecule spectroscopy is an excellent tool for probing molecular motions in heterogeneous materials, where the dynamics of individual environments are normally obscured in ensemble measurements. Single molecule rotational motion has proven to be a particularly accessible and useful reporter of dynamics in a variety of systems including liquids[1,2], polymer films[3], and biological systems[4]. The rotational motion of an individual molecule can be tracked by analyzing the polarization of a fluorescence signal. The dynamics can be analyzed from the correlation of the fluctuating polarization signal. To best compare to ensemble measurements of reorientation dynamics (fluorescence anisotropy[5,6], NMR[7], etc.), it would be ideal to measure the full three-dimensional orientation of the molecule, and to evaluate the same correlation that is measured in the ensemble experiments. While there are several schemes to measure the three-dimensional orientation of single molecules[8-10], these techniques typically require many photons to determine the orientation, thus limiting the length of the transient that can be collected. Since long trajectories are required to obtain useful correlations for the systems of interest, most experiments have simply measured the in-plane projection of the fluorescence. This dichroism signal is measured by detecting any two orthogonal polarizations in the plane of the sample, taking the difference in these two signals divided by their sum. The rotational dynamics of individual trajectories can then be quantified by correlating the dichroism.

This approach has been used to elucidate heterogeneous dynamics[11] in super-cooled liquids and in polymers near their glass transition[1]. These results show that the single molecule correlation functions calculated based on the reduced linear dichroism signals are single exponentials for short observation times and evolve into nonexponential decays at longer observation times. These results have been interpreted as indicative of purely diffusive dynamics at shorter times, while the molecule resided in one unique environment, with longer times reflecting sampling of multiple distinct environments. The implication is that the nonexponential relaxation seen in ensemble experiments is solely the result of ensemble averaging over many molecular environments, each of which has its own exponential relaxation. This interpretation was called into question by Hinze *et al.*[12] by performing a detailed formal analysis to show that the correlation of the reduced linear dichroism signal for a single molecule should not be a simple single exponential even for a homogeneous system with an isotropic diffusion tensor.

The earlier interpretation[1] as heterogeneous dynamics can be reconciled with this formal analysis[12] if one takes proper account of the impact of a high-numerical aperture (NA) objective. When this effect is included, a single exponential decay is recovered in the measurement, for the case of isotropic rotational diffusion. Moreover, the measured result will be equivalent to that measured in the ensemble rotational anisotropy experiment[6].

THEORETICAL ANALYSIS OF SINGLE MOLECULE AUTO-CORRELATION FUNCTIONS

The measure of a transition dipole orientation is usually represented with the reduced linear dichroism:

$$A(t) = \frac{I_s(t) - I_p(t)}{I_s(t) + I_p(t)} \tag{3.1}$$

where I_s and I_p are orthogonal polarizations of the fluorescence signal perpendicular to the objective. A schematic representation of the experimental arrangement, defining the azimuthal angle Φ and polar angle Θ, is shown in Figure 3.1.

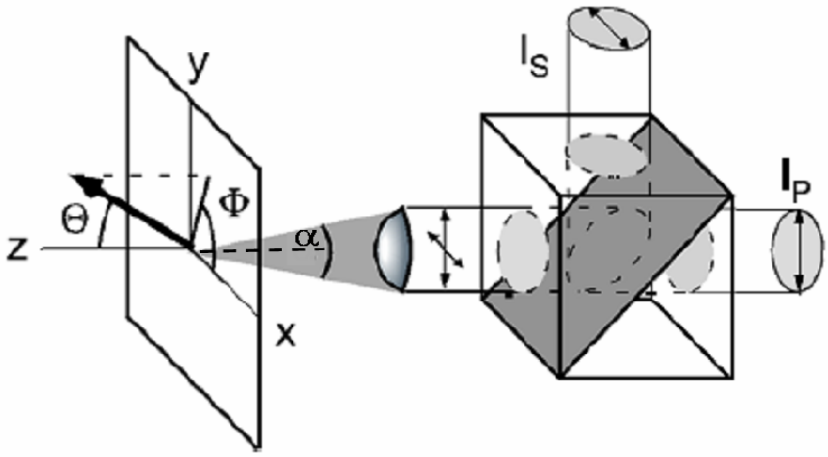

Figure 3.1: Schematic representation of fluorescence polarization measurement. The orientation of the dipole is prescribed by angles Φ and Θ. Z is the objective axis, α is the angle of collection. Is and Ip are orthogonal polarization components of the fluorescence signal separated by the cube beam splitter.

Assuming a plane wave emission polarized along the molecular transition dipole moment, the signals I_s and I_p are proportional to the projections of the transition moment onto the two polarization directions being measured. In the case where NA = 0, it is readily shown that the raw dichroism signal $A(t)_{raw}$ is given by:

$$A(t)_{raw} = \cos(2\Phi) \tag{3.2}$$

The only effect of the polar angle Θ on the fluorescence is that the total intensity will drop as the molecule tips out of the plane of the sample. However, this analysis fails to take into account the dipolar nature of the emission source which is critical if a large cone of the radiation is collected.

The cone of light collected by a lens is given by the NA for the collecting objective, such that the collection angle α is given by:

$$\alpha = \sin^{-1}(NA/n) \tag{3.3}$$

where n is the index of refraction of the medium. It has been shown that, when using high NA optics, even when the transition dipole is aligned along the Z axis, the dipole nature of the emission leads to collection of radiated fluorescence[8-10]. The Z component of the emission appears isotropic in the plane of the sample, contributing equally to I_s and I_p. This will clearly lead to a skewed measurement of Φ, as evident from Equation 3.2. Following Fourkas[8], the signals I_s and I_p can be related to the transition dipole orientation and the NA. The fluorescence signals that would be seen on the detectors are given by:

$$I_s(\Theta,\Phi) = I_{tot}(A + B\sin^2\Theta + C\sin^2\Theta\cos 2\Phi) \tag{3.4}$$

$$I_p(\Theta,\Phi) = I_{tot}(A + B\sin^2\Theta - C\sin^2\Theta\cos 2\Phi) \tag{3.5}$$

where A, B, and C are constants readily evaluated in terms of α. For example, for n = 1.4, with high NA of 1.2, α = 1.0297, giving A = 0.04928, B = 0.04730, C = 0.09421. In the lower NA limit, e.g. NA = 0.2, α = 0.14335, giving A = 0.00003, B = 0.00252, C = 0.00255. Taking into account these effects of the high-NA optics gives a very different reduced linear dichroism signal:

$$A(t)_{corrected} = \frac{I_s(\Theta,\Phi) - I_p(\Theta,\Phi)}{I_s(\Theta,\Phi) + I_p(\Theta,\Phi)} = \frac{C\sin^2\Theta\cos 2\Phi}{A + B\sin^2\Theta} \tag{3.6}$$

As NA approaches the limit of zero, $A \sim 0, B \cong C$, and the above dichroism signal becomes identical to Eq. 3.2. The correlation function for this corrected dichroism signal, or any other function of the angular coordinates, can be calculated following Hinze *et al.*[12], and Berne and Pecora[13]. The correlation function for the case of isotropic diffusion can be shown to be a sum of correlation functions:

$$C(t) = \sum_l a_l C_l(t) \tag{3.7}$$

with prefactors a_l corresponding to each of the harmonics. The individual $C_l(t)$ are given by:

$$C_l(t) = e^{-l(l+1)Dt} \tag{3.8}$$

where l labels a Legendre polynomial P_l, and D is the rotational diffusion constant.

For ensemble anisotropy experiments, the dipole-dipole correlation function can be expressed exactly in terms of only P_2, and the measured decay behaves as:

$$C_2 \sim \exp(-6Dt) \tag{3.9}$$

A critical consequence of Eq. 3.6, evident immediately from an expansion of the denominator, is that the correlation functions of the corrected and raw dichroism signals cannot be expressed in this simple form. In general, the coefficients a_l are given by the projections:

$$a_l = \frac{1}{4\pi}\sum_m \left| \int_0^{2\pi} d\Phi \int_0^{\pi} d\Theta \sin\Theta \; X(\Theta,\Phi)\, Y_{l,m}(\Theta,\Phi) \right|^2 \tag{3.10}$$

where $X(\Theta, \Phi)$ is the function of interest, and $Y_{l,m}(\Theta, \Phi)$ are the spherical harmonic functions[12]. Based on symmetry, only even l will be non-zero here.

EFFECTS OF HIGH NUMERICAL APERTURE ON CORRELATION FUNCTIONS

As noted earlier, Hinze *et al.*[12] showed, for the idealized case of zero-NA [Eq. 3.2], that the correlation function deviated significantly from a single exponential. To best compare to experiments, they fit their results to a stretched exponential function, $f(t) = e^{-(t/\tau)^{\beta}}$, with a best fit yielding $\beta = 0.871$.

Here, we take into account the effects of the numerical aperture on the collected dichroism signals. The prefactors for $l = 0 - 20$ are calculated numerically for a variety of numerical apertures by substituting the expression for the dichroism from Eq. 3.6 as the function $X(\Theta, \Phi)$ in Eq. 3.10, giving:

$$a_l = \frac{1}{4\pi}\sum_m \left| \int_0^{2\pi} d\Phi \int_0^{\pi} d\Theta \sin\Theta \, \frac{C\sin^2\Theta\cos 2\Phi}{A + B\sin^2\Theta} Y_{l,m}(\Theta,\Phi) \right|^2 \tag{3.11}$$

The index of refraction is assigned as 1.4. The calculated a_l are normalized and tabulated in Table 3.1, including the results corresponding to Hinze *et al.*[12] (i.e., NA = 0) for comparison.

NA / l	0	0.6	1.2
a_2	0.835013	0.921797	0.989387
a_4	0.100205	0.065315	0.010403
a_6	0.031014	0.010248	0.000205
a_8	0.013520	0.002043	$4.75313*10^{-6}$
a_{10}	0.007084	$4.54623*10^{-4}$	$1.17983*10^{-7}$
a_{12}	0.004171	$1.07522*10^{-4}$	$3.03458*10^{-9}$
a_{14}	0.002661	$2.63960*10^{-5}$	$7.96989*10^{-11}$
a_{16}	0.001801	$6.64136*10^{-6}$	$2.12247*10^{-12}$
a_{18}	0.001275	$1.69978*10^{-6}$	$5.62535*10^{-14}$
a_{20}	0.000936	$4.40450*10^{-7}$	$4.30060*10^{-16}$

Table 3.1: The numerical results for prefactors a_l from $l = 2$ to $l = 20$, calculated from Eq. 3.9, for NA = 0.6 and NA = 1.2. Column NA = 0 represents a_l values from Hinze *et al.*[12]

To illustrate more clearly the effects of NA on a_l terms, the results are also plotted, as shown in Figure 3.2. When the angular averaging effects implicit in collection with high NA are included, the higher order terms clearly rapidly decrease in importance, and a_2 increasingly dominates (note the logarithmic scale). Furthermore, these higher harmonic angular terms have inherently faster decays [see Eq. 3.8]. As a result, by NA ~ 0.6, the decay is virtually indistinguishable from a single exponential decay, characteristic of $l = 2$. It is precisely the $l = 2$ correlation function that is measured in a bulk fluorescence anisotropy experiment.

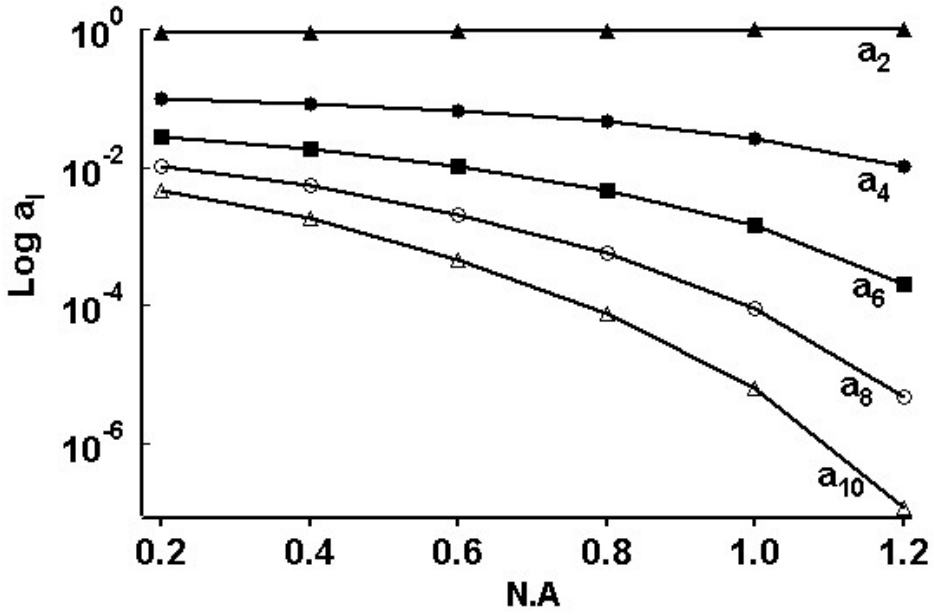

Figure 3.2: Numerical values of a_l, as a function of NA. As NA increases, a_2 dominates, and all higher-order a_l decrease rapidly. The limiting values for NA = 0 (see Table 3.1) are quite similar to the values at NA = 0.2.

SIMULATION OF SINGLE MOLECULE ROTATIONAL TRAJECTORIES

To gain further understanding of these analytical results and to test the effects of noise, single molecule rotational trajectories were simulated using a random walk on a sphere. The angular trajectories (Θ, Φ) were then used to compute fluorescence signals. To calculate the corrected dichroism signal, we use Eq. 3.4 and Eq. 3.5 to obtain $I_s(t)$ and $I_p(t)$, which were then augmented with a background and shot noise comparable to realistic single molecule data[14]. $A_{corrected}(t)$ was then calculated using Equation 3.6. For the raw data (NA = 0), $I_s(t)$ and $I_p(t)$ were taken to be simply $\cos^2(\Phi)$ and $\sin^2(\Phi)$. $A_{raw}(t)$ was then calculated using Equation 3.2.

The effect of the polarization on dichroism can be easily seen in a histogram of values. Figure 3.3 shows the distribution of $A_{raw}(t)$ and $A_{corrected}(t)$ along with a histogram of typical single molecule data of Rhodamine 6G in poly(methyl acrylate)[14]. The raw histogram simply gives the distribution of the cosine function, which is strongly peaked at $A(t) = \pm 1$. In contrast, both the corrected $A(t)$ and the experimental data are peaked at $A(t) = 0$, and have a vanishing amplitude for a magnitude larger than 0.8. For the dichroism to attain the values ± 1, one of the detectors needs to have a signal of zero, which cannot occur for finite NA. This effect is enhanced with increasing NA and also as the molecule tilts out of plane. As a result, the most probable observation becomes detection of equal signals on each detector, giving a most probable dichroism of zero.

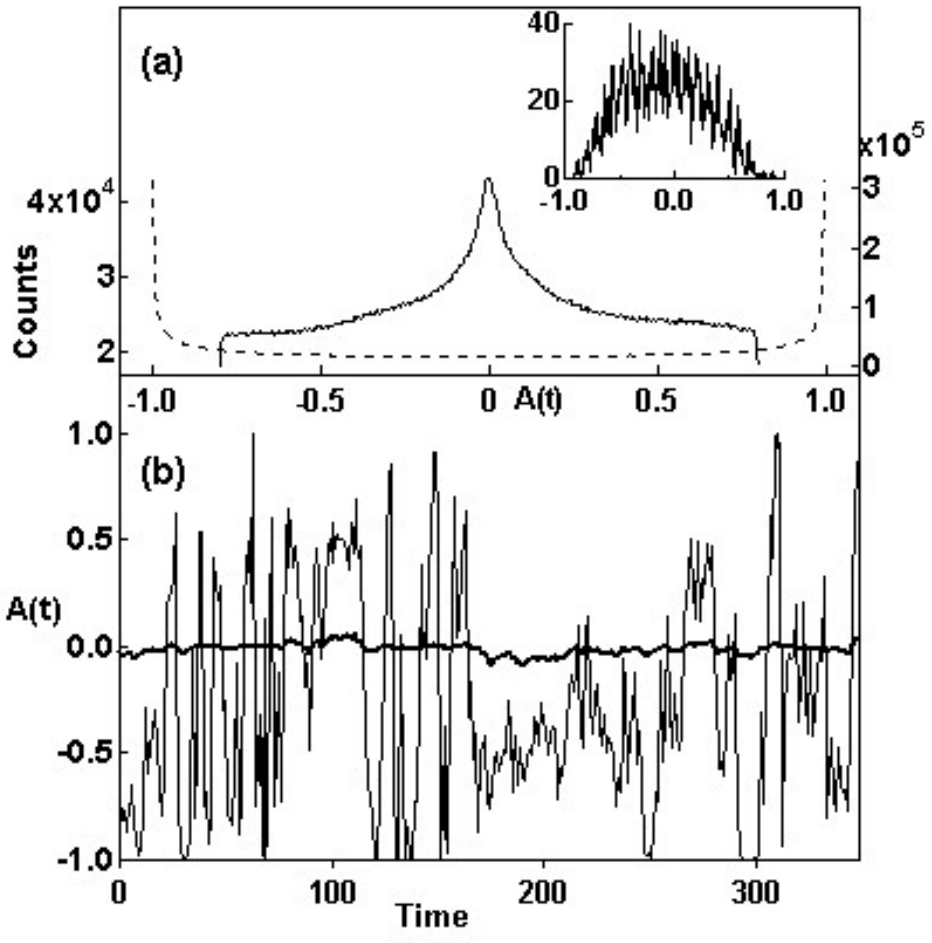

Figure 3.3: Dichroism signals from random walk simulation of isotropic diffusion. (a) Histogram of $A_{raw}(t)$ (NA = 0) (- - -) and $A_{corrected}(t)$ (NA = 1.25) (–). Inset: Histogram of measured dichrosim signal for Rhodamine 6G in poly(methyl acrylate) at room temperature (NA = 1.25)[14], showing the same pattern as $A_{corrected}(t)$. (b)Time history of $A_{raw}(t)$ and $A_{corrected}(t)$ for a segment near where $\Theta(t) \sim 0$. Note that $A_{corrected}(t) \sim 0$ at all times. Time in arbitrary units.

Correlation functions $C(t)$ for the raw and corrected data, for NA = 1.2, are shown in Figure 3.4. When each is fit with a stretched exponential, $C_{raw}(t)$ is best fit with $\beta = 0.91$, while the corrected $C(t)$ yields a single exponential best fit with $\beta = 1$. Most importantly, as demonstrated analytically above, the correlation function is the same correlation function measured in the bulk anisotropy experiments facilitating comparison to ensemble measurements. The uncorrected correlation function is nonexponential, and necessarily, well fit by Eq. 3.7.

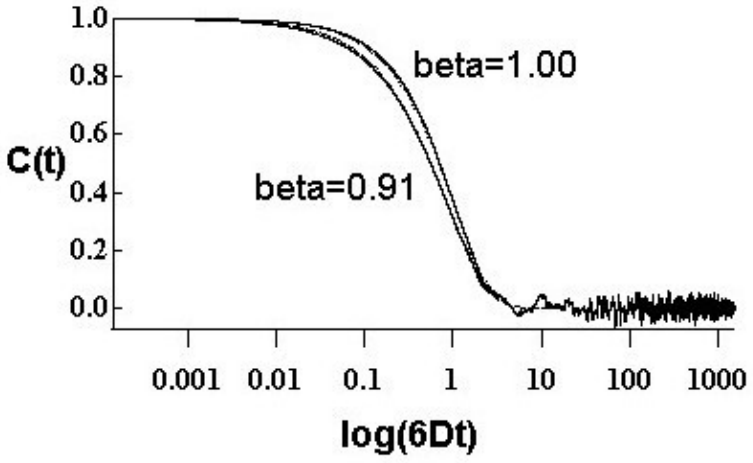

Figure 3.4 The correlation functions $C(t)$ for corrected (NA = 1.25) and raw (NA = 0) dichroism signals calculated from simulated data. Each is fit with a stretched exponential (dotted line). (Corrected, β = 1.0; raw, β = 0.91.) Time in arbitrary units.

It is interesting to see the origin of the nonexponential decay from examination of a trajectory. When the dipole is aligned on the objective axis, $\Theta = 0$, it is clear that any small change in Θ will result in a large change in the in-plane angle Φ, leading to rapid fluctuations in $A_{raw}(t)$. These rapid fluctuations in the vicinity of the poles will contribute higher order and faster terms in the correlation function $A_{raw}(t)$. Figure 3.3 shows a segment of a simulated trajectory for which the emission angle fluctuates around $\Theta = 0$. The uncorrected (NA = 0) data manifest the expected large fluctuations in $A_{raw}(t)$, while the signal that would be collected at large NA effectively removes all of the fluctuation. A molecule that is roughly perpendicular to the sample plane thus appears isotropic, and manifests an $A_{corrected}(t)$ that is always approximately zero. A related effect was noted by Hinze *et al.*[12] for large-angle jump diffusion. When the molecule only makes large angular displacements, the rapid fluctuations associated with small displacements near the pole are never sampled.

CONCLUSIONS

The effects of anisotropic rotation have not been explicitly investigated here. However, the conclusion must be the same. For anisotropic diffusion, the diffusion constant is replaced by a tensor and the angular description must be expanded. Nevertheless, the two essential elements at work in the isotropic case are unchanged: the components of the dichroism signal associated with more oscillatory angular functions will be averaged to a smaller amplitude by high NA, and the transient decay of the corresponding higher order terms in the correlation function will be inherently more rapid than those of lower order. Hence, the expected result is that in the absence of dynamical heterogeneity, the observed result will be indistinguishable from the ensemble

experiment. The fact that the measured angular function is nearly exactly described by $l = 2$ is consistent with this generalization.

This work shows that, in contrast to the idealized case of zero NA, the rotational correlation function associated with single molecule fluorescence dichroism should yield a single exponential when the effect of high-NA optics is taken into account, if the dynamics can be described by a single diffusion tensor. Therefore, the observation of single molecule transients that deviate from single exponential decays is a reflection of more complicated dynamics, not intrinsic polarization effects associated with the emission of radiation. Nonexponential decay of a single molecule transient is not in and of itself evidence of heterogeneous dynamics, as the decay could deviate from a single exponential due to the molecule having a non-spherical shape. However, one would expect heterogeneous dynamics to lead to nonexponential decays. Heterogeneity can be confirmed from differences between the rotational decays of individual molecules or the same molecule observed at different times. Moreover, since the dichroism signal at high NA reflects the same correlation function as the ensemble anisotropy measurements, deviations between single-molecule and ensemble measurements can be quantitatively analyzed with confidence[15].

ACKNOWLEDGEMENT

The author would like to thank Dr. Rossky and Richard Darst for their help on the simulation of single molecule rotational trajectories.

REFERENCES

(1) Deschenes, L. A.; Vanden Bout, D. A. *J. Phys. Chem. B* **2002**, *106*, 11438

(2) Ha, T.; Glass, J.; Enderle, T.; Chemla, D. S.; Weiss, S. *Phys. Rev. Lett.* **1998**, *80*, 2093

(3) Bartko, A. P.; Xu, K.; Dickson, R. M. *Phys. Rev. Lett.* **2002**, *89*, 026101

(4) Mei, E.; Tang, J.; Vanderkooi, J. M.; Hochstrasser, R. M. *J. Am. Chem. Soc.* **2003**, *125*, 2730

(5) Thurau, C. T.; Ediger, M. D. *J. Chem. Phys.* **2003**, *118*, 1996

(6) Ediger, M. D. *Ann. Rev. Phys. Chem.* **2000**, *51*, 99

(7) Böhmer, R.; Diezemann, G.; Hinze, G.; Rössler, E. *Prog. Nucl. Magn. Reson. Spectrosc.* **2001**, *39*, 191

(8) Fourkas, J. T. *Opt. Lett.* **2001**, *26*, 211

(9) Lieb, M. A.; Zavislan, J. M.; Novotny, L. *J. Opt. Soc. Am. B* **2004**, *21*, 1210

(10) Dickson, R. M.; Norris, D. J.; Moerner, W. E. *Phys. Rev. Lett.* **1998**, *81*, 5322

(11) Richert, R. *Condens. Matter* **2002**, *14*, R703

(12) Hinze, G.; Diezemann, G.; Basché, T. *Phys. Rev. Lett.* **2005**, *93*, 203001

(13) Berne, B. J.; Pecora, R. *Dynamic Light Scattering*; Dover: Mineola, N.Y., **2000**

(14) Deschenes, L. A. *Single-molecule studies of heterogeneous dynamics near the glass transition*, The University of Texas at Austin, 2002

(15) Wei, C.-Y. J.; Kim, Y. H.; Darst, R. K.; Rossky, P. J.; Vanden Bout, D. A. *Phys. Rev. Lett.* **2005**, *95*, 173001.

Chapter 4: Single-Molecule Studies of Polymer Rotational Dynamics

INTRODUCTION

When investigating dynamics in glass-forming materials using ensemble techniques, the observed result is a nonexponential relaxation which indicates that dynamics are not pure diffusion. The origin of this non-exponentiality has remained a challenging problem for many decades[1-6]. One question of particular interest is whether or not dynamics can be described by either of these possible scenarios: a heterogeneous scheme in which all molecules relax exponentially at different time, or the homogeneous scheme, where all molecules relax via inherently identical nonexponential decays[7-14]. Alternatively, the dynamics could lie between these two extremes. To explore which scheme can best describe dynamics in such inhomogeneous media, the single-molecule technique would be an ideal tool because it can probe individual molecular behaviors and measure individual properties that may be obscured in the ensemble average[15-18].

In this work, single-molecule fluorescence spectroscopy[19-26] is utilized to study rotational motions of single Rhodamine 6G molecules in poly(cyclohexyl acrylate). By following single transients, individually distinguishable differences in molecular dynamics may be identified, and a distribution of properties can be obtained for statistical analysis, instead of only an averaged value. We hope to investigate the underlying molecular motions that contribute to the observed inhomogeneous dynamics in glass-forming systems.

EXPERIMENTAL SECTION

Sample preparation

To ensure the probe molecules are well-isolated, a dilute solution containing 0.1nM R6G and 4% wt PCA was made. The solution was spin-cast onto glass cover slips to make thin films and dried in the hood prior to experiment. Transient data were taken at room temperature of 21 ˚C. No cryostat was used for these experiments.

Fluorescence measurement

The single-molecule experiment was done using a lab-built microscope, as shown in Figure 4.1. A 532-nm diode laser from Compass was focused onto the sample by an oil-immersion objective with a numerical aperture (NA) of 1.2. A ¼-wave plate was placed before the objective to change the polarization of the laser from linearly polarized to circularly polarized, so that R6G molecules in all orientations can be excited equally. Emission from the dye molecule was collected and collimated by the same objective, separated from the excitation wavelength by a dichroic mirror, a Notch filter, and long-pass filters. The signal was split by a cube beam splitter into two orthogonal polarizations, designated as I_s and I_p, on the plane perpendicular to the objective axis. Signals were collected by two PerkinElmer avalanche photodiodes on these two directions. The sample was mounted on an X-Y Piezo-scanning stage manufactured by Queensgate Instruments.

An image scan was first taken to locate single molecules, with typical scanning area of 10 μm x 10 μm, step size of 100 nm, and integration time of 50 ms per pixel. Once the image was obtained, positions of single R6G dyes were recorded, and then the target molecule was moved into the laser spot one at a time for excitation. The power

was attenuated 100 to 1000 fold (~ 0.5 μW) for recording transients. Typical transient lengths were about few hundred seconds long, and some were collected for longer than 2000 seconds.

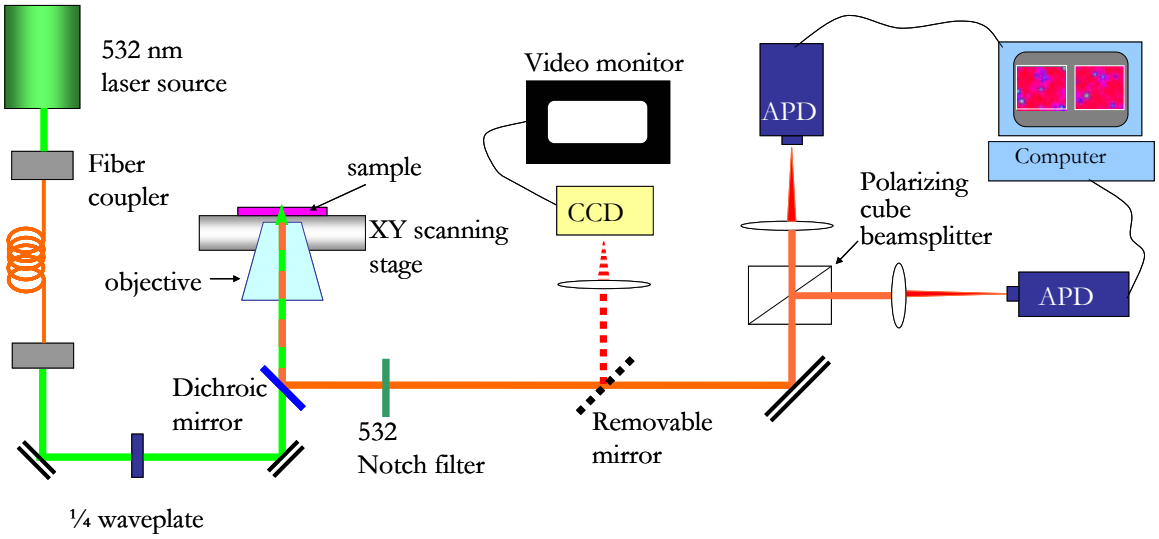

Figure 4.1: Schematic representation of single-molecule experimental setup. The ¼-wave plate is used to change the linearly-polarized laser beam to circularly-polarized. The objective focuses the excitation light onto the sample and also collects fluorescence photons from the sample. The X-Y piezo stage allows for image scans across the sample area to locate single molecule positions. The dichroic mirror and Notch filters are used to separate excitation source from fluorescence. CCD is confocal with the sample to help with initial alignment of the laser focus. Fluorescence signal is split by a cube beamsplitter onto two avalanche photodiodes (APD).

Quantifying rotational dynamics

From the raw data collected by the two APD, the reduced linear dichroism is readily calculated by:

$$A(t) = \frac{I_s(t) - I_p(t)}{I_s(t) + I_p(t)} \tag{4.1}$$

which is a relative measure of the dipole orientation as being projected onto the plane perpendicular to the objective. It is the difference between fluorescence intensities detected on both polarizations, divided by the total signals collected. This normalization removes artifacts from laser power fluctuation, out-of-plane rotation, triplet blinking, or any spectral diffusion. Ideally, the value $A(t)$ has possible maximum and minimum values at 1 and -1, but this is not the case when the signals are collected by a high-numerical aperture objective. Effects from high-NA optics will be discussed in the next section.

We can characterize the rotational time constant by taking the auto-correlation function of this timed dichroism signal, using the finite time series form:

$$C_A(t) = \langle A(t')A(t'+t) \rangle = \frac{\sum_{t'=0}^{T-t'-1} A(t')A(t'+t)}{\sum_{t'=0}^{T-1} A(t')A(t')} \tag{4.2}$$

The auto-correlation function is a measure of similarity between signal at two times, t' and $t + t'$. When t' is 0, the signal array is perfectly in-phase with itself, thus $C_A(t) = 1$;

as t' increases, difference between $A(t')$ and $A(t + t')$ increases and $C_A(t)$ becomes small. In general, the auto-correlation function will resemble an exponential form decaying from 1 to 0 [27,28].

Theoretically, for an isotropic diffusion case, $C_A(t)$ can be expressed in terms of spherical harmonic functions[29],

$$C_A(t) = \sum_l a_l C_l(t) = \sum_l a_l e^{-l(l+1)Dt} \tag{4.3}$$

where l labels a Legendre polynomial, P_l , and its corresponding coefficient, a_l , and the rotational diffusion constant, D. When taking into account the effects from using a high-numerical aperture objective as in all single-molecule experiments, the resulting correlation function $C_A(t)$ is dominated by the second harmonic term, $C_2 \sim \exp(-6Dt)$. In other words, the final result is that the measured correlation function is essentially a single exponential decay for a pure diffusion. The correlation function can be fit with a stretched exponential function, also know as the Kohlrausch-Williams-Watts (KWW) function:

$$C(t) \propto \exp[-(t/\tau)^{\beta}] \tag{4.4}$$

to obtain characteristic rotational time τ and stretching exponent β . This function is universally used because of an addition parameter β that provides flexibility for fitting than a single exponential form. $\beta = 1$ gives a single exponential function, and $\beta \neq 1$ gives a nonexponential function.

RESULTS AND DISCUSSION

Images of single molecules

Figure 4.2 shows orthogonal images obtained from scanning over a thin polymer film containing 0.1 nM of R6G dyes at 21 ˚C. The scan size is 10μm x 10μm, with each step size of 100 nm, and integration time of 50 ms.

Once we confirm that they are single dye molecules, their exact locations can be recorded from the images, which can be translated into the position of the Piezo stage. Then the target molecule can be moved into the center of laser focus spot for excitation. Usually after most of the single molecules from this image have been probed, a fresh area will be scanned to locate more single molecules to obtain transient data.

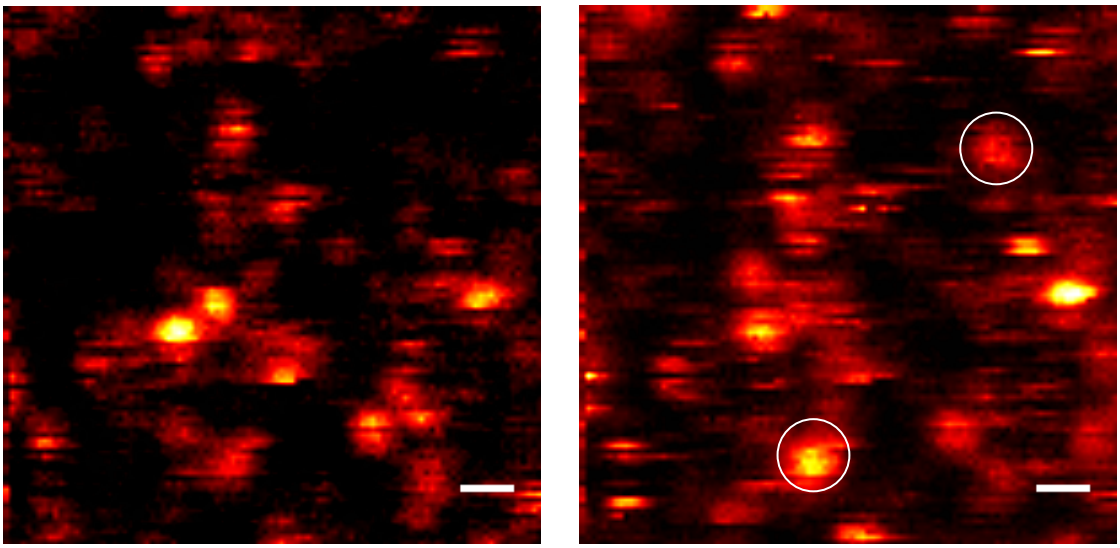

Figure 4.2: Example of single molecule fluorescence images obtained from two orthogonal polarizations. The scale bar is 1 μm.

There are several unique single-molecule characteristics that can be identified in this image. For example, the size of the spheres is on the submicron scale, which is approximately the laser focus size (~ ½ wavelength). Since a single R6G molecule is only about 15Å, one should expect single molecule image to be the laser focus spot size, and should be uniform across the scanned area. In addition, there are "stripes" on some of the single molecule images along the scanning direction (horizontal axis). This is the situation when the molecule rotates during the rest of the line scan and therefore the bright/dark stripes correspond to the times when the dipole moment is parallel/perpendicular to the horizontal direction. Alternatively, the excited state molecule will occasionally inter-system cross to the triplet state, and since the triplet state has a longer lifetime, the molecule is trapped in the "dark state" for some time before it returns to the ground state and can be excited again. This is also observed as brief discontinuity in the emitted fluorescence. Molecules of well-defined orientations or are less mobile will show more distinct linear dichroism, i.e. appear bright in one polarization and dark in the other (such as the circled molecules in Figure 4.2). The final piece of evidence for single transient is single-step photobleaching, which occurs when irreversible photochemistry happens to the excited-state fluorophore and it becomes a non-fluorescent species. In an ensemble of molecules, because photobleaching takes place at different times for different molecules, the result is a gradual decrease in fluorescence intensity; however, with only one fluorophore, it is either "on" or "off" and the effect is a sudden drop in fluorescence signal. By observing these features unique to individual molecules, we can confirm that single transient data were obtained in our experiments.

Analysis of single molecule transients

Once the locations of the single molecules on the image have been determined, the target molecule will be moved into the laser focus for excitation one at a time. Fluorescence photons are collected at 200 ms intervals, and the recorded raw data consist of two simultaneous signals of orthogonal polarizations.

The measure of transition dipole orientation can be represented by the reduced linear dichroism [Eq. 4.1], using the collected raw signals I_s and I_p. As the molecule rotates in space, the dichroism value varies with time. Since $A(t)$ is a noise signal that fluctuates around a timed average, we can extract this periodic component associated with the rotational dynamics by taking the auto-correlation function of $A(t)$ [Eq. 4.2]. To characterize this correlation function, the KWW stretched exponential function is used [Eq. 4.4], which would yield $\beta = 1$ for single exponential and $\beta \neq 1$ for nonexponential decays.

Depicted in Figure 4.3 is an example of a typical single molecule transient, including: (a) raw signals collected on two orthogonal polarizations: I_s and I_p; (b) the dichroism signals calculated from I_s and I_p.; and (c) the auto-correlation function of dichroism, $C_A(t)$, and the dashed line is the fit to the KWW stretched exponential function.

Qualitatively, the two orthogonal signals in Fig. 4.3(a) display some anti-correlation relation at some periods, which makes sense as the transition dipole moment rotates around the axes and will result in a larger intensity on one polarization if it is well-aligned on that direction.

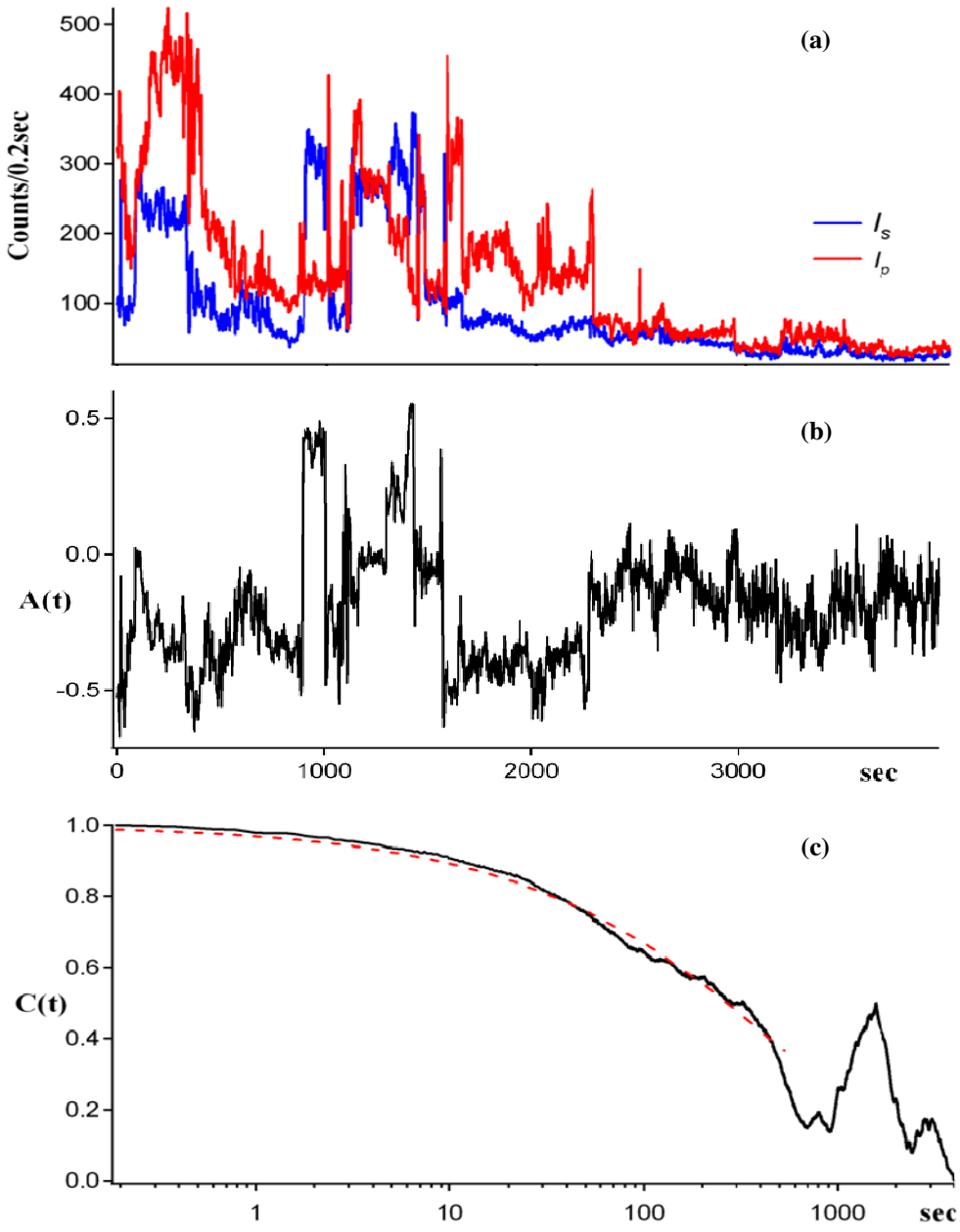

Figure 4.3: Typical single molecule transient in PCA at 21˚C throughout data analysis procedure. Panel (a) shows the raw signals collected on the two orthogonal polarizations, from I_s and I_p. (b) is the reduced linear dichroism calculated by $(I_s - I_p)/(I_s + I_p)$. (c) is the auto-correlation of the dichroism signal on a logarithmic time scale, with the fit (dashed line) to the KWW stretched exponential function, yielding $\tau = 524.21 \pm 2.04$ sec, $\beta = 0.546 \pm 0.002$.

The linear dichroism is calculated using Eq. 4.1. Intuitively, Eq. 4.1 can be reduced to cos (2Θ), where Θ is the dipole angle projected on the plane perpendicular to the objective axis. It appears that the limits for dichroism are ±1, which can be described by the situation when the dipole is aligned perfectly parallel to either direction (*s* or *p*). However, this is the ideal case when no effect from optics is considered, i.e. NA = 0. In reality, especially for a single-molecule experiment where a high-NA objective is used to collect most radiated photons, the dichroism values do not reach ±1 because the polarizing effects from the high-NA objective do not give zero intensity on one polarization at any given dipole orientation[30,31]. Instead, the most probable value of measured dichroism is zero when the dipole is aligned nearly parallel to the objective axis, in which case the projections of the emission polarization become almost equal onto the two detection axes. This effect is shown in Figure 4.4, where the histogram of dichroism values from single-molecule experiment is compared to the simulated data without consideration of NA.

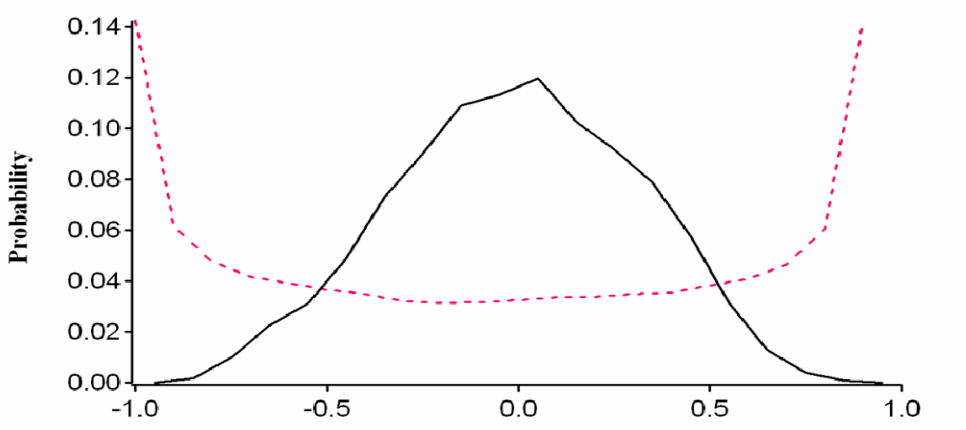

Figure 4.4: Histogram of linear dichroism signals for all singlemolecule data collected by a NA = 1.2 objective (dark line), and for simulated NA = 0 single molecule transient data (dotted line). The simulation histogram peaks at ±1 whereas the experimental histogram is peaked at 0 and does not reach the limits of ±1.

There are also many discrete large value changes in the calculated linear dichroism [Fig. 4.3(b)], i.e. it appears that the molecule undergoes large orientational changes occasionally. These large jumps are rarely observed in the simulated transients. Such sudden changes can be explained as situations when the molecule experiences different environments throughout the course of observation and thus the switching in dynamics. We have not yet developed a quantitative method to analyze these distinct dichroism changes in terms of comparing the frequencies or amplitudes of $|\Delta A/\Delta t|$ to the simulated data. Qualitatively speaking, these large changes are unique only in experimental results. Future work could include a simulation of single molecule transients with large-angle jumps or switching in rotational constants to explore the origins for such phenomenon.

The correlation function $C_A(t)$ in Figure 4.3(c) is fit with the KWW stretched exponential function to obtain rotational time τ and β. We have noticed that fitting result is sensitive to fitting criteria and may vary slightly when given different constraints. Upon using the stretched exponential function to characterize dynamics, β is usually constrained in the range of $0 < \beta \leq 1$ so that $\beta = 1$ defines a homogeneous case, and vanishes in an extreme heterogeneous limit. Statistically speaking, there is no need to constrain β within unity. Having $\beta < 1$ may seem unphysical, but it could happen as a result of statistical fluctuation when fitting the correlation function by the method of least squares. The result of confining $\beta \leq 1$ would be forcing all β values greater than 1 to be exactly equal to 1. In addition, the theoretical auto-correlation function is essentially zero after a certain time lag q, beyond which the standard errors will be greater than the estimated auto-correlation function itself. Therefore the fitting should be restricted to time lag q instead of the whole range[27].

Measurement of distributions of properties

We collected a set of 58 single transients of R6G in PCA film at room temperature 21˚C, which is 2 ˚C above T_g of PCA. Each transient has distinguishable correlation functions that have different rotational times. However, they are not all single exponential functions. Several select transient correlation functions are shown in Figure 4.5 to illustrate their distinct differences.

The correlation functions are each fit with the stretched exponential function [Eq. 4.4]. The average values for these 58 single transients are $< \tau >$ = 149.22 sec, and $< \beta >$ = 0.78, when fitted to time lag q with no constraint on β. If β is constrained to $0 < \beta \leq 1$, then the fitting results yield $< \tau >$ = 150.54 sec, and $< \beta >$ = 0.76. The difference is rather trivial and does not affect the shape of the distributions, except that all the $\beta > 1$ values become $\beta = 1$.

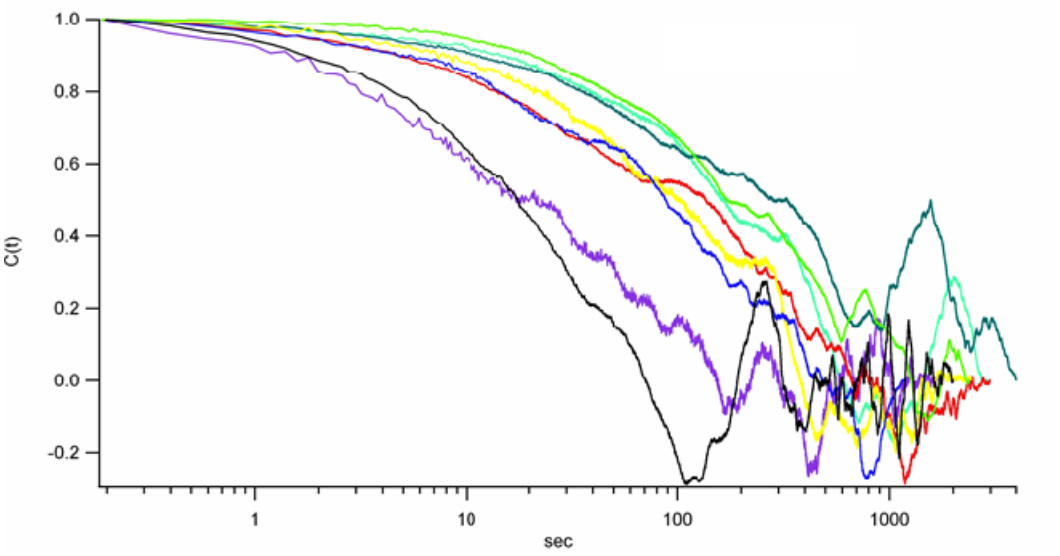

Figure 4.5: Example of select single molecule rotational correlation functions on a logarithmic time scale. All transients have different correlation functions with different decay times, and they are not all single exponentials.

When comparing fitting results of correlation functions for all the molecules, we see wide distributions for τ and β, as shown in Figure 4.6. The distribution for τ appears to be quite broad with the longest times more than an order of magnitude longer than the shortest. The stretching exponent β also exhibits a broad distribution ranging from single exponential to highly nonexponential decays. Note that if β is constrained to within 1, then the values that are greater than 1 will be reduced to 1, and the histogram for β will have a slightly larger peak at the limit of 1.

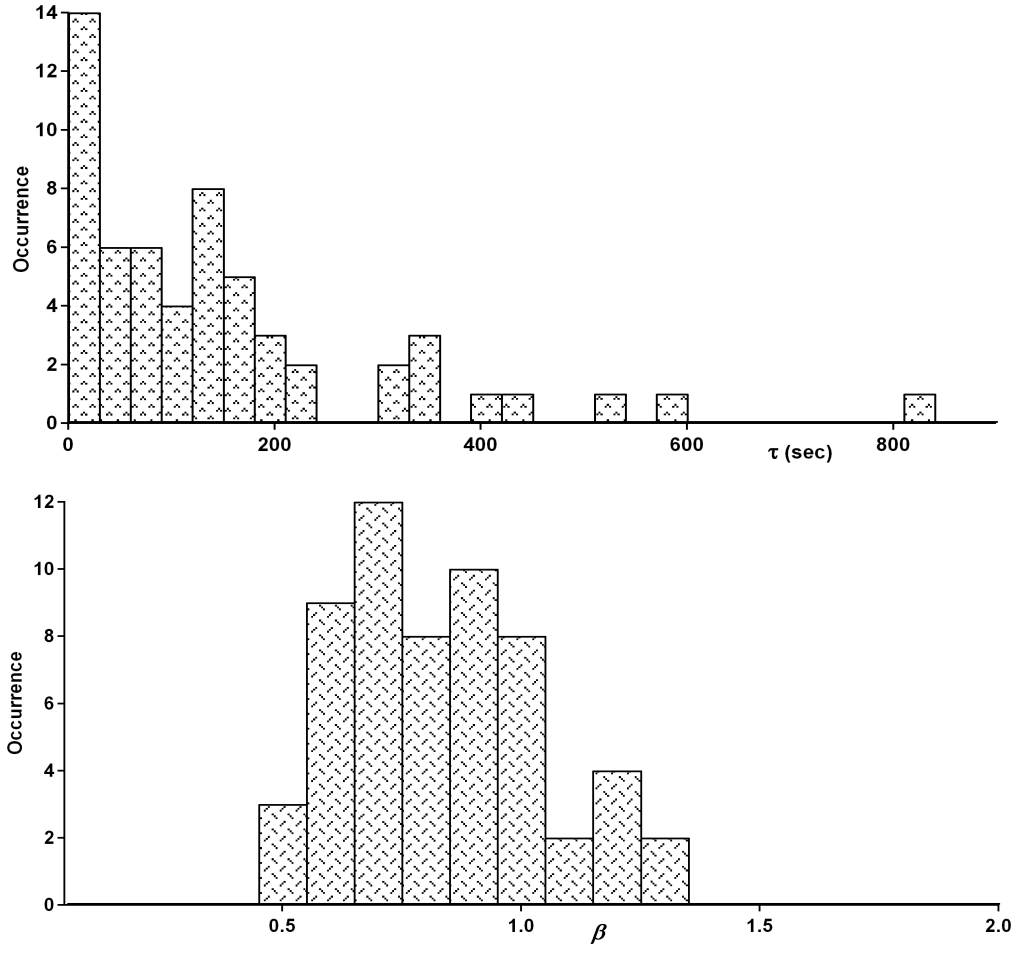

Figure 4.6: Distributions of fitted τ (top) and β (bottom) for a set of 58 single molecule transients in PCA at 21˚C. $< \tau >$ = 149.22 sec, $< \beta >$ = 0.78.

Intuitively, upon examining the results shown in Fig. 4.5 and Fig. 4.6, one would be very tempted to conclude right away that the differences in correlation functions and the distributions of τ and β are evidence of spatial heterogeneity. While this interpretation seems fairly reasonable, one needs to keep in mind that the observed single transients have limited lengths and thus the effects from statistics need to be considered very carefully in order to properly describe the dynamics.

Intrinsic statistical errors for single molecule distributions

While not ensemble-averaged, the single-molecule measurement is inherently time-averaged as the data for a single molecule are collected over a period of repeated excitation. The signals carry information about local environments as a function of time, thus a single transient monitored during a finite period of time may not be able to sample the entire space of possible configurations to yield sufficient statistical results that represent the whole system. It can be shown that for a stationary process, the variance of the correlation function is inversely proportional to the trajectory length[28,32]. Thus, even if the system is stationary, the correlation function calculated from a trajectory of finite length exhibits fluctuations. As a consequence, if one characterizes the correlation function by fitting it to a parameterized function, a stretched exponential for our analysis, the variances in the correlation function will propagate to the other parameters. Another way to iterate this is that if one wants to characterize the time scale for molecular rotation, one needs to observe the molecule long enough for it to reorient.

In a previous work done by Lu and Vanden Bout[33], a "natural distribution" in τ_F and β_F is calculated from simulated isotropic rotational diffusion trajectories of given length T. As shown in Figure 4.7, the results are wide distributions of τ_F and β_F even though there is only one true rotational constant, and all correlation functions

should be single exponentials with $\beta = 1$. Moreover, in each case the distributions of both τ_F and β_F broaden as T shortens, and the average values begin to deviate from the true value of the system. These broadening effects in τ_F and β_F are purely due to finite sampling, and theoretically the distributions can be applied to correlation functions of any rank l. Given these inherent statistical fluctuations, one needs to evaluate carefully an experimental distribution and determine if it varies significantly from what would be expected based on the statistics and normal diffusion.

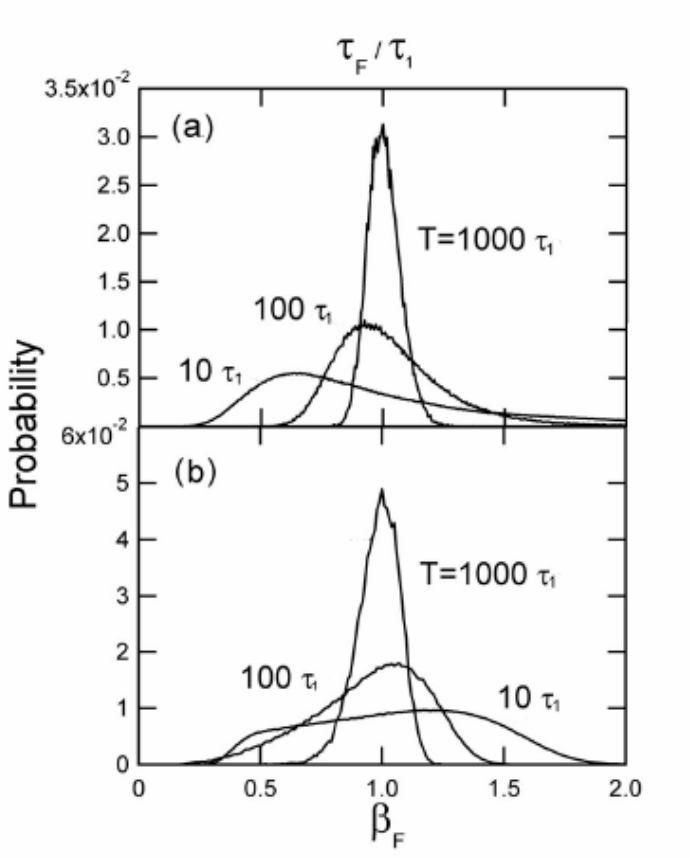

Figure 4.7: Distributions of τ_F and β_F with respect to different sample sizes T ($10\tau_1$, $100\tau_1$, and $1000\tau_1$). Each curve is calculated from 1000 independent trajectories $l = 1$, $\tau_1 = 200$, length 10^7 broken into pieces of desired length T.

To compare the distributions, we used a chi-square test to see if the standard deviation of experimental data is the same as the simulated data. If the chi-square test value is greater than the upper critical value χ^2_α or smaller than the lower critical value $\chi^2_{1-\alpha}$ at significance level α, then we can say that the standard deviation of the experimental data is not the same as the simulation of pure rotational diffusion. If the test value falls inside the upper and lower critical values, then the two standard deviations are not different from each other[34]. To draw an analogy to the simulation, the experimental single-molecule results from fitting with non-restricted β is used, and the standard deviation is: $S(\tau_{exp})$ = 1.080 for the distribution of τ_{exp} [Fig. 4.6(a)] normalized to $< \tau_{exp} >$. (For clarity, here we add subscript *exp* to denote experimental results, and *F* for simulated results.) The distribution of τ_F for simulated data is normalized to the true rotational constant τ_1, which is unknown in the experimental data, therefore we use the average rotational constants $< \tau_{exp} >$ for normalization. The average ratio of transient length *T* over $<\tau_{exp}>$ is 12.75 for this entire set of 58 single molecule data, hence we use the standard deviation for simulated $T = 12.75\ \tau_1$ trajectories for comparison, which is : $S(\tau_F)$ = 0.823. The calculated one-way chi-square test value for τ is:

$$P(\tau) = (N-1)\left(\frac{S(\tau_{\exp})}{S(\tau_F)}\right)^2 = 98.157 \qquad (4.5)$$

where *N*-1 is the degree of freedom. The upper critical chi-square value at 0.1% significance level is $\chi^2_{0.001} = 95.751$, and therefore the single-molecule data have a different distribution of rotational constants than the simulated distributions. The calculated chi-square test value for β yields $P(\beta)$ = 20.425, which falls below the lower critical value of $\chi^2_{0.999} = 29.592$. Therefore the distribution of β_{exp} is not the same as the simulated distribution, either.

If we plot the distributions from simulated transients on top of the experimental data, shown in Figure 4.8, we can see their differences immediately. The distribution of τ_{exp} for single-molecule data is peaked at very small times, and tails off at a larger extreme than the simulated data. The distribution of β_{exp} for single-molecule data is not centered at 1, whereas the simulated transients have a broader range of β_F values that are slightly peaked at $\beta_F > 1$. It should also be mentioned that for simulated transients, despite the trajectory lengths and the broad distribution, the average β_F value is always ≈ 1 (for example, for $T = 12.75\,\tau_1$ transients, $<\beta_F> = 1.030$); for experimental transients, $< \beta_{exp} > = 0.780$.

This basic comparison demonstrates that single-molecule results are very different from pure diffusion. Our transient lengths, however, are only on the order of 10 times the average rotational time, which unfortunately inherit greater statistical fluctuations in the estimation of the true rotational dynamics of the system than an ideal case of infinitely long trajectory. In practice, fluorescent probe molecules cannot be observed infinitely because of irreversible photobleaching, hence it is very difficult to obtain transients that have sufficient lengths (at least 100 times longer than the true rotational time) to reduce the impacts of statistical errors. Even if our transients are as long as any reported lengths, we are still limited by effects from finite sampling.

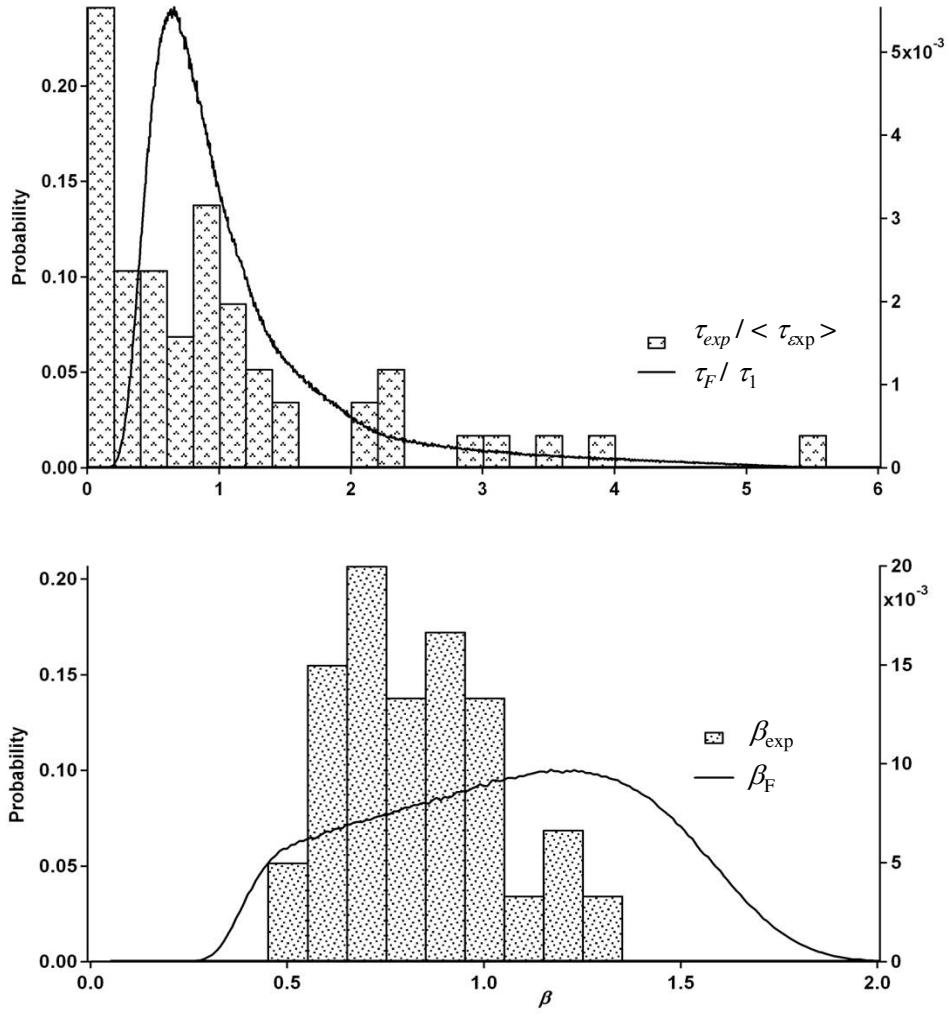

Figure 4.8: Distributions of τ_{exp} / $<\tau_{exp}>$ and β_{exp} for a set of 58 single molecule transients (bar). The overlapping lines are the distributions from simulated transients of T = 12.75 τ_1 for comparison.

On the other hand, the chi-square test may not be an ideal test for evaluating single molecule distributions, because the distributions of τ and β from both the experiment and simulation are not normal distributions, therefore they do not quite meet the criteria for chi-square test. Statistical tests, however, are used mainly to decide if two cases are the same based on the subtle differences between them. If the results already appear to be quite different, it is unlikely that the null hypothesis of the two being the same will be accepted.

In the single-molecule experiment, each transient has different lifetimes, but the simulated transients are all of the same length. Therefore we tried a different method for analysis by selecting single transients that have trajectory length T longer than $10\times<\tau_{exp}>$, and truncating each trajectory to the same length, $10\times<\tau_{exp}>$. Unfortunately, we are now only left with half of the transient data for analysis. This group of transients has a larger average τ, which in turn yields an average ratio of $T/<\tau'_{exp}> \approx 6$, resulting in even shorter relative transient lengths that will have larger statistical fluctuations, thus we stop carrying out further statistical comparisons. Moreover, due to the fact that we are not able to determine the "true" correlation time of the system in the first place, we use $<\tau_{exp}>$ as the reference for defining relative transient lengths, which is already a biased estimation of the true rotational constant under the condition of insufficient transient lengths. In other words, finite sampling results in inherent statistical errors that impose limitations on the analyses of correlation functions and thus extra consideration is needed when interpreting the distributions. Nevertheless, qualitative comparison and simple statistical tests show that the experimental results are still very different from the simulated results for a pure diffusion.

CONCLUSIONS

Single-molecule spectroscopy was utilized to study rotational dynamics of R6G probe molecules in poly(cyclohexyl acrylate) matrix. Numerical analysis demonstrates that by taking into account the effects of high-NA objectives, auto-correlation function of the measured dichroism signal from a single fluorophore undergoing pure rotation still manifests a single exponential decay. This suggests that a nonexponential decay can be interpreted as an indication for complex dynamics.

Statistical analysis based on simulated trajectories shows that even a pure rotation could yield a distribution of values as a result of finite sampling, which implies that in real experiments, the quality of the single transient data needs to be evaluated carefully because it is affected by trajectory lengths. From the experimental results of R6G probe rotations in PCA, the average transient length is about 12.75 $< \tau >$, which implicates that the broad distributions in both time constants and stretching exponents can possibly be the result of large statistical errors. (It should be noted that the length of trajectories in these studies is as long or longer than any single molecule rotational trajectory present in the literature.) The experimental distributions of both τ and β from single molecule transients, however, are very different from the simulated distributions for a pure diffusion. The experimental single molecule transients also have discrete large changes in the dichroism signals, which are rarely seen in the simulated trajectories.

Referring back to the introduction, there are two possible underlying schemes that can lead to the same final result of nonexponential decay in an ensemble measurement: the *heterogeneous* case, consisting of pure diffusions on different time scales, and the *homogeneous* case, where all molecules have identical nonexponential relaxations. From the results of single molecule rotational correlation functions, the system can be

described as inhomogeneous because each of the transient is different from one another, and the average β is not 1. But whether or not the system is truly spatially heterogeneous is not so easily determined by examining a distribution of rotational times and β. The system could be a pure rotation, but due to insufficient transient lengths or background signals, the correlation functions are not single exponential functions, and thus wide distributions for β and τ can arise merely as the result of poor statistics. Alternatively, any heterogeneity could be shadowed by the statistical errors and the limitation of correlation function analysis prevents such observation. The dynamics are more complicated than the two extreme schemes of homogeneous or heterogeneous, and could be better described by a combination of both pictures.

In conclusion, single-molecule experiments can measure a distribution of properties to reveal individual differences that are concealed in an ensemble measurement. Unfortunately, one of the biggest challenges in single-molecule fluorescence spectroscopy is that the "lifetime" of a probe molecule is often shortened by irreversible photobleaching, thus the resulting short transient length imposes limitation on the analysis of its rotational correlation function. To obtain a better estimation of the true rotation time of the system, one can extend the transient length, for example, by using very low probing power, reducing exposure time, or removing triplet quenchers such as oxygen[35,36], etc. Future exploration of non-pure diffusion models should also be able to provide more insights for determining system heterogeneity.

REFERENCES

(1) Ediger, M.D.; Angell, C.A.; Nagel, S.R. *J. Phys. Chem.* **1996**, *100*, 13200.

(2) Angell, C.A.; Ngai, K. L.; McKenna, G. B.; McMillan, P. F.; Martin, S.W. *J. Appl. Phys.* **2000**, *88*, 3113.

(3) Phillips, J. C. *Rep. Prog. Phys.* **1996**, *59*, 1133.

(4) Sillescu, H. *J. Non-Crys. Solids* **1999**, *243*, 81.

(5) Stickel, F.; Fischer, E. W.; Richert, R. *J. Chem. Phys.* **1995**,*102*, 6251.

(6) Lubchenko, V.; Wolynes, P. G. *Annu. Rev. Phys. Chem* **2007**, *58*, 235.

(7) Arbe, A.; Colmenero, J.; Monkenbusch, M.; Richter, D. *Phys. Rev. Lett.* **1998**, *81*, 590.

(8) Cicerone, M. T.; Blackburn, F. R.; Ediger, M. D. *Macromolecules* **1995**, *28*, 8224.

(9) Ediger, M. D. *Ann. Rev. Phys. Chem.* **2000**, *51*, 99.

(10) Richert, R. *J. Phys.: Condens. Matter* **2002**, *14*, R703.

(11) Russell, E. V.; Israeloff, N. E. *Nature* **2000**, *408*, 695.

(12) Schmidt-Rohr, K.; Spiess, H. W. *Phys. Rev. Lett.* **1991**, *66*, 3020.

(13) Simdyankin, S. I.; Mousseau, N. *Phys. Rev. E* **2003**, *68*, 041110.

(14) Glotzer, S. C.; Jan, N.; Lookman, T.; MacIsaac, A. B.; Poole, P. H. *Phys. Rev. E* **1998**, *57*, 7350.

(15) Moerner, W. E.; Fromm, D. P. *Rev. Sci. Instrum.* **2003**, *74*, 3597.

(16) Xie, X. S.; Trautman, J. K. *Annu. Rev. Phys. Chem* **1998**, *49*, 411.

(17) Weiss, S. *Science* **1999**, *283*, 1676.

(18) Plakhotnik, T.; Donley, E. A.; Wild, U. P. *Ann. Rev. Phys. Chem.* **1997**, *48*, 181.

(19) Mei, E.; Tang, J.; Vanderkooi, J. M.; Hochstrasser, R. M. *J. Am. Chem. Soc.* **2003**, *125*, 2730.

(20) McCain, K. S.; Hanley, D. C.; Harris, J. M. *Anal. Chem.* **2003**, *75*, 4351.

(21) Michalet, X.; Weiss, S.; Jäger, M. *Chem. Rev.* **2006**, *106*, 1785.

(22) Nie, S.; Zare, R. N. *Annu. Rev. Biophys. Biomol. Struct.* **1997**, *26*, 567.

(23) Rosenberg, S. A.; Quinlan, M. E.; Forkey, J. N.; Goldman, Y. E. *Acc. Chem. Res.* **2005**, *38*, 583.

(24) Tomczak, N.; Vallee, R. A. L.; van Dijk, E. M. H. P.; Garcia-Parajo, M.; Kuipers, L.; van Hulst, N. F.; Vancso, G. J. *Eur. Polym. J.* **2004**, *40*, 1001.

(25) Uji-i, H.; Melnikov, S. M.; Deres, A.; Bergamini, G.; DeSchryver, F.; Herrmann,A.; Müllen,K.; Enderlein, J.; Hofkens, *J. Polym.* **2006**,*47*, 2511.

(26) Bartko, A. P.; Xu, K.; Dickson, R. M. *Phys. Rev. Lett.* **2002**, *89*, 026101.

(27) Box, G. E. P.; Jenkins, G. M. *Time Series Analysis Forecasting and Control*; Holden-Day: San Francisco, 1970.

(28) Brockwell, P. J.; Davis, R. A. *Time series: theory and methods*, 2nd ed.; Springer-Verlag: New York, NY, 1991.

(29) Berne, B. J.; Pecora, R. *DynamicLight Scattering*; Dover: Mineola,N.Y., 2000.

(30) Fourkas, J. T. *Opt. Lett.* **2001**, *26*, 211.

(31) Wei, C.-Y. J.; Kim, Y. H.; Darst, R. K.; Rossky, P. J.; Vanden Bout, D. A. *Phys. Rev. Lett.* **2005**, *95*, 173001.

(32) Zwanzig, R.; Ailawadi, K. *Phy. Rev.* **1969**, *182*, 280.

(33) Lu, C.-Y.; Vanden Bout, D. A. *J. Chem. Phys.* **2006**, *125*, 124701.

(34) NIST/SEMATECH *e-Handbook of Statistical Methods* http://www.itl.nist.gov/div898/handbook/.

(35) Deschenes, L. A.; Vanden Bout, D. A. *Chem. Phys. Lett.* **2002**, 365, **387**.

(36) Lakowicz, J. R. *Principles of Fluorescence Spectroscopy*, 2nd ed.; Kluwer Academic/Plenum Publishers: New York, NY, 1999.

Chapter 5: Comparison of Single-Molecule and Ensemble Measurements

This chapter will summarize our studies on the relaxation dynamics of polymers, including brief reviews on the techniques already described in detail in the preceding chapters, with the emphasis on the comparison of ensemble and single-molecule experiments. Concluding remarks will be made on the heterogeneity of polymer dynamics near the glass transition temperature based on our current results.

INTRODUCTION

The nature of non-crystalline materials such as viscous liquids, polymers, and glassy solids, is a very intriguing and challenging field of research. When these liquids cool, viscosity increases several orders of magnitude, until eventually the rearranging dynamics are too slow that the structure of supercooled liquid is considered *frozen*, and becomes a glass. At temperatures near the glass transition, not only does the relaxation time increase dramatically, the relaxation function itself is rarely an exponential form, which would be the case if there was only one time constant in the system[1-9].

On the other hand, these nonexponential relaxations are often measured by ensemble techniques, but there are some intriguing questions about the underlying dynamics that lead to the observed nonexponential behavior. How do the molecules rotate? Are there different time scales? If so, are they pure diffusions? Or do the individual molecules orient in the same nonexponential fashion as the ensemble? To answer these questions, one would have to investigate system dynamics on a single-

molecule level, because the subtle differences between individual molecular properties are often obscured in a bulk measurement. For instance, a nonexponential decay can be the superposition of many single exponential decays with different decay times. Alternatively, each component can have exactly the same nonexponential form as the ensemble decay. An even more complicated case would be the scheme that entails both.

The development of single-molecule spectroscopy has facilitated investigations of such inhomogeneous systems, and has shown to be a powerful tool for directly observing individual properties that are different from the bulk property and provides a great means for understanding chemical reactions and molecular interactions on a single-molecule basis as delineated in text books or theoretical models[10-18].

We performed an ensemble experiment to study anisotropy relaxations of poly(cyclohexyl acrylate) by polarized fluorescence recovery after photobleaching (FRAP)[19-22], and measured the average rotational times for this polymer at various temperatures. The results yield nonexponential decays which suggest that dynamics are not pure diffusion. In order to gain further understanding of the origins of the observed inhomogeneous dynamics, we exploited single-molecule spectroscopy to study rotational dynamics of the same polymer system, and obtained a broad distribution of rotational correlation functions[23]. In addition, to ensure that the probe rotations are reflective of the polymer dynamics, the measured rotational time from both experiments should agree with each other and be compared to the literature to determine if indeed the primary relaxation of polymer is measured.

EXPERIMENTAL SECTION

Samples

The polymer under study is poly(cyclohexyl acrylate), with approximate MW = 150,000, and literature T_g of 19 ˚C. The probe molecules are Rhodamine 6G dyes, which are very popular fluorescent probes because of their large quantum yield.

For the ensemble experiment, a polymer melt containing 10-100 ppm (wt) R6G is made inside a 4-mm quartz cuvette, which allows for a 90˚-detection configuration. Temperature is controlled either by a water chiller or a continuous-flow liquid nitrogen cryostat equipped with a digital temperature controller.

For the single-molecule experiment, a thin film sample is made by spin-casting a polymer solution doped with very little amount of R6G . The low concentration of R6G (0.1 ~ 1 nM) ensures that the probe molecules will be spatially isolated in the film.

Ensemble FRAP technique

Rotational dynamics of fluorescent molecules can be studied by polarized fluorescence recovery after photobleaching (FRAP) technique, also known as dynamic hole-burning. The basic principle is to intentionally create anisotropy in an isotropic system, and then measure the time it takes for the remaining ensemble to return to a normal distribution. To create initial anisotropy, a linearly-polarized, high-intensity bleaching beam is used to selectively photobleach probe molecules that have absorption dipoles oriented along the excitation polarization. This is why it is also called "hole-burning" because now one specific orientation has been depleted. A weaker reading beam either parallel or perpendicular to the bleaching beam is then followed to

probe the orientation of the remaining molecules. The fluorescence signals that have polarization parallel to the bleaching beam will initially have smaller intensity because molecules aligned along this direction have been photobleached most effectively, whereas the perpendicular polarization will have greater intensity. As the remaining fluorophores reorient, the depleted polarization will recover, i.e. as the ensemble gradually returns to isotropic distribution, anisotropy decays to zero[20, 21]:

Anisotropy is calculated by:

$$r(t) = \frac{(I'_{//} - I^0_{//}) - (I'_{\perp} - I^0_{\perp})}{(I'_{//} - I^0_{//}) + 2(I'_{\perp} - I^0_{\perp})} = \frac{\Delta I_{//} - \Delta I_{\perp}}{\Delta I_{//} + 2\Delta I_{\perp}} \tag{5.1}$$

where $I^0_{//}, I^0_{\perp}$ are signals *before* photobleaching, and $I'_{//}, I'_{\perp}$ are signals *after* photobleaching. Subscripts // and $\perp$ denote fluorescence emissions parallel and perpendicular to the bleaching beam polarization, respectively.

The experimental setup includes a 532-nm continuous-wave laser source for excitation. The laser polarization is modulated at 10 Hz frequency between +/- 45° by the use of an electro-optic modulator, a ½-wave plate, and a function generator. The switching between high-intensity bleaching beam and low-intensity reading beam is achieved by a solenoid and a neutral density filter of optical density OD = 3 or 4. Bleaching power is typically in the range of 0.5 to 3.5 mW, and reading power is 0.5 to 3.5 μW. Bleaching duration is usually between 1 to 6 sec. Bleaching power and duration can be manipulated to produce different bleach depths. By employing a polarizer at the "magic angle" of 35.3° from vertical in front of the detector, fluorescence signals collected at 90° will be proportional to the number of molecules excited by the reading beam polarization[19]. A single photomultiplier tube collects emitted

fluorescence photons continuously as a single wave, and raw data are later sorted into separate signals that are parallel ($I_{//}$) and perpendicular ($I_{\perp}$) to the bleaching polarization.

Single-molecule spectroscopy

The single-molecule experiment is performed using a different instrumental setup from the ensemble experiment. To obtain single molecule transient data, we need to first locate dye molecules in the film sample. An image scan is thus taken using a lab-built confocal microscope equipped with an X-Y Piezo translational stage. Once the positions of the individual probe molecules are recorded, they can be observed one molecule at a time. Each single transient ends when irreversible photochemical reaction (photobleaching) takes place.

The single-molecule experiment is different from the ensemble FRAP experiment in the way that it directly probes molecular orientations so no initial anisotropy needs to be created. If using linearly-polarized beam, however, only molecules aligned in that direction can be effectively excited. This would lead to difficulty in detecting fluorescence signals on only two orthogonal directions because the molecule may not be perfectly aligned parallel to either direction during the course of observation, which would result in small signals and poor data quality. Instead, a circularly-polarized light is used to provide uniform excitation to the probe molecule regardless of its orientation.

A 532-nm diode laser is used as the excitation source, focused onto the sample by a high-numerical aperture objective (NA = 1.2, oil immersion lens), which also collects and collimates the emitted photons. The excitation wavelength is filtered out from the emission wavelength using a dichroic mirror, a Notch filter, and several long-pass filters. Fluorescence signal is separated by a polarizing cube beamsplitter into two orthogonal

directions (I_s and I_p) perpendicular to the objective axis, and detected by two avalanche photo diodes simultaneously.

The molecular orientation can be measured by calculating the reduced linear dichroism, $A(t)$, which can be thought of as the projection of the dipole onto the plane of detection:

$$A(t) = \frac{I_s(t) - I_p(t)}{I_s(t) + I_p(t)} \tag{5.2}$$

When the dipole is aligned preferentially with one of the directions, fluorescence signals collected at this channel will be larger than the orthogonal channel, and vice versa. Ideally, by looking at this equation, as the molecule rotates around space, $A(t)$ should fluctuate with possible maximum and minimum values of ± 1. However, in a single-molecule experiment where one would like to collect as many emitted photons as possible from one fluorophore, a high-NA objective is used which has depolarization effects resulting in a measured dichroism signal that is not a simple function of the projected in-plane angle Φ of the dipole, and does not reach the limits of ± 1.

The auto-correlation function of $A(t)$ is calculated using the equation for discrete data points in a finite time series:

$$C_A(t) = \left\langle A(t')A(t'+t) \right\rangle = \frac{\sum_{t'=0}^{T-t-1} A(t')A(t'+t)}{\sum_{t'=0}^{T-1} A(t')A(t')} \tag{5.3}$$

where T is the total number of points in the transient. The auto-correlation function is a "memory function" which calculates the overlap of the signal array with itself, i.e. at first

point, the signal including noise overlaps with itself perfectly, thus the auto-correlation has maximum value. When t' is very small, $A(t'+t)$ will be very close to $A(t)$. As t' becomes large compared to the periodic fluctuation of this signal, the correlation between $A(t')$ and $A(t'+t)$ is lost. At the last point when the signal array is totally out-of-phase with itself, the auto-correlation function is zero. Thus auto-correlation function can be used to remove any random noise inherent in the signal, and identify a periodic time component for this dichroism measurement[24-26].

COMPARING ENSEMBLE AND SINGLE-MOLECULE MEASUREMENTS

To make a quantitative comparison between ensemble and single-molecule experiments, we need to understand how to relate the measured quantity $A(t)$ and $C_A(t)$ to the molecular rotational correlation function. It has been shown that for an isotropic diffusion case, the rotational correlation function can be expressed in terms of spherical harmonic functions[24,27]:

$$C(t) = \sum_l a_l C_l(t) \tag{5.4}$$

Each $C_l(t)$ is given by:

$$C_l(t) = e^{-l(l+1)Dt} \tag{5.5}$$

where l labels a Legendre polynomial P_l and its corresponding coefficient, a_l, and D is the rotational diffusion constant. Optical techniques that measure ensemble anisotropy yield a decay that results from only the $l = 2$ correlation function, $C_2(t)$. For the single-molecule case, one must expand the measured dichroism into the spherical harmonics to

examine all the terms that will constitute the correlation function. The coefficients a_l can be calculated by projecting the dichroism into spherical harmonic coordinates:

$$a_l = \frac{1}{4\pi}\sum_m \left| \int_0^{2\pi} d\Phi \int_0^{\pi} d\Theta \sin\Theta \; A(\Theta,\Phi)\, Y_{l,m}(\Theta,\Phi) \right|^2 \tag{5.6}$$

In an ideal case where no optics is considered, the dichroism signal can be reduced to $A(t) = \cos(2\Phi)$, where Φ is the azimuthal angle of the dipole moment. Therefore, $A(t)$ is simply representative of the projected in-plane orientation of the emission dipole, and has most probable values at ±1. Refer to Figure 5.1 for an illustration of the experimental geometry for collecting transient data.

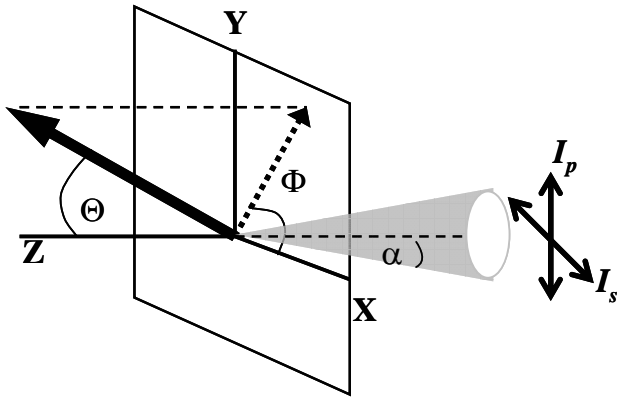

Figure 5.1: Schematic representation of the experimental geometry for analyzing single molecule dipole orientation. The emission dipole can be prescribed by the spherical coordinate angles Θ and Φ. Z is the objective axis, α is the collection angle, and Is, Ip are the orthogonal fluorescence components projected on the plane perpendicular to Z.

The correlation function for $A(t) = \cos(2\Phi)$ can be computed by expanding $A(t)$ into the spherical harmonics [Eq. 5.6] and summing the correlation functions for each l weighted by their coefficients [Eq. 5.4 and 5.5]. Hinze *et al.*[27] had demonstrated that for $A(t)$ in the limit of zero-NA, including terms from $l = 2$ up to $l = 20$ results in a decay that would be multi-exponential, but can be fit by the Kohlrausch-Williams-Watts (KWW) stretched exponential function:

$$f(t) = e^{-(t/\tau)^{\beta}} \tag{5.7}$$

The fit yielded $\tau = 0.87/6D$ and $\beta = 0.87$. This result suggested that rotational correlation function cannot be related to optical anisotropy $C_2(t) = \exp(-6Dt)$, and there is an inherent nonexponential factor for an isotropic decay thus only decays with $\beta < 0.84$ could be regarded as indications for nonexponential behaviors.

While the results from Hinze hold in the limit of zero-NA, single-molecule experiments generally require high-NA objectives in order to efficiently collect the most photons from the single emitter. The high-NA has the effects of altering the polarization of the light that is collected so that the dichroism signal is no longer simply related to the in-plane projection of the dipole. Such effects from high-NA optics should be considered for any analysis of single molecule polarizations[28]. The fluorescence signals that are detected on two directions are functions of the dipole orientation angles Φ and Θ, NA, and the index of refraction of the medium, n. Putting together all these parameters gives a more complicated reduced linear dichroism:

$$A(t)_{NA} = \frac{\mathrm{C}\sin^2\Theta\cos 2\Phi}{\mathrm{A} + \mathrm{B}\sin^2\Theta} \tag{5.8}$$

where A, B, C are constants defined by NA and n. When NA = 0, Equation 5.8 reduces to $\cos(2\Phi)$. Following the previous analysis, the correlation function of $A(t)_{NA}$ can be readily calculated by expanding the measured quantity into spherical harmonics [Eq. 5.6].

In the high-NA case (e.g. NA = 1.2), the coefficients a_l decrease dramatically with l [Figure 5.2], and the resulting decay is nearly entirely described by the $l = 2$ component : $C_2 = \exp(-6Dt)$, which is the same exponential decay measured in the ensemble anisotropy experiments. When fitting the correlation function that includes the terms from $l = 2$ to $l = 20$ with the stretched exponential, it yields a decay whose $\tau = 1/6D$ and $\beta = 1$. The end result is that the polarization effects from the high-NA optics cause the measured rotational correlation function to return to an essentially single exponential decay[29]. While homogeneous diffusion will yield single exponential correlation functions for the single molecule transients, this does not lead to the conclusion that a nonexponential decay is a proof for heterogeneous environments. What we have demonstrated here is that we can now directly compare the measured single molecule dichroism signal and its auto-correlation function to the ensemble FRAP measurements of optical anisotropy decays.

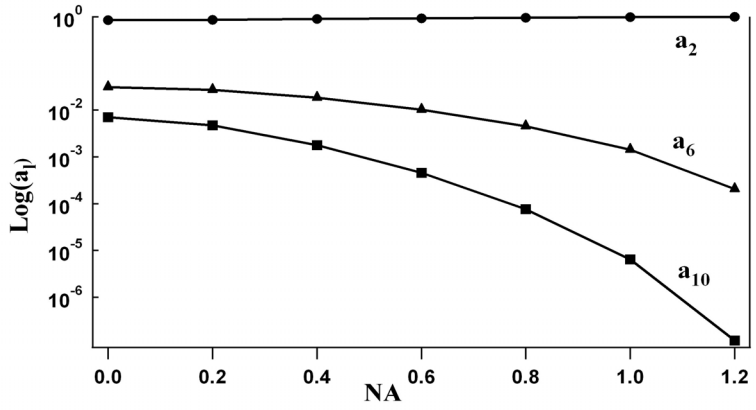

Figure 5.2: The effects of high NA on the correlation function coefficients, a_l. Numerical values of a_2, a_6, and a_{10} are shown here for NA = 0 to 1.2. Except for a_2, all higher-order a_l terms decrease rapidly as NA increases. NA is plotted on logarithmic scale to emphasize this dramatic effect.

RESULTS AND DISCUSSION

Examples of ensemble anisotropy decay and single molecule transient data are depicted in Figure 5.3.

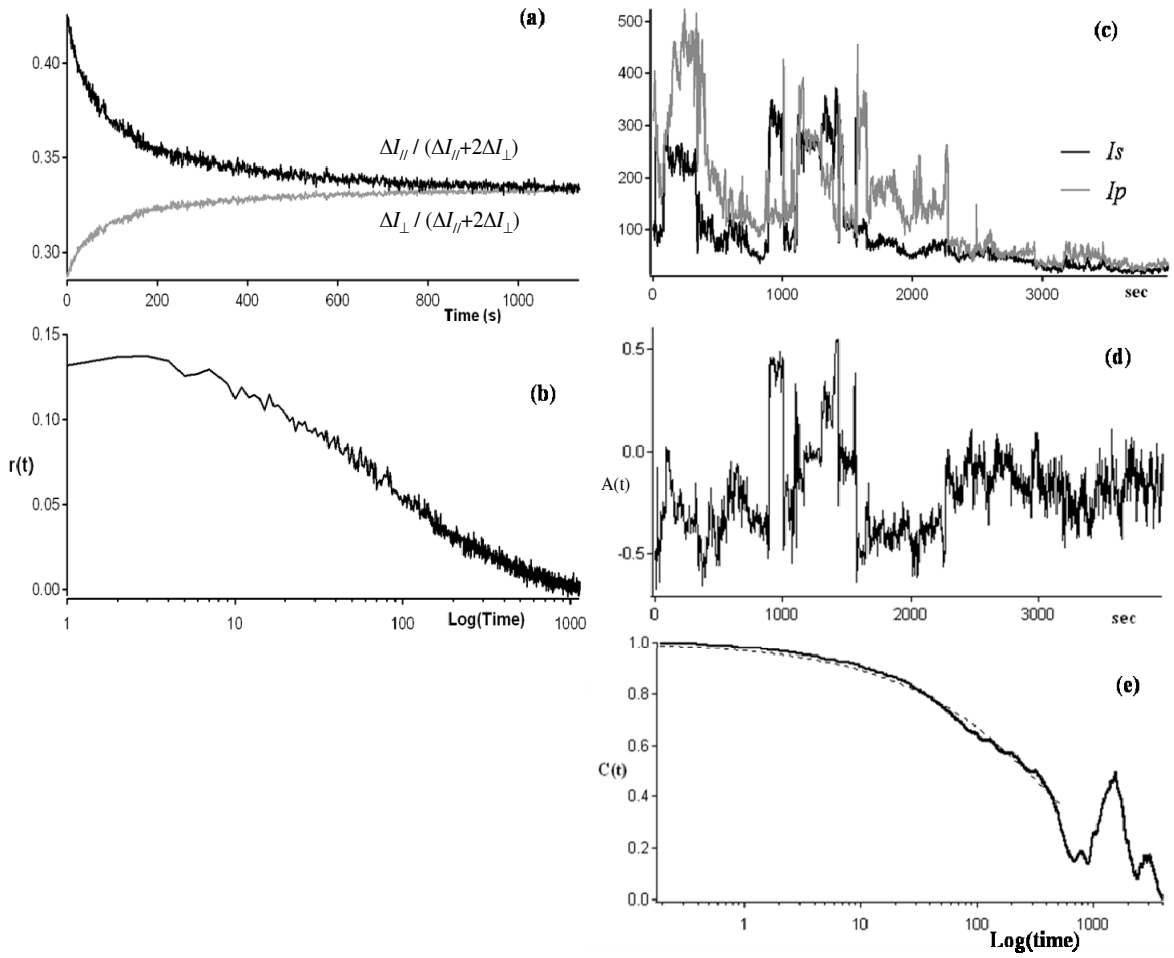

Figure 5.3: Anisotropy decay from ensemble experiment (left) and single molecule transient data (right). (a) shows the fluorescence signals from unbleached molecules, $\Delta I_{//}$ and $\Delta I_{\perp}$ normalized to $(\Delta I_{//} +2\Delta I_{\perp})$, which are used to calculate the anisotropy in (b). Raw data for single molecule transient are shown in (c), and I_s, I_p are used to calculate the reduced linear dichroism in (d). From (d), auto-correlation function is calculated, shown in (e).

Ensemble data are collected and sorted as $\Delta I_{//}$ and $\Delta I_{\perp}$, fluorescence signals parallel and perpendicular to the bleaching beam polarization, from the molecules that were not photobleached. To make clear how the polarization "hole" is filled as molecular orientations become more randomly distributed, $\Delta I_{//}$ and $\Delta I_{\perp}$ are normalized to $(\Delta I_{//} + 2\Delta I_{\perp})$, as shown in Figure 5.3(a). $\Delta I_{//}$ starts out low while $\Delta I_{\perp}$ is high, and eventually they become equal when the system is isotropic again. Fig. 5.3(b) shows the anisotropy as a function of time calculated by these two signals [Eq. 5.1], and decays to 0 when $\Delta I_{//} = \Delta I_{\perp}$. The decay is fit with the stretched exponential function [Eq. 5.7] to characterize the rotational time τ_{ens} and β_{ens}.

Fig. 5.3(c) shows the raw data for a single molecule transient, in which I_s and I_p are orthogonal fluorescence signals. The reduced linear dichroism signal $A(t)$ calculated from I_s and I_p [Eq. 5.2] is shown in Fig. 5.3(d). Note that the values of dichroism do not reach ± 1, and there are discrete large dichroism changes that suggest non-diffusion dynamics. The auto-correlation function of $A(t)$ is calculated and plotted on a logarithmic time scale, shown in Fig. 5.3(e). The dashed line is the fit to the stretched exponential function [Eq. 5.7] to obtain τ_{sm} and β_{sm} for single molecule transients. Statistically speaking, there is no need to constrain β within 0 and 1, although it is common practice when fitting to the stretched exponential as the values greater than one are non-physical (but could occur as a result of the statistical fluctuations). Rather than fitting all the points in the decay, the fit can be restricted to a certain time lag q, beyond which the standard errors will be greater than the estimated auto-correlation[25].

The average values for a set of 58 R6G single transients are calculated from individual fits of the correlation functions:

$$< \tau_{sm} >= \frac{1}{58}\sum_{i=1}^{58}\tau_i , < \beta_{sm} >= \frac{1}{58}\sum_{i=1}^{58}\beta_i \tag{5.9}$$

yielding $<\tau_{sm}>$ = 149.22 sec and $< \beta_{sm} >$ = 0.78, when fitted to time lag q with no constraint on β. When β was constrained to $0 < \beta \leq 1$, the fitting results yield $<\tau_{sm}>$ = 150.54 sec and $< \beta_{sm} >$ = 0.76. The difference is rather trivial and does not affect the shape of the distributions, except that all the $\beta_{sm} >1$ values become $\beta_{sm} = 1$.

The average ensemble relaxation time and β for the three PCA samples at their respective T_g + 2˚C are calculated as :

$$\begin{aligned} < \tau_{ens} >&= \frac{1}{3}\left[\tau_{ens(PCA1)} + \tau_{ens(PCA2)} + \tau_{ens(PCA3)}\right] \\ < \beta_{ens} >&= \frac{1}{3}\left[\beta_{ens(PCA1)} + \beta_{ens(PCA2)} + \beta_{ens(PCA3)}\right] \end{aligned} \tag{5.10}$$

The result of $<\tau_{ens}>$ = 132.46 sec agrees with the average of all single molecules, $<\tau_{sm}>$ 149.22 sec, while the value of $< \beta_{ens} >$ = 0.562 is smaller than the single-molecule result, $< \beta_{sm} >$ = 0.78. This discrepancy can be attributed to the fitting to the single molecule correlation functions, where statistical errors can bias the results when transient lengths are not long enough (this was discussed in the previous chapter). Nevertheless, the fact that β from both experiments is not equal to 1 clearly indicates that dynamics are not homogeneous in the polymer. Moreover, the smaller β in the ensemble data is evidential of the dynamics being heterogeneous.

If we sum up of all rotational correlation functions we can compare the "ensembled" single molecules to the bulk measurements. Equation 5.11 calculates the sum of all single molecule correlation functions, normalized to the first point:

$$C(t)_{sum} = \sum_{i=1}^{58} C_i(t) \tag{5.11}$$

Equation 5.12 combines all the ensemble anisotropy decays $r(t)$ obtained from the three ensemble samples at their respective T_g + 2 ˚C:

$$r(t)_{sum} = r(t)_{PCA1} + r(t)_{PCA2} + r(t)_{PCA3} \tag{5.12}$$

Both decays are depicted together in Figure 5.4, with the sum of all single molecule correlation functions shown as the red dashed line, and the sum of ensemble anisotropy shown as the dark line. We can see immediately that the two decays almost overlap. When fitting each of both decays to the stretched exponential function, the sum of single molecule correlation functions, $C(t)_{sum}$, yields $\tau_{sm,sum}$ = 84.66 sec and $\beta_{sm,sum}$ = 0.51; the sum of ensemble decays, $r(t)_{sum}$, yields $\tau_{ens,sum}$ = 132.69 sec and $\beta_{ens,sum}$ = 0.58. It is very clear that the superposition of all single molecules is a nonexponential decay that is almost identical to the ensemble relaxation in terms of β. Note that the ensemble results of τ and β calculated from Eq. 5.10 and 5.12 are the same, but fitting of $C(t)_{sum}$ gives $\tau_{sm,sum}$ and $\beta_{sm,sum}$ values that are smaller than the average of independently fitted trajectories, $<\tau_{sm}>$ and $<\beta_{sm}>$ [Eq. 5.9]. This effect can be rationalized by the fact that even if we sum up a series of single exponential functions (β = 1) with different decay times (τ), the overall function will not be a single exponential. Since our single molecule transients all have different τ and β, it can be expected that the sum of all correlation functions will be more "stretched" than the individual decays.

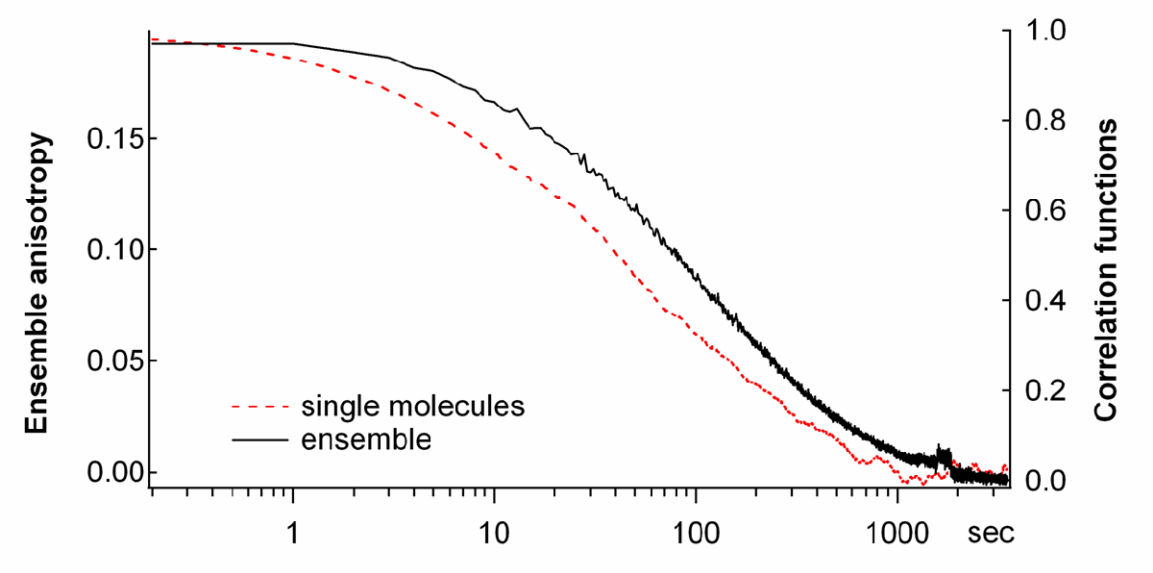

Figure 5.4: Comparison of ensemble anisotropy decay at T_g + 2 ˚C and the sum of all single molecule correlation functions. Both are fit with the KWW stretched exponential function, and the results for all single molecules are: $\tau_{sm,sum}$ = 84.66 sec, $\beta_{sm,sum}$ = 0.51; for the ensemble anisotropy decays: $\tau_{ens,sum}$ = 132.69 sec, and $\beta_{ens,sum}$ = 0.58. Time is on logarithmic scale.

This comparison demonstrates that the same properties are being measured in both experiments, and further confirms that the single-molecule experiment did not probe a subset of molecules that were not representative of the ensemble. The fitting to the stretched exponential function also yields $\beta < 1$ for both experiments, which suggests that the dynamics cannot be pure diffusion.

CONCLUSIONS

In this chapter, analysis of single molecule correlation functions for comparison to the ensemble measurements is presented. Polarization detection of emission from a single dipole through a high-NA objective is very sensitive to the relative position of the dipole in the collimated beam. The reduced linear dichroism calculated from the orthogonal fluorescence signals detected on the plane perpendicular to the objective axis will not be a simple cosine function of the azimuthal angle Φ, but dependent on both spherical angles (Φ, Θ), NA, and the index of refraction. This results in dichroism signals smaller than the ideal limits of $|\pm 1|$. The consequence of using high-NA optics, however, turns out to be a favorable situation, where the auto-correlation function of the measured dichroism signal from a single fluorophore undergoing pure rotation actually manifests a single exponential function, which has the same form as the optically measured bulk anisotropy decay. This analogy therefore enables us to compare the single molecule correlation times directly to the ensemble anisotropy decay times.

When comparing polymer rotational dynamics measured using the ensemble FRAP technique and single-molecule spectroscopy, both experiments yield coherent results for poly(cyclohexyl acrylate) at 2 ˚C above its glass transition temperature. The average correlation time from single transients matches the ensemble rotational time. Both the ensemble β and the average β for single molecule correlation functions are not equal to 1, with the ensemble β smaller than the average single-molecule β, suggesting the system has heterogeneous dynamics. Nevertheless, the dynamics cannot be described by an ensemble of molecules that are rotating with different diffusion constants.

Single-molecule spectroscopy has shown to be a unique tool for probing individual properties that are different from the bulk measurement. Rotational correlation functions for individual transients are very different from one another, and each decay is unlike the bulk decay, either. Yet, as discussed in this chapter, the average of all rotational constants is the same as the ensemble anisotropy relaxation time, which in a way validates the applicability of single molecule auto-correlation functions for characterizing rotational dynamics. Referring back to the very first question about how to describe on a molecular basis the nonexponential relaxations observed in non-crystalline systems, our results of single-molecule measurements suggest that rather than concluding the system is *heterogeneous* (consisting of localized pure diffusions with different time scales), or *homogeneous* (in which each single component has identical nonexponential decays as the bulk decay), one should regard the underlying dynamics as a complex inhomogeneous system that consists of molecules with different rotational constants, but each of them may not be a pure diffusion tensor. Although single molecule transients which cannot be observed for an infinite long period will produce inherent statistical errors that need to be taken into consideration when interpreting results[30], our conclusion remains the same, i.e., the system is not pure diffusion. Figure 5.5 can serve as a schematic summary of our discussions on the microscopic scenarios for nonexponential dynamics in polymers and other glass-forming materials.

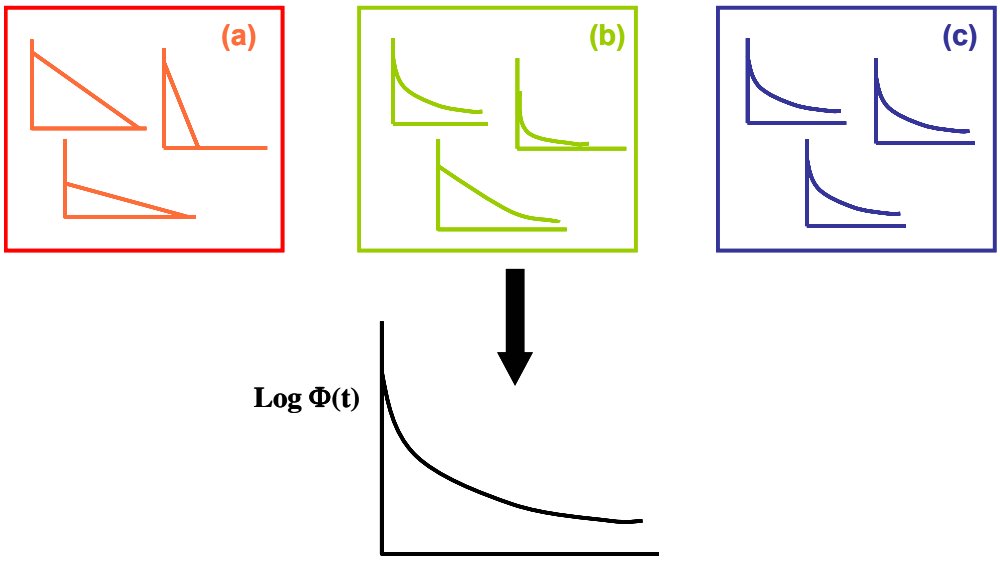

Figure 5.5: Possible scenarios for describing a bulk nonexponential decay. (a) is a heterogeneous extreme in which each molecule relaxes in single exponential fashions, but with different decay times; (c) is a homogeneous extreme in which all molecules exhibit identical nonexponential relaxations; and (b) depicts an intermediate case consisting of different relaxation behaviors, which may and may not be single exponential decays.

Future work can include investigation of non-diffusion models which can produce nonexponential decays similar to those observed in single-molecule experiments. There is still room for improvement of single-molecule data quality, such as extending transient lifetime, improving signal-to-noise ratio, and employing a 3-dimensional determination of the dipole orientation. Analytical methods other than auto-correlation functions can also be explored, and measuring faster dynamics at higher temperatures may also reduce statistical errors inherent in finite-sampling situations.

REFERENCES

(1) Stickel, F.; Fischer, E. W.; Richert, R. *J. Chem. Phys.* **1995**, *102*, 6251.

(2) Phillips, J. C. *Rep. Prog. Phys.* **1996**, *59*, 1133.

(3) Ediger, M.D.; Angell,C.A.; Nagel,S. R. *J. Phys. Chem.* **1996**, *100*, 13200.

(4) Böhmer, R.;Chamberlin, R.V.; Diezemann, G.; Geil, B.; Heuer, A.; Hinze,G.; Kuebler,S.C.; Richert,R.; Schiener,B.; Sillescu,H.; Spiess,H.W.; Tracht,U.; Wilhelm,M. *J. Non-Crys. Solids* **1998**, *235-237*, 1.

(5) Sillescu, H. *J. Non-Crys. Solids* **1999**, *243*, 81.

(6) Angell, C. A.; Ngai, K. L.; McKenna, G. B.; McMillan, P.F.; Martin, S.W. *J. Appl. Phys.* **2000**, *88*, 3113.

(7) Richert, R. *J. Phys.: Condens. Matter* **2002**, *14*, R703.

(8) Simdyankin, S. I.; Mousseau, N. *Phys. Rev. E* **2003**, *68*, 041110.

(9) Lubchenko, V.; Wolynes, P. G. *Annu. Rev. Phys. Chem* **2007**, *58*, 235.

(10) Basché, T.; Moerner, W. E.; Orrit, M.; Wild, U. P. *Single-molecule optical detection, imaging and spectroscopy*; VCH: Cambridge, 1997.

(11) Xie, X. S.; Trautman, J. K. *Annu. Rev. Phys. Chem* **1998**, *49*, 411.

(12) Ha, T.; Glass, J.; Enderle, T.; Chemla, D. S.; Weiss, S. *Phys. Rev. Lett.* **1998**, *80*, 2093.

(13) Barkai, E.; Jung, Y.J.; Silbey, R. *Ann. Rev. Phys. Chem.* **2004**, *55*, 457

(14) Moerner, W. E.; Fromm, D. P. *Rev. Sci. Instrum.* **2003**, *74*, 3597.

(15) Tomczak, N.; Vallee, R. A. L.; van Dijk, E. M. H. P.; Garcia-Parajo, M.; Kuipers, L.; van Hulst, N. F.; Vancso, G. J. *Eur. Polym. J.* **2004**, *40*, 1001.

(16) Barbara, P. F. *Acc. Chem. Res.* **2005**, *38*, 503.

(17) Rosenberg, S. A.; Quinlan, M. E.; Forkey, J. N.; Goldman, Y. E. *Acc. Chem. Res.* **2005**, *38*, 583.

(18) Michalet, X.; Weiss, S.; Jäger, M. *Chem. Rev.* **2006**, *106*, 1785.

(19) Wegener, W. A. *Biophys. J.* **1984**, *46*, 795.

(20) Velez, M.; Axelrod, D. *Biophys. J.* **1988**, *53*, 575.

(21) Cicerone, M. T.; Ediger, M. D. *J. Phys. Chem.* **1993**, *97*, 10489.

(22) Wang, C.-Y.; Ediger, M. D. *J. Phys. Chem. B* **1999**, *103*, 4177.

(23) Deschenes, L. A. *Single-molecule studies of heterogeneous dynamics near the glass transition*, The University of Texas at Austin, 2002.

(24) Berne, B. J.; Pecora, R. *Dynamic Light Scattering*; Dover: Mineola, N.Y., 2000.

(25) Box, G. E. P.; Jenkins, G. M. *Time Series Analysis Forecasting and Control*; Holden-Day: San Francisco, 1970.

(26) Brockwell, P. J.; Davis, R. A. *Time series: theory and methods*, 2nd ed.; Springer-Verlag: New York, NY, 1991.

(27) Hinze, G.; Diezemann, G.; Basché, T. *Phys. Rev. Lett.* **2005**, *93*, 203001.

(28) Fourkas, J. T. *Opt. Lett.* **2001**, *26*, 211.

(29) Wei, C.-Y. J.; Kim, Y. H.; Darst, R. K.; Rossky, P. J.; Vanden Bout, D. A. *Phys. Rev. Lett.* **2005**, *95*, 173001.

(30) Lu, C.-Y.; Vanden Bout, D. A. *J. Chem. Phys.* **2006**, *125*, 124701.

Appendix A

LABVIEW VI FOR FRAP EXPERIMENT

This is the main LabVIEW VI used to do FRAP experiment, including data-collection and photobleaching. The software version is LabVIEW 7.0.

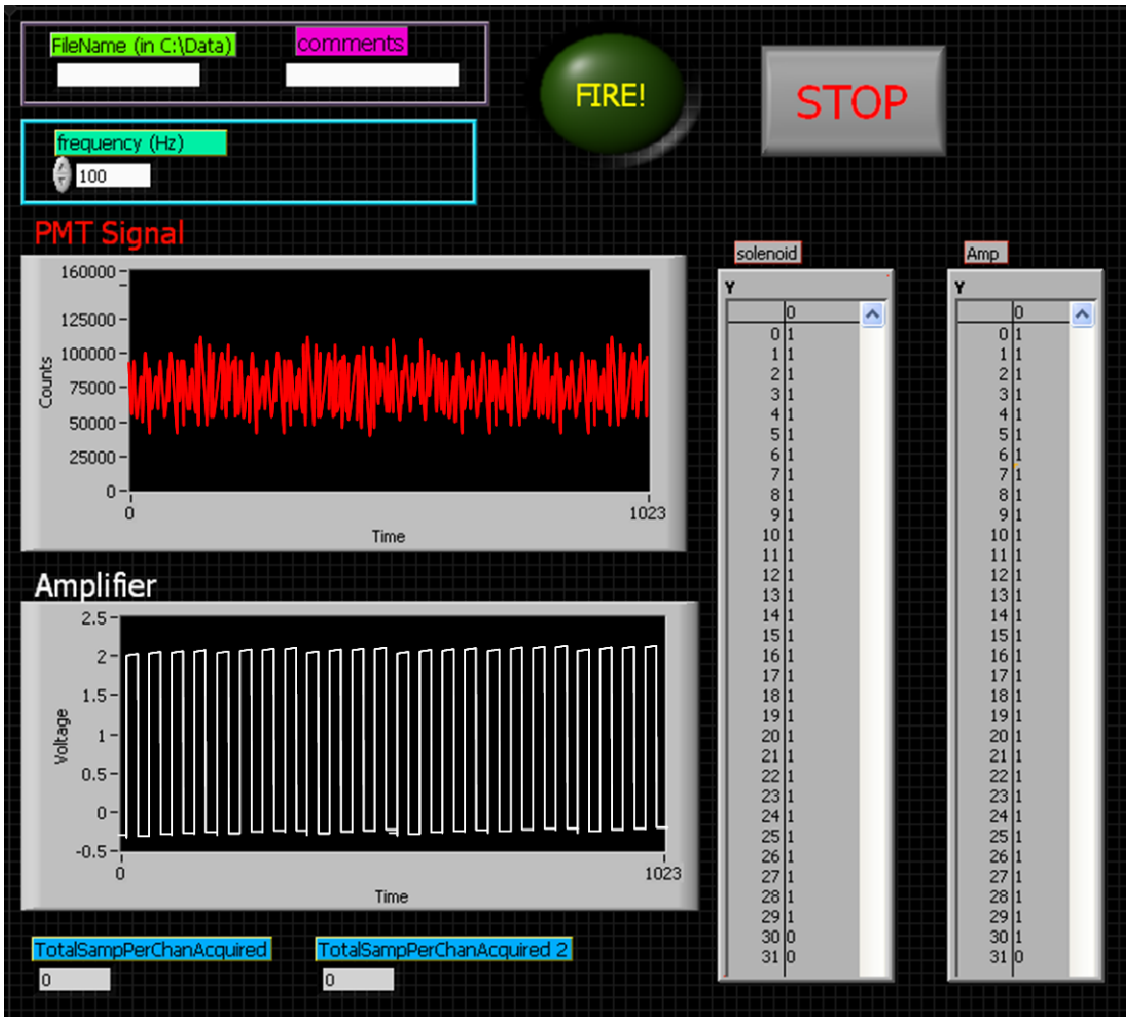

Figure A.1: Front Panel of FRAP.vi.

The Front Panel description of FRAP.vi:

(1) Counter1 measures the photon counts from PMT, using Counter0 as the source of sample clock, counting the number of "period ticks" in each "measurement time". Counter0 clock is triggered by the digital pulse from the function generator. When the PMT is off or when the signal frequency is smaller than the sampling rate (1/measurement time), the program fails because it doesn't support the DuplicateCountPrevention function.

(2) Analog input reads the amplifier "monitor output voltage", which is 1/200 of the actual output voltage supplied to the EOM.

(3) Use the "solenoid" and "amp" digital table to control the bleaching mechanism. "1" pulls the solenoid and removes the filter. "1" disables the output of the voltage amplifier. “0” puts the filter back and enable the voltage amplifier output. Each Y point is 100ms (e.g. to bleach for 3 sec, enter 30 columns of “1”). The solenoid has a slower response time than the amplifier so need to turn it on and off before the amplifier (give it "0" one digit before the amplifier).

(4) Must enter a name for the file to be saved in “FileName” or an error message will occur. Type in any information regarding experimental conditions in “Comments” so it will be saved in the text file as well. Run the vi, and click “FIRE” to photobleach the sample. Data is saved as two text waves “Photon_counts” and “Amplifier”.

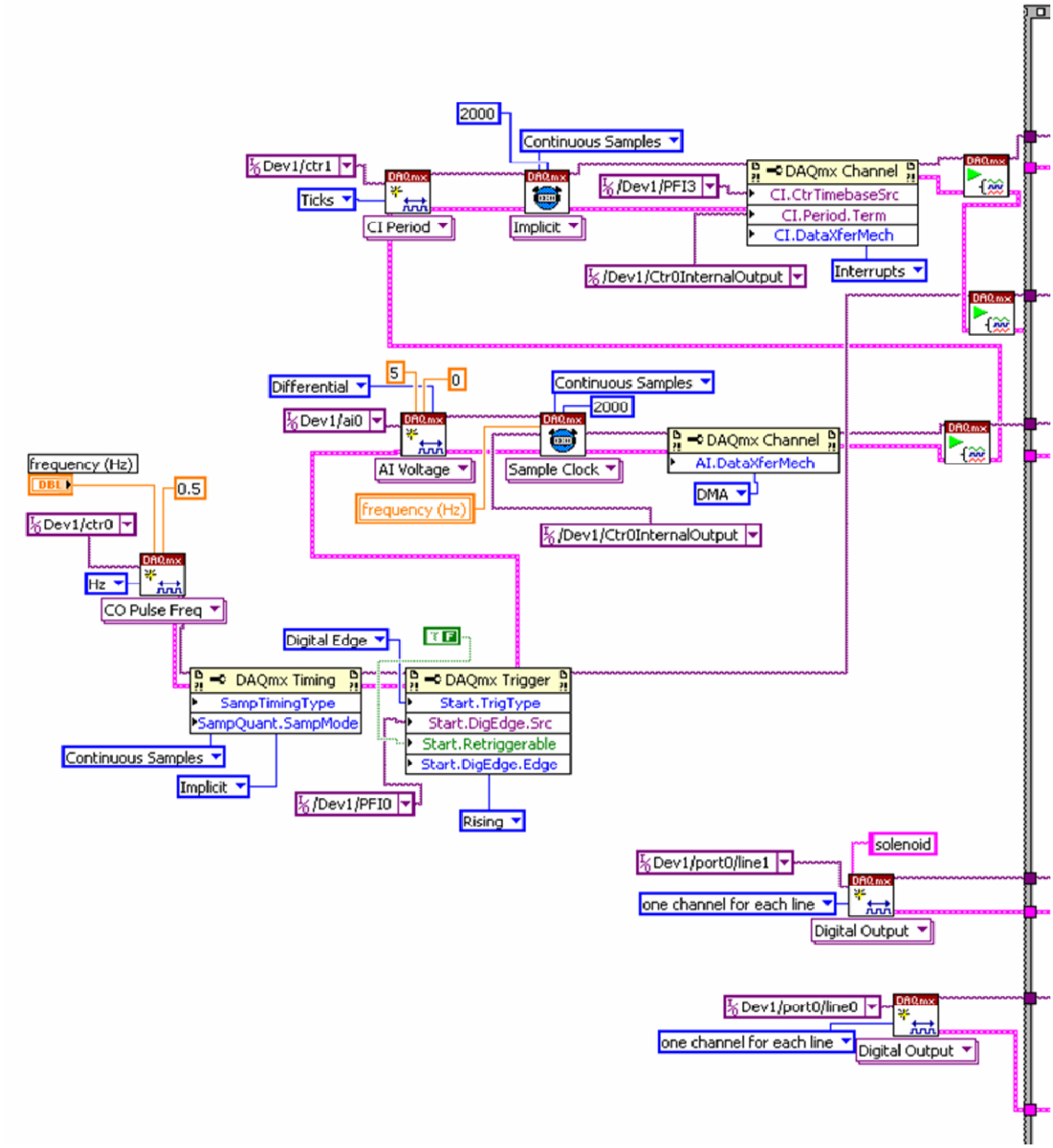

Figure A.2: Block Diagram of FRAP.vi - Part 1. The diagram continues on the right-hand side (Figure A.3).

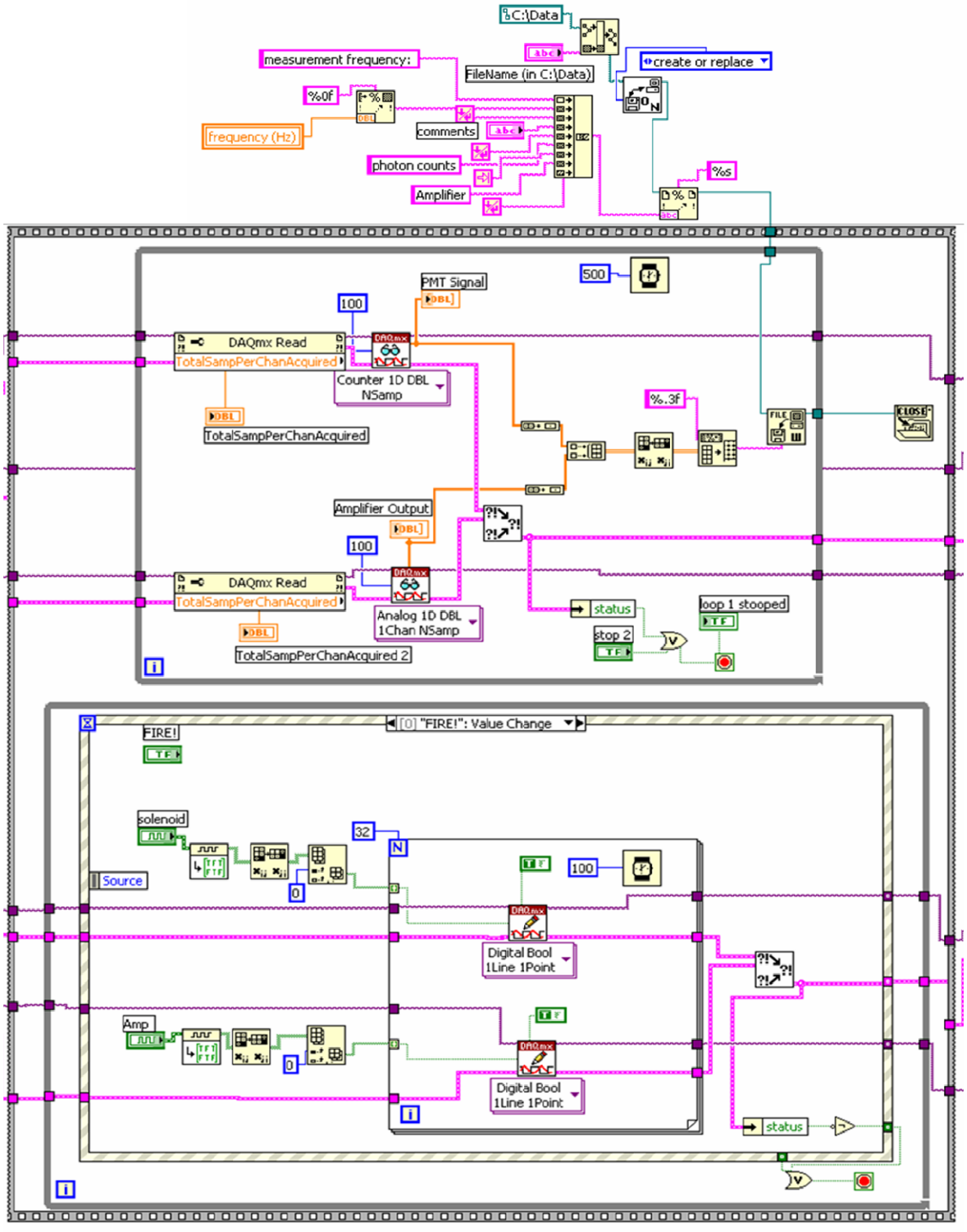

Figure A.3: Block Diagram of FRAP.vi - Part 2.

Description of channel configuration:

The LabVIEW PCI 6014 DAQ card has a total of 64 channels (which will be referred to as I/O:) including two counters. One counter (I/O ctr0) is used to generate a pulse train with a certain period, also called the measurement time; while the second counter (I/O ctr1) counts the number of events in each period. The default frequency (1/ measurement time) is 100 Hz. This pulse train (**CO Pulse Freq**) is triggered by a TTL pulse from the function generator (I/O PFI0) so it is synchronized to the polarization modulation.

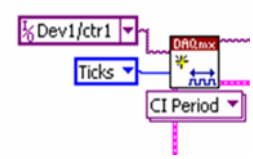

CI Period configures counter 1 to count the number of "ticks" within each period of the pulse train generated from Ctr0, thus CI PeriodTerminal = I/O Ctr0InternalOutput (Ctr0 and Ctr1 are interconnected on DAQ so it's unnecessary to connect the physical pins with a wire). CI CtrTimeBaseSource is the signal that we want to count, so the detector is connected to I/O PFI3. CI DataTransferMechanism is set as Interrupts because there is only one DMA (Direct Memory Access) transfer route, which is assigned to the **AI Voltage** task (switching them around causes unsynchronized sample acquisition rate in **AI**).

AI Voltage measures the monitor voltage of the amplifier (I/O ai0), using I/O Ctr0InternalOutput as the **sample clock source**. Take note that timing control is different for analog and counter tasks. For counters, the "timing" is when the event happens so cannot be controlled by a "sample clock", and therefore timing is **implicit**. For an analog task, a clock must be assigned so it will take measurements at each clock tick.

Select Continuous Samples to create buffered sampling for better accuracy. **CI** and **AI** samples are then read from the buffer every 500 ms and concatenated into two parallel arrays. The commands to create/close the file for writing the arrays are placed outside the **While** loop, so that the file is opened/closed only once.

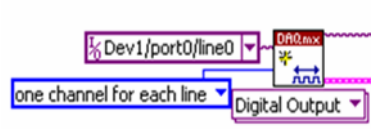

The other important function of the FRAP.vi is to control the photobleaching mechanism. The goal is to produce linearly-polarized, high-intensity bleaching beam, therefore polarization modulation needs to be paused while the neutral density filter is removed from the beam path. This is achieved by outputting TTL signals to control the voltage amplifier (I/O line0) and the solenoid (I/O line1). Because the solenoid has a slower response time than the amplifier, two separate digital Booleans are used so that the solenoid can receive pull/release signaling before the amplifier (the Boolean sequences are controlled by the front panel). Each TTL lasts 100 ms, so change the iteration number accordingly to create desired bleaching period. A high-TTL signal ("1") will disable the amplifier (pause polarization modulation) and pull the solenoid (remove ND filter); a low-TTL signal ("0") will enable the amplifier output (start polarization modulation) and release the solenoid (put ND filter back).

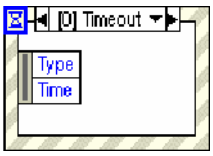

Event Structure is configured so that digital arrays will be sent when there is "Value Change" of the "FIRE" Boolean control in the front panel. This is designed so that we can first record initial fluorescence signals and then photobleach the sample to create anisotropy by clicking on the "FIRE" command.

Initial alignment

This Align.vi is used to monitor the signals so that the ½-wave plate can be fine-adjusted until the parallel and perpendicular signals have the same intensities. It splits the incoming signal array into two arrays and plots them on the same graph.

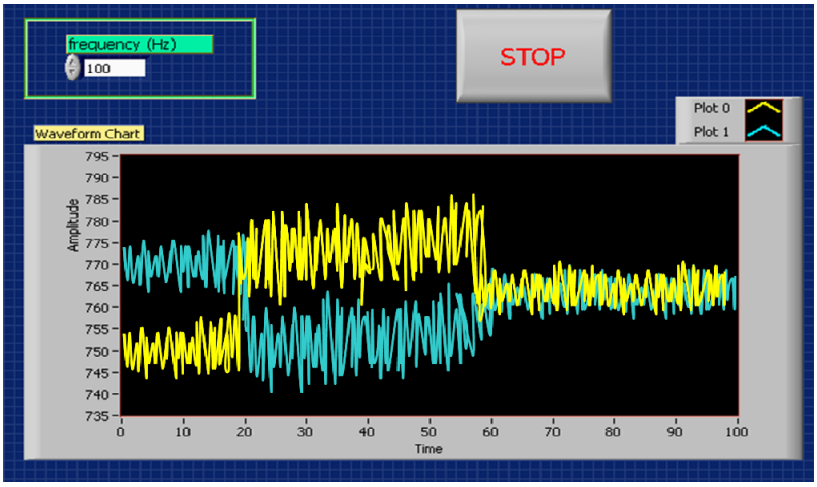

Figure A.4: Front panel of Align.vi.

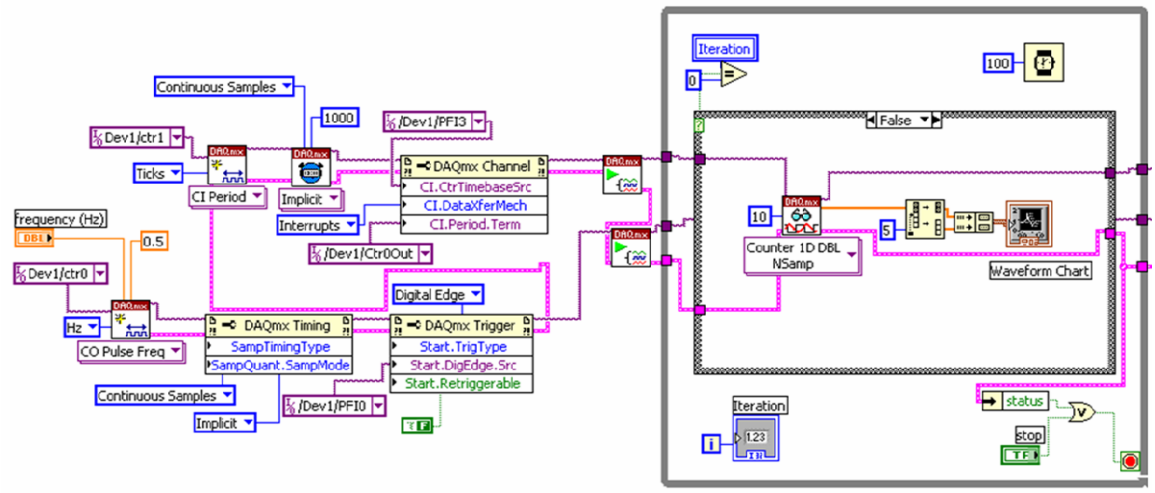

Figure A.5: Block Diagram of Align.vi.

IGOR PROCEDURE FOR ANALYSING FRAP DATA

The following procedure is for analyzing data taken at modulation frequency of 10 Hz, acquisition frequency of 100 Hz. First sort the raw wave "Photon_counts" into before-bleaching:"raw"(delete the first point), and after-bleaching:"raw_ab"(omit first 0.2s of data). Each wave starts with the parallel signal (when amplifier is 0).

```
//This separates parallel and perpendicular signals for the before-bleaching data//
Function AssignIni()
    wave raw
    SetScale/P x 0, 0.01," ",raw
    Make/o/n=(numpnts(raw)/2) para_raw, perp_raw
    Variable i=0
    For (i=0; i<(numpnts(para_raw)); i+=1)
        para_raw[i*5, i*5+4] = raw [i*5+p]        //first 5 points in a cycle are parallel//
        perp_raw[i*5,i*5+4] = raw[5*i+5+p]     //next 5 points are perpendicular//
    Endfor
    DeletePoints i-1, 1, para_raw, perp_raw
    SetScale/P x 0, 0.01," ", para_raw, perp_raw
    Make/o/n=(numpnts(para_raw)/5) para0, perp0
    Variable j=0
    For (j=0; j<(numpnts(para0)); j+=1)              //average every 5 points//
        para0[j] = mean(para_raw, pnt2x(para_raw,5*j), pnt2x(para_raw,4+5*j))
        perp0[j] = mean(perp_raw, pnt2x(perp_raw,5*j), pnt2x(perp_raw,4+5*j))
    Endfor
    SetScale/P x 0,0.05,"", perp0,para0
    Display/N= Raw_Signals para0, perp0;
    ModifyGraph rgb(perp0)=(0,43520,65280);Legend/C/N=text0/F=0/A=RB;
    Label left "counts/0.01sec" ;Label bottom "sec";
    TextBox/C/N=text1/F=0/A=MT "Raw signals before bleaching"
End

// This separates parallel and perpendicular signals for the after-bleaching data//
Function AssignAB()
    wave raw_ab
    SetScale/P x 0, 0.01, " ", raw_ab
    Make/o/n=(numpnts(raw_ab)/2) para, perp, para_time, perp_time
    Duplicate/o raw_ab, xarray
    xarray=x
    variable i
    For (i=0; i<(numpnts(para)); i+=1)
        para[i*5, i*5+4] = raw_ab [i*5+p]
        para_time[i*5,i*5+4] = xarray[i*5+p]
        perp[i*5,i*5+4] = raw_ab[5*i+5+p]
        perp_time[i*5,i*5+4]= xarray[i*5+5+p]
    Endfor
    DeletePoints i-1, 1, para, para_time, perp, perp_time
End
```

```
//This gives the binned data of parallel and perpendicular signals in each modulation//
Function AssignAvg()
    wave para, perp , para_time, perp_time
    make/O/N=(numpnts(para)/5) para_avg=0, perp_avg=0, para_avgtime=0, perp_avgtime=0
    variable i
    for (i=0; i<(numpnts(para_avg)); i+=1)
        para_avg[i] = mean(para, pnt2x(para,5*i), pnt2x(para,4+5*i))
        para_avgtime[i]=para_time[5*i]
        perp_avg[i] = mean(perp, pnt2x(perp,5*i), pnt2x(perp,4+5*i))
        perp_avgtime[i]=perp_time[5*i]
    endfor
    DeletePoints i-1, 1, para_avg, para_avgtime, perp_avg, perp_avgtime
    Display/N=AfterBleach para_avg vs para_avgtime;
    AppendToGraph perp_avg vs perp_avgtime;ModifyGraph
    Label left "counts/0.01sec";Label bottom "sec";
    TextBox/C/N=text1/F=0/A=MT/E=2 "Raw signals after bleaching"
End

//This corrects for the intensities using the initial ratio//
Function AssignCorre1()
    Wave para0, perp0, para_avg, perp_avg, para_avgtime
    Duplicate/O para_avg, para_cori    //correts the parallel signals
    Duplicate/O perp_avg, perp_cori    //these two are the same
    variable ratio
    ratio = mean(para0)/mean(perp0)
    para_cori= para_avg/ratio
End

//Calculates anisotropy using unbinned data//
Function Anis()
    wave para, para0, perp0, perp
    duplicate/O para, dpara
    duplicate/O perp, dperp, ani
    ani=0
    dpara = mean(para0)-para
    dperp=mean(perp0)-perp
    ani=(dpara-dperp)/(dpara+2*dperp)
End

//Calculates anisotropy using binned points in each modulation cycle//
Function AnisRaw()
    wave para_avg, para0, perp0, perp_avg
    duplicate/O para_avg, dpara_avg, dpara_n0    // _n0 stands for normalized raw data
    duplicate/O perp_avg, dperp_avg, dperp_n0, ani_avg
    ani_avg=0
    dpara_avg = mean(para0)-para_avg
    dperp_avg=mean(perp0)-perp_avg
    dpara_n0=dpara_avg/(dpara_avg+2*dperp_avg)
    dperp_n0=dperp_avg/(dpara_avg+2*dperp_avg)
    ani_avg=dpara_n0-dperp_n0
    Display/N=DeltaN dpara_n0, dperp_n0 vs para_avgtime;
    ModifyGraph rgb(dperp_n0)=(0,43520,65280);Legend/C/N=text0/F=0/A=RB
    Label left "normalized delta";Label bottom "sec";
```

```
    TextBox/C/N=text1/F=0/A=MT/E=2 "Normalized raw delta signals"
    Display/N=Anisotropy ani_avg vs para_avgtime;
    ModifyGraph rgb=(32768,65280,49152);ModifyGraph lowTrip(left)=0.01
    Label left "anisotropy";Label bottom "sec";
    TextBox/C/N=text0/F=0/A=MT/E=2 "Raw Anisotropy"
End

//Calculates anisotropy based on signals corrected using the initial ratios//
Function AnisCorre1()
    wave para0, perp0,para_avg, perp_avg, para_avgtime
    duplicate/O para_avg, dpara_cori, dperp_cori, dpara_ni, dperp_ni, ani_cori //dpara_ni is the
    variable ratio                                          //normalized delta para signals
    ratio = mean(para0)/mean(perp0)
    dpara_cori = (mean(para0)-para_avg)/ratio
    dperp_cori= mean(perp0)-perp_avg
    dpara_ni = dpara_cori/(dpara_cori+2*dperp_cori)
    dperp_ni=dperp_cori/(dpara_cori+2*dperp_cori)
    ani_cori= dpara_ni-dperp_ni
    Display dpara_ni, dperp_ni vs para_avgtime
    ModifyGraph rgb(dperp_ni)=(0,43520,65280);Legend/C/N=text0/F=0/A=RB ;
    Label left "normalized delta";Label bottom "sec" ;
    TextBox/C/N=text1/F=0/A=MT/E=2 "Normalized delta signals \r(corrected to initial ratio)
    Display ani_cori vs para_avgtime
    ModifyGraph rgb=(65280,32768,58880); ModifyGraph lowTrip(left)=0.01
    Label left "corrected anisotropy" ;Label bottom "sec";
    TextBox/C/N=text0/F=0/A=MT/E=2 "Corrected Anisotropy (to initial ratio)
End

//Calculates anisotropy based on signals corrected to the final values that make anisotropy 0//
Function AnisCorre2()
    wave dpara_avg, dperp_avg
    variable a, b
    wavestats/q dpara_avg
    a=V_endrow
    b=mean(dpara_avg, pnt2x(dpara_avg, a-200), pnt2x(dpara_avg, a))
    variable c, d, e
    wavestats/q dperp_avg
    c=V_endrow
    d=mean(dperp_avg, pnt2x(dperp_avg, c-200), pnt2x(dperp_avg, c))
    e= b/d
    print a, b, c, d, e
    duplicate/o dpara_avg, dpara_corf, dperp_corf, dpara_nf, dperp_nf, ani_corf
    dpara_corf =dpara_avg/e
    dperp_corf=dperp_avg
    dpara_nf=dpara_corf/(dpara_corf+2*dperp_corf)
    dperp_nf=dperp_corf/(dpara_corf+2*dperp_corf)
    ani_corf=dpara_nf-dperp_nf
    Display ani_corf vs para_avgtime
    ModifyGraph rgb=(51456,44032,58880); ModifyGraph lowTrip(left)=0.01
    Label left "corrected anisotropy"; Label bottom "sec"
    TextBox/C/N=text0/F=0/A=MT/E=2 "Corrected Anisotropy (to final values)"
    Display dpara_nf, dperp_nf vs para_avgtime
    ModifyGraph rgb(dperp_nf)=(0,43520,65280); Legend/C/N=text0/F=0/A=RB
```

```
    Label left "normalized delta"; Label bottom "sec"
    TextBox/C/N=text1/F=0/A=MT/E=2 “Normalized delta signals \r(corrected to final values)"
End

//Adds to the equation the fit error & coefficient parameters//
Function addeqn(fit,error)
    wave fit, error          // input must be two waves W_coef & W_sigma
    variable tkww, bkww, etkww, ebkww, correlationtime
    string final
    tkww = fit [2]           //in stretched exponential function Tkww is parameter k2
    bkww = fit [1]            // in stretched exponential funtion bkww is parameter k1 (amp is k0)
    etkww = error [2]
    ebkww = error [1]
    final = "\[1\F'symbol't\F]1\BKWW\M=\t" + num2str(tkww) + " ± " + num2str(etkww)
    final = final +"\r\[1\F'symbol'b\F]1\BKWW\M=\t" + num2str(bkww) + " ± " + num2str(ebkww)
    TextBox/A=RC/F=0 final
End
```

Although “Decimation” is a nice command to bin data, it cannot be written in a user-defined function. (Type #include<decimation> in the procedure to activate this macro.)

```
//This bins and plots all data //
Function bindata(bin)       // Usually bin size =10//
    variable bin
    Wave para_avg, perp_avg
    Make/O/N= (numpnts(para_avg)/bin) para_avgb, perp_avgb, time2
    SetScale/P x 0, (0.1*bin), "", para_avgb, perp_avgb, time2
    time2=x
    variable i
    For (i=0; i<(numpnts(para_avgb)); i+=1)
        wavestats/Q/R=(bin*i, bin*i+bin-1) para_avg
        para_avgb[i] =V_avg
    Endfor
    variable j
    For (j=0; j<(numpnts(perp_avgb)); j+=1)
        wavestats/Q/R=(bin*j, bin*j+bin-1) perp_avg
        perp_avgb[j] =V_avg
    Endfor
    wave para_avgb, perp_avgb
    Duplicate/O para_avgb, dpara_avgb, dperp_avgb, dpara_n0b, dperp_n0b, ani_avgb
    dpara_avgb = mean(para0)-para_avgb
    dperp_avgb=mean(perp0)-perp_avgb
    dpara_n0b=dpara_avgb/(dpara_avgb+2*dperp_avgb)
    dperp_n0b=dperp_avgb/(dpara_avgb+2*dperp_avgb)
    ani_avgb=dpara_n0b-dperp_n0b
    Display/N=AfterBleach_bin para_avgb , perp_avgb
    ModifyGraph rgb(perp_avgb)=(0,43520,65280)
    Legend/C/N=text0/F=0/A=LB; Label left "counts/0.01sec"; Label bottom "sec"
    TextBox/C/N=text1/F=0/A=MT/E=2 "Signals after bleaching(binned/sec)"
    Display/N=Delta_bin dpara_n0b, dperp_n0b
    ModifyGraph rgb(dperp_n0b)=(0,43520,65280)
    Legend/C/N=text0/F=0/A=RB; Label left "normalized delta"; Label bottom "sec"
```

```
    TextBox/C/N=text1/F=0/A=MT/E=2 "Normalized delta signals (binned /sec)"
    Display/N=Anisotropy_bin ani_avgb vs time2
    ModifyGraph lowTrip(left)=0.01;ModifyGraph rgb=(32768,65280,49152)
    Legend/C/N=text1/F=0/A=RC;Label left "Anisotropy (binned/sec)";Label bottom "sec"
    TextBox/C/N=text0/F=0/A=MT/E=2 "Anisotropy (binned/sec)"
End

//Calculates bleach depth//
Function bleachdepth()
    Wave para0, para_avg, perp0, perp_avg
    variable a, b, c, d, e, f
    Wave bdepth
    Variable/G index          //If only analyzing one data file, omit the “Variable/G index”.
    wavestats/q para0
    a=V_avg
    b=mean(para_avg, pnt2x(para_avg, 0), pnt2x(para_avg, 10))
    c= (a-b)/a
    bdepth[index]=c
    printf "para bleach depth is %g\r", c
    wavestats/q perp0
    d=V_avg
    e=mean(perp_avg, pnt2x(perp_avg, 0), pnt2x(perp_avg, 10))
    f= (d-e)/d
    printf "para bleach depth is %g\r", f
End


//Calls out the filename and put it on the graph//
Function addfilename()
    SVAR S_filename
    TextBox/A=MT/F=0 S_filename
End


//This fits anisotropy to the stretched exponential by changing the initial guess values//
Function FitAni(ani_avg, para_avgtime)
    Wave ani_avg, para_avgtime
    Wave Amp, Beta, Tau
    Variable/G iA=0.4 ,iB=0.5 , iT=50, iy0=0
    Variable/G V_FitQuitReason, V_FitError =0
    Variable/G FitNum=0
    Variable/G Index
    Make/D/N=4/O W_coef
    W_coef [0]= {iA, iB, iT, iy0}
    Make/O/T/N=2 T_Constraints
    T_constraints[0]={"K1>0", "K1<1"}
    Print "test1"
    FuncFit stretched W_coef ani_avg /X=para_avgtime /D/C=T_Constraints
    FitNum +=1

    if (V_FitQuitReason!=0 || V_FitError!=0)
        print "test2"
        W_coef[0]={iA, iB,iT*0.1, iy0}
```

```
        V_FitError=0
        FuncFit stretched W_coef ani_avg /X=para_avgtime /D/C=T_Constraints
        FitNum+=1
    Endif

    if (V_FitQuitReason!=0 || V_FitError!=0)
        print "test3"
        W_coef[0]={iA, iB,iT*05, iy0}
        V_fitError=0
        FuncFit stretched W_coef ani_avg /X=para_avgtime /D/C=T_Constraints
        FitNum+=1
    Endif

    if (V_FitQuitReason!=0 || V_fitError!=0)
        print "test4"
        W_coef[0]={iA, iB,iT*2, iy0}
        V_fitError=0
        FuncFit stretched W_coef ani_avg /X=para_avgtime /D/C=T_Constraints
        FitNum+=1
    Endif
End
```

This will process each data file and save the results into designated waves. Need to upload the files one by one manually.

```
Function doeverything()
    Wave/T f_name
    Variable/G index     //Index is the counter for appending results
    SVAR s_filename
    f_name[index] = s_filename
    Wave Amp, Beta, Tau, Amp_b, Beta_b, Tau_b    //make these waves first
    Assignini()
    Assignab()
    AssignAvg()
    AnisRaw()
    Bleachdepth()
    fitani(ani_avg, para_avgtime)
    Wave W_coef
    Amp[index]=W_coef[0]
    Beta[index]=W_coef[1]
    Tau[index]=W_coef[2]
    Bindata(10)
    fitani(ani_avgb, time2)
    Amp_b[index]=W_coef[0]
    Beta_b[index]=W_coef[1]
    Tau_b[index]=W_coef[2]
    index += 1
    Save/J/M="\r\n"/W/F/I raw,raw_ab     //saves the sorted raw and raw_ab into a new file
End
```

```
//kill graphs before executing the next “doeverything”//
Function killgraphs()
    Dowindow/K Raw_signals
    Dowindow/K AfterBleach
    DoWindow/K DeltaN
    DoWindow/K Anisotropy
    Dowindow/K AfterBleach_bin
    DoWindow/K Delta_bin
    DoWindow/K Anisotropy_bin
    killwaves/A/Z
End
```

The Stretched Exponential function and WLF equation.

```
Function stretched(w,t) : FitFunc
    Wave w
    Variable t
    //CurveFitDialog/ These comments were created by the Curve Fitting dialog. Altering them will
    //CurveFitDialog/ make the function less convenient to work with in the Curve Fitting dialog.
    //CurveFitDialog/ Equation:
    //CurveFitDialog/ f(t) = y0+amp*exp(-(t/tau)^beta)
    //CurveFitDialog/ End of Equation
    //CurveFitDialog/ Independent Variables 1
    //CurveFitDialog/ t
    //CurveFitDialog/ Coefficients 4
    //CurveFitDialog/ w[0] = amp
    //CurveFitDialog/ w[1] = beta
    //CurveFitDialog/ w[2] = tau
    //CurveFitDialog/ w[3] = y0
    return w[3]+w[0]*exp(-(t/w[2])^w[1])
End

Function WLF(w,T) : FitFunc
    Wave w
    Variable T
    //CurveFitDialog/ These comments were created by the Curve Fitting dialog. Altering them will
    //CurveFitDialog/ make the function less convenient to work with in the Curve Fitting dialog.
    //CurveFitDialog/ Equation:
    //CurveFitDialog/ f(T) = A+(-c1*(T-Tg)/(c2+T-Tg))
    //CurveFitDialog/ End of Equation
    //CurveFitDialog/ Independent Variables 1
    //CurveFitDialog/ T
    //CurveFitDialog/ Coefficients 4
    //CurveFitDialog/ w[0] = c1
    //CurveFitDialog/ w[1] = c2
    //CurveFitDialog/ w[2] = Tg
    //CurveFitDialog/ w[3] = A
    return w[3]+(-w[0]*(T-w[2])/(w[1]+T-w[2]))
End
```

FRAP RESULTS FOR PPEMA

Anisotropy relaxation for Poly(2-phenylethyl methacrylate) was also measured by ensemble FRAP, following the sample preparation and experimental procedure described in Chapter 2. Experiment temperature was controlled by a water chiller. The T_g value reported by the manufacturer and literature for PPEMA is 26 ˚C, and fitting to the WLF equation yields the same T_g.

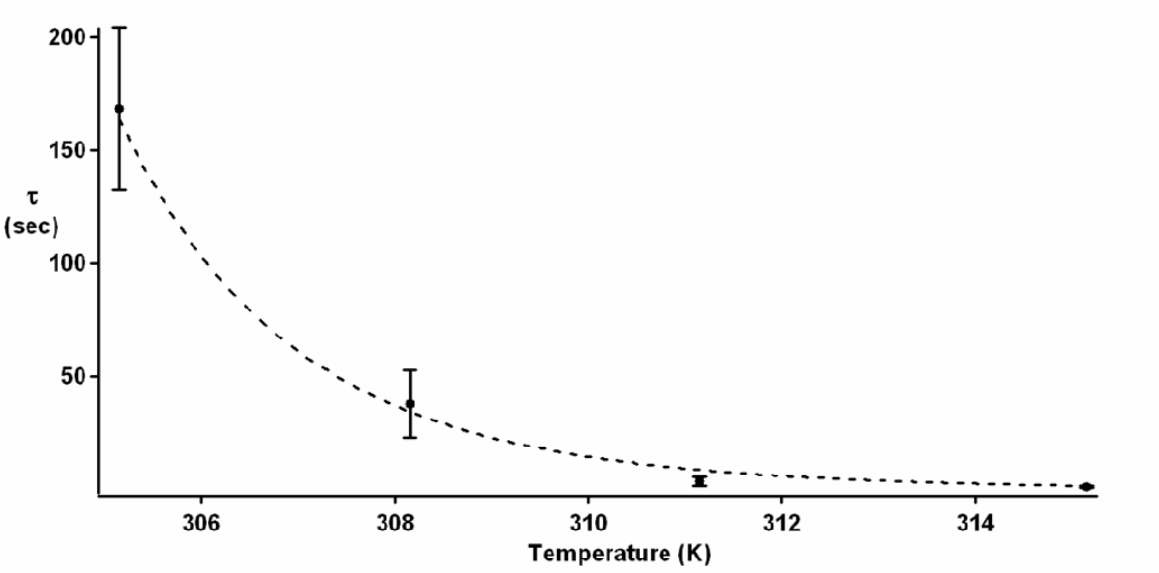

Figure A.6: Anisotropy decay time vs temperature for PPEMA. The dashed line is the fit to the WLF equation.

Appendix B

IGOR PROCEDURE FOR ANALYZING SIMULATED SINGLE MOLECULE TRAJECTORIES

The following procedure is for the analysis of simulated single molecule trajectories discussed in Chapter 3. The raw data are "theta" and "phi".

```
//Calculates corrected and uncorrected linear dichorism(d)//
Function Cal_Intensity(theta, phi,NA)
    wave theta, phi
    variable NA
    variable alpha, A, B, C
    make/o/n=(numpnts(theta)) i0, i90, itotal,d_cor, d_uncor
    alpha=asin(NA/1.41)
    A=1/6-1/4*cos(alpha) + 1/12*cos(alpha)*cos(alpha)*cos(alpha)
    B=1/8*cos(alpha)-1/8*cos(alpha)*cos(alpha)*cos(alpha)
    C=7/48-1/16*cos(alpha)-1/16*cos(alpha)*cos(alpha)-1/48*cos(alpha)*cos(alpha)*cos(alpha)
    printf "A is: %g; B is: %g; C is: %g\r", A, B, C
    i0=A+B*sin(theta)*sin(theta)+C*sin(theta)*sin(theta)*cos(phi+phi)
    i90=A+B*sin(theta)*sin(theta)-C*sin(theta)*sin(theta)*cos(phi+phi)
    itotal=i0+i90
    wavestats/Q itotal
    i0=i0/V_max
    i90=i90/V_max
    d_cor=(i0-i90)/(i0+i90)
    d_uncor=cos(phi+phi)
    AppendToTable i0, i90, d_cor, d_uncor
End

//This adds noise to the raw signals//
Function Add_Noise(signal, newsignal)
    wave signal, newsignal
    newsignal=signal*2000+50 // Multiply intensity by 2000, and add dark counts 50
    newsignal=round((gnoise(sqrt(newsignal))+newsignal)) // add a Poisson noise which is
                                                          proportional to sqrt of total signal
End


//Fits the correlation function to a stretched exponential//
Function FitSimToStretched(correlation)
    wave correlation
    Make/D/N=3/O W_coef
    W_coef[0] = {1,1, 6}
    Make/O/T/N=3 T_Constraints
    T_Constraints[0] = {"K1 > 0","K1 < 1", "K2>0"}
    FuncFit/N/H="100" stretched W_coef correlation[0,100000] /D /C=T_Constraints
End
```

```
//Fits the uncorrected correlation function to the Hinze equation//
Function FitToHinze(uncorrected)
    wave uncorrected
    Make/D/N=1/O W_coef
    W_coef[0] = {0.0002}
    FuncFit/N Hinze W_coef uncorrected[0,100000] /D
End

//Generate the correlation function//
Function make_CofT(transient)
    wave transient
    correlate transient, transient
    wavestats/Q transient
    DeletePoints 0, V_npnts/2, transient
    transient = transient/V_max
End

// makes linear dichroism from x & y signals//
Function make_AofT(x,y,AofT)
    wave x, y, AofT
    AofT = (x-y)/(x+y)
End

//Generate the quarter angle from x & y data
Function make_angle(x,y,angle)
wave x, y, angle
angle = atan(sqrt(x/y))
End

//Fits correlation function of corrected and uncorrected dichroism to stretched exponential//
    Function FitCorrelation()
    wave d_cor,d_uncor
    duplicate/o d_cor, c_cor
    make_coft(c_cor)
    SetScale/P x 1,1,"", c_cor
    display c_cor; ModifyGraph log(bottom)=1
    FitSimToStretched(c_cor); RemoveFromGraph fit_c_cor
    addeqn(W_coef, W_sigma); TextBox/C/N=text0/E=0
    duplicate/o d_uncor, c_uncor
    make_coft(c_uncor); SetScale/P x 1,1,"", c_uncor
    AppendToGraph c_uncor; ModifyGraph log(bottom)=1;ModifyGraph rgb(c_uncor)=(0,0,39168)
    FitToHinze(c_uncor); RemoveFromGraph fit_c_uncor
    Wave W_coef
    variable D
    D=W_coef[0]
    String final
    final="cos(2phi) fit to Hinze"+ "\rD is " + num2str(D) +"\r and tau is " + num2str(1/6/D)
    TextBox/A=LC/F=0/X=0.1/Y=0.00/E=0 final
End

Function FitCorreWithNoise()
    wave i0, i90
    make/o/n=(numpnts(i0)) i0noise, i90noise
```

```
    add_noise(i0, i0noise)
    add_noise(i90,i90noise)
    AppendToTable i0noise, i90noise
    make/o/n=(numpnts(i0)) cnew
    make_Aoft(i0noise, i90noise, cnew)
    make_Coft(cnew); SetScale/P x 1,1,"", cnew
    display cnew; modifyGraph log(bottom)=1
    FitSimToStretched(cnew)
    addeqn(W_coef, W_sigma); RemoveFromGraph fit_cnew; Label left "C(t) with added noise"
End

//Makes histograms of d(inplane angle)/dt
Function Make_Histogram()
    wave i0, i90, i0noise, i90noise //from original intensity and with added noise//
    make/o/n=(numpnts(i0)) angle
    make_angle(i0, i90, angle)
    Differentiate/METH=1 angle/D=dif_angle
    Make/N=450/D/O hist_dif_angle;DelayUpdate;
    Histogram/B=1 dif_angle,hist_dif_angle
    make/o/n=(numpnts(i0)) anglenew
    make_angle(i0noise, i90noise, anglenew)
    Differentiate/METH=1 anglenew/D=dif_anglenew
    Make/N=450/D/O hist_dif_anglenew;DelayUpdate
    Histogram/B=1 dif_anglenew,hist_dif_anglenew
    display hist_dif_angle, hist_dif_anglenew
    CurveFit/N gauss hist_dif_angle /D
    wave W_coef
    variable width1
    width1=W_coef[3]
    CurveFit/N gauss hist_dif_anglenew /D
    wave W_coef
    variable width2
    width2=W_coef[3]
    Legend/C/N=text0/A=LB/F=0/X=0.05
    String final
    final="Width of d(ang)/dt is " + num2str(width1)+"\rWidth of d(ang)/dt with noise is " +
    num2str(width2)
    TextBox/A=RT/F=0/X=0.1/Y=0.00/E=2 final
    RemoveFromGraph fit_hist_dif_angle, fit_hist_dif_anglenew
    ModifyGraph lstyle(hist_dif_anglenew)=12,rgb(hist_dif_anglenew)=(0,0,39168)
End

//Makes histogram of dichroism signals//
Function HistOfDichroism()
    wave d_cor, d_uncor, i0noise, i90noise
    make/o/n=(numpnts(i0noise)) d_cornoise
    make_aoft(i0noise, i90noise, d_cornoise)
    Make/N=450/D/O hist_d_cor;DelayUpdate
    Histogram/B=1 d_cor,hist_d_cor
    Make/N=450/D/O hist_d_uncor;DelayUpdate
    Histogram/B=1 d_uncor,hist_d_uncor
    Make/N=450/D/O hist_d_cornoise;DelayUpdate
    Histogram/B=1 d_cornoise, hist_d_cornoise
```

```
    Display hist_d_cor, hist_d_uncor, hist_d_cornoise
    ModifyGraph rgb(hist_d_uncor)=(0,52224,0),rgb(hist_d_cornoise)=(0,15872,65280)
    Legend/C/N=text0/A=LT/X=5.00/Y=5.00/E=0
End
```

The rotational correlation function from Hinze's paper.

```
Function Hinze(w,t) : FitFunc
    Wave w
    Variable t
    //CurveFitDialog/ These comments were created by the Curve Fitting dialog. Altering them will
    //CurveFitDialog/ make the function less convenient to work with in the Curve Fitting dialog.
    //CurveFitDialog/ Equation:
    //CurveFitDialog/ f(t) = (.835013*exp(-6*D*t))+(.100205*exp(-20*D*t))
                              +(0.0310139*exp(- 42*D*t))+(0.0135202*exp(-72*D*t))
                              +(0.00708445*exp(-110*D*t))+(0.00417137*exp(-156*D*t))
                              +(0.00266071*exp(-210*D*t))+(0.00180131*exp(-272*D*t))
                              +(0.00127513*exp(-342*D*t))+(0.00093625*exp(-420*D*t))
    //CurveFitDialog/ End of Equation
    //CurveFitDialog/ Independent Variables 1
    //CurveFitDialog/ t
    //CurveFitDialog/ Coefficients 1
    //CurveFitDialog/ w[0] = D
    return (.835013*exp(-6*w[0]*t))+(.100205*exp(-20*w[0]*t))+(0.0310139*exp(-42*w[0]*t))
          +(0.0135202*exp(-72*w[0]*t))+(0.00708445*exp(-110*w[0]*t))
          +(0.00417137*exp(-156*w[0]*t))+(0.00266071*exp(-210*w[0]*t))
          +(0.00180131*exp(-272*w[0]*t))+(0.00127513*exp(-342*w[0]*t))
          +(0.00093625*exp(-420*w[0]*t))
End
```

The following functions are for statistical analysis to characterize jumps or exchanges (for trial only).

```
//Calculates avg and sdev of raw data, each segment differs by one point//
Function make_stats (raw, average, standev, x)
    wave raw, average, standev    // x+1 is the number of points in each segment//
    variable x
    variable i
    for (i=0; i <=(numpnts(raw)-x); i+=1)
          wavestats/Q/R=[i,i+x] raw
          average[i]= V_avg
          standev[i]=V_sdev
    endfor
End

//Calculates avg and sdev of raw data, divided into several bins//
Function make_stats2 (raw, average, standev,y)
    wave raw, average, standev // y+1 is the bin width//
    variable y
    variable i, j
    for (i=0, j=0 ; i <= (numpnts(raw)-y); i =i+y+1, j=j+1 )
          wavestats/Q/R=[i, i+y] raw
```

```
            average[j]=V_avg
            standev[j]=V_sdev
    endfor
End

//To find exchange based on average+/- standev*factor //
Function find_exchange (average, standev, exchange, factor)
    wave average, standev, exchange
    variable factor    //returns true only when the next 2 avg are outside the range
    exchange = 0
    variable i
    for (i=0;i<(numpnts(average));i+=1)
        if (average[i+1] > (average[i]+factor*standev[i]))
            if (average[i+2] > (average[i]+factor*standev[i]))
                exchange[i]=5
                print "exchange"
            endif
        else
            if (average[i+1] < (average[i]-factor*standev[i]))
                if (average[i+2] < (average[i]-factor*standev[i]))
                        exchange[i]=5
                        print "exchange"
                endif
            endif
        endif
    endfor
End

//T-test //
Function do_Ttest(average, standev, n, t_cal, t,true) //n is the number of points in each average
                                                        (n=x+1 in make_stats)
    wave average, standev, t_cal, true              // enter value of t from desired confidence level
    variable n , t                                      and number of degrees of freedom (2n-2)
    variable i
    for (i=0; i<(numpnts(average)); i+=1)
        t_cal[i]=((average[i+1]-average[i])/sqrt(((standev[i+1])^2+(standev[i])^2)/n))
            if (abs(t_cal[i])>t)
                true[i]=5
                print "true"
            else
                true[i]=0
            endif
    endfor
End

//Another T-test//
Function do_Ttest2(average, standev, n, t_cal, t,true) // n is the number of points in each average
                                                        (n=x+1 in make_stats)//
    wave average, standev, t_cal, true     // enter value of t from desired confidence level
    variable n , t                                  // and number of degrees of freedom (2n-2)
    variable i // compare consecutive t-pairs to pick up exchange correctly//
    for (i=0; i<(numpnts(average)); i+=1)
        t_cal[i]=((average[i+1]-average[i])/sqrt(((standev[i+1])^2+(standev[i])^2)/n))
```

```
            if (abs(t_cal[i])>t)
                if (abs((average[i+2]-average[i])/sqrt(((standev[i+2])^2+(standev[i])^2)/n))>t )
                    if (abs((average[i+3]-average[i])/sqrt(((standev[i+3])^2+(standev[i])^2)/n))>t)
                  if (abs((average[i+4]-average[i])/sqrt(((standev[i+4])^2+(standev[i])^2)/n))>t)
                      if (abs((average[i+5]-average[i])/sqrt(((standev[i+5])^2+(standev[i])^2)/n))>t)
                              true[i]=5
                              print "true"
                        endif
                    endif
                      endif
                endif
            else
                true[i]=0
            endif
    endfor
End

//To do a F-test for comparison of standard deviations//
Function do_Ftest(standev, f_cal, f, true)
    wave standev, f_cal, true
    variable f
    variable i
    for (i=0; i<(numpnts(standev)); i+=1)
        f_cal[i]= (standev[i]^2/standev[i+1]^2)
            if (f_cal[i] < 1 )
               f_cal[i] = 1/f_cal[i]
            endif

            if (f_cal[i] > f)
               true[i]=5
               print "true"
            else
               true[i]=0
            endif
    endfor
End

//To find change points//
Function change_point(data, change)
    wave data, change
    wave f,g
    variable i, j
    for (i=10, j=0 ;i<numpnts(data); i+=i+1, j+=j+1 )
        wavestats/Q/R=[0, j+9] data
        f[i]=(V_sdev^2)*(V_npnts-1)
        wavestats/Q/R=[j+10, ] data
        g[i]=(V_sdev^2)*(V_npnts-1)
        change[i]=f[i]+g[i]
        print "hi"
    endfor
End
```

CALCULATING ROTATIONAL CORRELATION FUNCTIONS

Examples of calculation for a_l coefficients of the rotational correlation functions (see Chapter 3) using Mathematica. This was carried out for even l from l =2 to l = 20. Numerical solutions obtained for each a_l were normalized and tabulated in Table 2.1.

a_l coefficients calculated using d = cos (2ϕ)

This is for NA = 0 (example: l = 2).

$$\frac{1}{4\pi}\sum_{m=-2}^{2}\left(\int_0^{2\pi}\int_0^{\pi}\text{Sin}[\theta]*\text{SphericalHarmonicY}[2,\ m,\ \theta,\ \phi]*\text{Cos}[2\,\phi]\,d\theta\,d\phi\right)^2$$

a_l coefficients calculated using the corrected I_0 and I_{90}

Each a_l can be computed using different parameters A, B, C, defined by the NA and index of refraction (example: l = 4).

$$\text{h4}[A\_,\ B\_,\ C\_] :=$$

$$\frac{1}{4\pi}\sum_{m=-4}^{4}\left(\int_0^{2\pi}\int_0^{\pi}\text{Sin}[\theta]*\text{SphericalHarmonicY}[4,\ m,\ \theta,\ \phi]*\frac{C*\text{Sin}[\theta]\,\hat{}\,2*\text{Cos}[2\,\phi]}{A+B*\text{Sin}[\theta]\,\hat{}\,2}\,d\theta\,d\phi\right)^2$$

A, B, and C are defined by $\alpha = \sin^{-1}(NA/n)$

$$\text{cofA}[\alpha\_] := 1/6 - 1/4*\text{Cos}[\alpha] + 1/12*\text{Cos}[\alpha]^3$$

$$\text{cofB}[\alpha\_] := 1/8*\text{Cos}[\alpha] - 1/8*\text{Cos}[\alpha]^3$$

$$\text{cofC}[\alpha\_] := 7/48 - 1/16*\text{Cos}[\alpha] - 1/16*\text{Cos}[\alpha]^2 - 1/48*\text{Cos}[\alpha]^3$$

Appendix C

IGOR PROCEDURE FOR ANALYZING SINGLE MOLECULE EXPERIMENTAL DATA

The procedure file includes all the user-defined functions useful for analyzing experimental data. The raw data are “Cont_ref” , “Right” and “Rear” text waves.

```
//Converts reference signal into time wave//
Function make_time(time_wav, freq)
    wave time_wav
    variable freq                    // frequency of reference signal
    variable index = 1
    variable c1
    wavestats/Q time_wav
    time_wav [ index ] = time_wav [index ] + time_wav[ index -1 ]
    index += 1
    while (index < V_npnts)
    time_wav = time_wav/freq              // calibrate to seconds
    c1=time_wav [0]
    time_wav = time_wav - c1              // set first point = 0
End

//Plots right and rear signals and calculates linear dichroism//
Function plotall(right, rear, cont_ref, dich)
    wave rear, right, cont_ref, dich
    String TimeX
    Make_time(cont_ref, 5000)
    TimeX= NameOfWave(cont_ref )+ "1"     //make a new time wave for displaying signals//
    Duplicate/O cont_ref, $TimeX
    wavestats/Q cont_ref
    Deletepoints V_endrow, 1,cont_ref //delete last point and use this as time for correlation fxn//
    wavestats/Q right
    right=right-V_min
    wavestats/Q rear
    rear=rear-V_min
    make_time($TimeX, 5000)        //use TimeX to display raw signlas//
    display/N= Raw_signal right, rear vs $TimeX; ModifyGraph rgb[0]=(0,0,52224);
    Legend/C/N=text0/F=0; Label left "counts/0.2sec";Label bottom "sec"
    make_aoft(right, rear, dich)
    make_coft3(dich)                      //take out first point in the correlation fxn//
    Display/n=Correlation_dichroism dich vs cont_ref
    ModifyGraph mode[0]=0,lsize[0]=1
    Label left "C(t)";DelayUpdate
    Label bottom "sec";
    ModifyGraph log(bottom)=1
End
```

```
//Generates correlation function, gets rid of the first point and normalizes to the 2nd point//
Function make_CofT3(transient)
    Wave transient
    correlate transient, transient
    Wavestats/Q transient
    DeletePoints 0, 1+(V_npnts/2), transient
    Wavestats/Q transient
    transient = transient/V_max
End

//This calculates the Standard Deviation of autocorrelation fxn at time lag k//
Function SD_corre(corre, k)
    Wave corre
    Variable k
    Variable N, sd1, Var
    sd1=0; var=0
    Wavestats/Q/R=[1, k] corre
    sd1=(V_rms)^2*V_npnts
    Wavestats/Q corre
    N=V_npnts
    Var=(1/N)*(1+2*sd1)
    printf "The standard deviation is:%g\r", sqrt(var); printf "The time lag q is: %g\r", k
    printf "The autocorre is :%g\r", corre[k]
End

//This finds the large-lag standard error for the autocorrelation function. Beyond this lag q the
theoretical autocorrelation fxn may have died out//
Function FindLargeLag(corre)
    wave corre
    variable N
    wavestats/Q corre
    N= V_npnts
    Duplicate/o corre, corre2
    corre2 = corre2*corre2
    Variable sdcor =0
    variable/G lagQ=0
    Do
        sdcor= sqrt(1/N*(1+2*sum(corre2, pnt2x(corre2, 1), pnt2x(corre2, lagQ))))
            If (sdcor <= corre[lagQ])
                lagQ+=1
            Else
               If (sdcor > corre[lagQ])
                    break
               Endif
                 Endif
    While (lagQ<=N)
    printf "The sufficient time lag q is: %g\r", lagQ
    printf "The autocorre at time lag q is:%g\r", corre[lagQ]
    printf "The standard deviation is: %g\r" ,sdcor
End
```

The following CorrFit functions fit the correlation function by varying fitting range, amp, and beta. There are five different criteria:

CorrFit0: fit the whole range, Amp =1, $0 < \beta \leq 1$

CorrFit1: fit to lag q, Amp =1, no constraint on β

CorrFit2: fit to lag q, no constraint on Amp and β

CorrFit3: fit to lag q, Amp =1, $0 < \beta \leq 1$

CorrFit4: fit to lag q, no constraint on Amp, $0 < \beta \leq 1$

Shown here is CorrFit3.

```
Function CorrFit3(dich, cont_ref)
    Wave dich, cont_ref
    Wave FitMethod3, Amp3, Beta3,Tau3
    Variable/G iA=1 ,iB=1 , iT=100              //initial guesses. They will be changed if fitting fails//
    Variable/G V_FitQuitReason, V_FitError =0
    Variable/G FitNum=0
    Variable/G Index
    Variable/G LagQ
    FindLargeLag(dich)
    Make/D/N=3/O W_coef
    W_coef [0]= {iA, iB, iT}
    Make/O/T/N=2 T_Constraints
    T_constraints[0]={"K1>0", "K1<1"}          //This constrains beta//
    Print "test1"
    FuncFit/H="100" stretched W_coef dich[0, lagQ] /X=cont_ref /D/C=T_Constraints
    FitNum +=1                                              //H=”100” hold amp at 1//
    If (V_FitQuitReason!=0 || V_FitError!=0)
        print "test2"
        W_coef[0]={iA, iB,iT*0.1}
        V_FitError=0
        FuncFit/H="100" stretched W_coef dich[0, lagQ] /X=cont_ref /D/C=T_Constraints
        FitNum+=1
    Endif

    If (V_FitQuitReason!=0 || V_FitError!=0)
        print "test3"
        W_coef[0]={iA, iB,iT*5}
        V_fitError=0
        FuncFit/H="100" stretched W_coef dich[0, lagQ] /X=cont_ref /D/C=T_Constraints
        FitNum+=1
    Endif

    If (V_FitQuitReason!=0 || V_fitError!=0)
        print "test4"
        W_coef[0]={iA, iB*0.5,iT*0.1}
        V_fitError=0
        FuncFit/H="100" stretched W_coef dich[0, lagQ] /X=cont_ref /D/C=T_Constraints
        FitNum+=1
    Endif

    If (V_FitQuitReason!=0||V_fitError!=0)
        print "test5"
```

```
        W_coef[0]={iA, iB*0.5,iT*5}
        V_fitError=0
        FuncFit/H="100" stretched W_coef dich[0, lagQ] /X=cont_ref /D/C=T_Constraints
        FitNum+=1
    Endif
    FitMethod3[index]=3                    //Save the fitting results into these waves//
    Amp3[index]=W_coef[0]
    Beta3[index]=W_coef[1]
    Tau3[index]=W_coef[2]
End

//This is a do-it-all function that plots raw data, fits correlation fxns, and saves the results. Upload
data file one by one and track by the counting variable “index” //
Function AutoFit(right, rear, cont_ref, dich)
    wave right, rear, cont_ref, dich
    plotall(right, rear, cont_ref, dich)
    Variable/G index
    Corrfit0(dich, cont_ref)
    Corrfit1(dich,cont_ref)
    Corrfit2(dich, cont_ref)
    Corrfit3(dich,cont_ref)
    Corrfit4(dich, cont_ref)
    index+=1
End
```

The following functions are useful for batch processing when all the raw files are already uploaded into the data folder.

```
//This calls all the right and rear waves to calculate delta_dichrosim, and make histograms//
Function delta_A()
    String List = WaveList ("*right*", ";", "") //Get all the "right_mmddno” names//
    String theWave
    variable windex=0
    String AofT
    Do
        theWave= StringFromList(windex, List)
            If (strlen(theWave)==0)
                break
            Endif
        String filenum
        filenum = theWave[5,9]          //extract the wavename associated with the original file//
        AofT = "A"+filenum
        Duplicate/o $theWave, $AofT
        String w_rear= "rear"+ filenum     //find the corresponding rear and cont_ref waves//
        String W_contref= "cont_ref" + filenum
        make_aoft($theWave, $w_rear, $AofT)   //Make linear dichroism and make a histogram//
        Display/R/T $AofT vs $W_contref as filenum
        String A_Hist = AofT + "_Hist"
        Make/N=40/D/O $A_Hist;DelayUpdate
        Histogram/B=1 $AofT, $A_Hist
        String A_dif = AofT+ "_Dif"          //calculate Delta_dichroism and make a histogram//
        Differentiate/METH=1 $AofT/D=$A_Dif                    //dA
```

```
        //Differentiate/METH=1 $A/X=$W_contref/D=$A_Dif              // dA/dT
        String A_Dif_Hist = AofT+ "Dif_Hist"
        Make/N=40/D/O $A_Dif_Hist;DelayUpdate
        Histogram/B=1 $A_Dif, $A_Dif_Hist
        AppendToGraph/L/B $A_Hist, $A_Dif_Hist
        ModifyGraph axisEnab(right)={0.5,1},axisEnab(left)={0,0.5};Legend/C/N=text1/F=0/A=RC
        ModifyGraph rgb[2] = (0,0,0); ModifyGraph lstyle[2] =3
        printf "The waves are: %s, %s, %s, %s\r", theWave, w_rear, AofT, W_contref
        Windex+=1
    While (1)
End

//This calls sorted right and rear and cont_ref waves to calculate dichroism and Correlation fxns//
Function FitAllWaves()
    Wave/T Filename
    Wave Length
    String WholeList= WaveList("right*", ";", "")   //list all waves containing “right_mmddnn”//
    String Targetwave
    Variable/G Index
    Variable Findex=0
    Do
        Targetwave = StringFromList(Findex, WholeList)
            If (strlen(Targetwave)==0)
                break
            Endif
        String Fnum
        Fnum = Targetwave[5,9]                  //get data file name “_mmddnn”//
        String Rear= "Rear" + fnum              //find the corresponding “rear_mmddnn”//
        String Cont_ref = "cont_ref"+fnum       //find the corresponding “cont_ref_mmddnn”//
        String TofC = "Ctime" + fnum            //make new time for correlation fxn//
        String AofT = "A"+ fnum
        String CofT = "C" + fnum
        Duplicate/O $Targetwave, $AofT
        Duplicate/O $Cont_ref, $TofC
        Wavestats/Q $TofC
        Deletepoints V_endrow, 1, $TofC
        Make_Aoft($Targetwave, $Rear, $AofT)
        Duplicate/O $AofT, $CofT
        Make_Coft3($CofT) ;Appendtotable $CofT
        Display $CofT vs $TofC
        Corrfit0($CofT, $TofC)                  //fit correlation fxn with 5 different criteria//
        Corrfit1($CofT, $TofC)
        Corrfit2($CofT, $TofC)
        Corrfit3($CofT, $TofC)
        Corrfit4($CofT, $TofC)
        Wavestats/Q $Cont_ref
        Length[index]=V_max                     //report transient length//
        Filename[index]= Fnum
        index+=1
        Findex+=1
    While (1)
End
```

```
//This calls out all the A_dif waves and concatenate them to make histogram//
Function combine_DifA()
    String DifAlist= Wavelist("A*_Dif", ";", "")
    Variable items= ItemsInList(DifAlist)
    Make/O/T/N= (items) textwave= StringFromList(p, DifAlist)
    Edit textwave
    Make/O DifAwaves=0; Appendtotable DifAwaves
    Concatenate/NP/O DifAlist, DifAwaves
End

//this calls out all the A(dichroism) waves and contatenate them to make histogram//
Function combineA()
    String Alist = Wavelist("A*", ";", "")
    String checkstr
    Variable i=0
    Do
        checkstr = StringFromList(i, Alist)
          If (strlen(checkstr)==0)
              break
          Endif

           If (strlen(checkstr)!= 5) //Remove other waves that are not dichroism (but contain "A" )
    Alist =RemoveListItem(i, Alist, ";")
          Else
              i+=1
          Endif
    While (1)
    Variable items= ItemsInList(Alist) //makes a text wave of the AList//
    Make/O/T/N=(ItemsInList(Alist)) Alistname = StringFromList(p, Alist)
    Edit Alistname
    Make/O allAwaves=0; Appendtotable allAwaves
    Concatenate/NP/O Alist, allAwaves
End

//This is used to truncate the transients to a certain length//
Function truncate()
    String Listall = WaveList("*", ";", "")
    String w1
    variable z1 = 0
    String neww1
    Do
        w1 = StringFromList(z1, Listall)                    //calls out all the waves in the folder//
            if (strlen(w1)==0)
              break
            endif
        neww1 = w1+"_s"                                              //s stands for short//
        Duplicate/o $w1, $neww1
        wavestats/Q $neww1
        Deletepoints 7676, V_npnts-7676, $neww1          //delete points after certain length//
        Appendtotable $neww1
        z1+=1
    While(1)
End
```

Vita

Chia-Yin Wei was born in Taiwan on July 4, 1979, the daughter of Ho-Ching Wei and I-Hsiu Chen Wei. After graduating from Taipei First Girls' High School in 1997, she entered National Taiwan University majoring in chemistry. Chia-Yin also attended Harvard Summer School in 1999. She received the degree of Bachelor of Science from National Taiwan University in June 2001, and was a recipient of the Award of the Dean of Natural Science College. She worked as a full-time teaching assistant for the Department of Chemistry at National Taiwan University for one year. She entered the Graduate School of The University of Texas at Austin in September 2002 to pursue physical chemistry studies under the supervision of Dr. David A. Vanden Bout.

Permanent address: 666, Section 1, Chungshan Rd., Shetou, Changhua, 51199, Taiwan

This dissertation was typed by Chia-Yin Wei.